Cellular Analysis by Atomic Force Microscopy

James J. Muys

A thesis presented for the degree of Doctor of Philosophy in

Electrical and Computer Engineering,

University of Canterbury,

Christchurch, New Zealand.

November 2006

Acknowledgments

I would like to thank both my supervisors for their support throughout this project. To Dr Maan Alkaisi - for initiating the Biochip project and for all your encouragement and guidance. To Professor John Evans - thank you for your patience and without your biological expertise we would have been truly lost. Strength and success of this work was ultimately a result of the strong collaborative efforts between both supervisors and associations.

Further acknowledgment goes to Research Fellow Junko Nagase for her enormous help in cell culture techniques and preparation of materials and reagents. I acknowledge Dr Peter Sykes for tumour removal and Nurse Diane Harker for coordinating their delivery and the patient approval process. For useful discussions I acknowledge the efforts made by D.O.S Melville, M. Allen, E.S Berthier, V. Nock, F. L'Hostis, L. Pearson, R.J Blaikie, G. Turner, H. Devereux, C.P Moore and A. Parbhu.

This research was supported by the MacDiarmid Institute for Advanced Materials and Nanotechnology and the Canterbury Medical Research Foundation, New Zealand.

To Mum, Dad and Nanda
with love, James

Preface

This document discusses research undertaken at the Electrical & Computer Engineering Department at the University of Canterbury, and the Christchurch School of Medicine & Health Sciences at the University of Otago between August 2003 and November 2006.

Aspects of research contained in this dissertation are discussed in the following publications:

Peer-Reviewed Journal Articles

1. Muys JJ, Alkaisi MM, Evans JJ, *Cellular Replication and AFM Imaging using a UV-Bioimprint Technique.* Nanomedicine: Nanotechnology, Biology, and Medicine, 2(3) 2006.

2. Muys JJ, Alkaisi MM, Nagase J, Sykes P, Parguez G, Melville DOS, Evans JJ. *Cellular transfer and AFM imaging of cancer cells using Bioimprint.* Journal of Nanobiotechnology, 4(1) 2006.

3. Muys JJ, Alkaisi MM, Evans JJ, *Bioimprint: Nanoscale analysis by replication of cellular topography using soft lithography.* Journal of Biomedical Nanotechnology, 2(1) 2006.

4. Muys J, Alkaisi MM, Evans JJ, Nagase J, *Analysis of dielectrophoretically trapped biological cells by atomic force microscopy using an integrated biochip platform.* Japanese Journal of Applied Physics, 44(7B) 2005.

Conference Proceedings[1]

1. Moore CP, Blaikie RJ, Muys JJ, *Biochip Multi-function Signal Generator*. Proceedings of the Thirteenth Electronics New Zealand Conference, (ENZCon06), November 13-14, 2006, Christchurch, New Zealand.

2. Muys JJ, Alkaisi MM, Evans JJ, *Bioimprint*$^{\circ}$. International Conference on Nanoscience and Nanotechnology (ICONN) Proceedings, 3-7 July, 2006, Brisbane, Australia.

3. Muys JJ, Alkaisi MM, Nagase J, Evans JJ, *Analysis of cells by atomic force microscopy*. Proceedings of the Canterbury Health Research Conference, The New Zealand Medical Journal (ISSN 1175 8716) 119(1231) 2006.

4. Muys JJ et al. *AC dielectrophoresis of spherical particles using 2-D interdigitated microelectrode array structures*. Proceedings of the Eleventh Electronics New Zealand Conference (ENZCon04), (ISBN 0-476-01106-X) pg. 61-66, November 15-16, 2004, Palmerston North, New Zealand.

Presentations

1. Muys JJ, Alkaisi MM, Mohammed K*, Evans JJ, *Soft Replication of Biological Cells using a Bioimprint Technique*$^{\diamond}$. 5th Conference on Nanoimprint and Nanoprint Technology (NNT), 15-17 November, 2006, San Francisco, CA.

2. Muys JJ, Alkaisi MM*, Evans JJ, *Bioimprint : Cellular Replication for Nanoscale Imaging*$^{\bullet}$. International Conference on Micro- and Nano-Engineering (MNE), 17-20 September, 2006, Barcelona, Spain.

3. Evans JJ*, Muys JJ, Alkaisi MM, *Atomic Force Microscopy technique for imaging pituitary cells*$^{\circ\diamond}$. 6th International Neuroendocrinology Congress, Frontiers in Neuroendocrinology, 27:118, June 19-22 2006, Pittsburgh, PA.

[1] **presenting author*, $^{\diamond}$*poster presentation*, $^{\bullet}$*oral presentation*, $^{\circ}$*peer-reviewed*, †*young author's award*.

4. Muys JJ, *AFM imaging of cell replicas*, The MacDiarmid Institute Student Symposium$^{\bullet}$, 12-13 November 2005, Wellington, New Zealand.

5. Muys JJ, Melville DOS, Alkaisi MM, Blaikie RJ, *Bioimprint* $^{\diamond}$, The Nanochallenge, 9-11 November 2005, Padua, Italy.

6. Muys JJ, Alkaisi MM, Nagase J, Evans JJ, *Analysis of cells by atomic force microscopy*$^{\bullet}$. Canterbury Health Research Conference, 26-27 August 2005, Christchurch, New Zealand.

7. Alkaisi MM*, Muys JJ, Evans JJ, *Imaging of Biological Cells by Atomic Force Microscopy Using an Integrated Biochip Platform*$^{\diamond\dagger}$. 1st International Workshop of NANO Systems Institute (IW-NSI), 30-31 May, 2005, Seoul, Korea 2005.

8. Muys JJ, *Dielectrophoretic Control of Biological Cells on a Biochip*$^{\bullet}$, IEEE Evening Event, 11 May 2005, University of Canterbury, New Zealand.

9. Muys JJ, Alkaisi MM, Evans JJ, *Atomic force microscopy of pituitary gonadotroph cells*$^{\diamond}$, and *Characterisation of endometrial cancer cells by atomic force microscopy*$^{\diamond}$. BioMEMS and Nanotechnology II, SPIE Microelectronics, MEMS, and Nanotechnology, 11-14 December 2005, Brisbane, Australia.

10. Muys JJ, Alkaisi MM, Evans JJ, Nagase J, *Analysis of dielectrophoretically trapped biological cells by atomic force microscopy using a biochip platform*$^{\bullet}$. Advanced Materials & Nanotechnology (AMN-2), 6-11 February 2005 Queenstown, New Zealand.

11. Muys J, Alkaisi MM, Evans JJ, Nagase J, *Analysis of dielectrophoretically trapped biological cells by atomic force microscopy using an integrated biochip platform*$^{\bullet}$. International Microprocesses and Nanotechnology Conference (MNC) 26-29 October, 2004, Osaka, Japan.

Patents

1. Alkaisi MM, Muys JJ, *'Moulding': A Bioimprint process for creating casts of biomaterials*, Provisional N.Z Application Patent Nos. 540713 and 543463, Filed by AJ Park Intellectual Property Lawyers & Consultants, 13 June 2005, Wellington, New Zealand.

Table of Contents

List of Figures

Abstract

Exocytosis is a fundamental cellular process where membrane-bound secretory granules from within the cell fuse with the plasma membrane to form fusion pore openings through which they expel their contents. This mechanism occurs constitutively in all eukaryotic cells and is responsible for the regulation of numerous bodily functions. Despite intensive study on exocytosis the fusion pore is poorly understood. In this research micro-fabrication techniques were integrated with biology to facilitate the study of fusion pores from cells in the anterior pituitary using the atomic force microscope (AFM). In one method cells were chemically fixed to reveal a diverse range of pore morphologies, which were characterised according to generic descriptions and compared to those in literature. The various pore topographies potentially illustrates different fusion mechanisms or artifacts caused from the impact of chemicals and solvents in distorting dynamic cellular events. Studies were performed to investigate changes in fusion pores in response to stimuli along with techniques designed to image membrane topography with nanometre resolution.

To circumvent some deficiencies in traditional chemical fixation methodologies, a Bioimprint replication process was designed to create molecular imprints of cells using imprinting and soft moulding techniques with photo and thermal activated elastomers. Motivation for the transfer of cellular ultrastructure was to enable the non-destructive analysis of cells using the AFM while avoiding the need for chemical fixation. Cell replicas produced accurate images of membrane topology and contained certain fusion pore types similar to those in chemically fixed cells. However, replicas were often dehydrated and overall experiments testing stimuli responses

were inconclusive. In a preliminary investigation, a soft replication moulding technique using a PDMS-elastomer was tested on human endometrial cancer cells with the aim of highlighting malignant mutations.

Finally, a Biochip comprised of a series of interdigitated microelectrodes was used to position single-cells within an array of cavities using positive and negative dielectrophoresis (DEP). Selective sites either between or on the electrode were exposed as cavities designed to trap and incubate pituitary and cancer cells for analysis by atomic force microscopy (AFMy). Results achieved trapping of pituitary and cancer cells within cavities and demonstrated that positive DEP could be used as a force to effectively position living cells. AFM images of replicas created from cells trapped within cavities illustrated the advantage of integrating the Biochip with Bioimprint for cellular analysis.

Chapter 1

Introduction

1.1 Exocytosis

Constitutive exocytosis is a fundamental physiological process occurring ubiquitously in all eukaryotic cells. It is responsible for controlling membrane traffic essential for a range of functions including; cell growth, division, cell-to-cell communication, cell polarity establishment and maintenance of cellular architecture, to name a few. As well as occurring constitutively, exocytosis can be tightly regulated by stimulation triggers, which control the release of physiological critical molecules to the extra-cellular space, such as the secretion of hormones or neurotransmitters in neuroendocrine cells. Current understanding of exocytosis is derived from vesicular fusion with the plasma membrane based on morphological, electrophysiological and biochemical studies [1]. Traditionally, techniques used to monitor exocytosis have included [2]; time-resolved capacitance measurements, amperometry, fluorescence, evanescence wave/total internal reflection microscopy and electron microscopy. More recently, AFMy has been introduced as a potential tool for imaging dynamic events *in situ*.

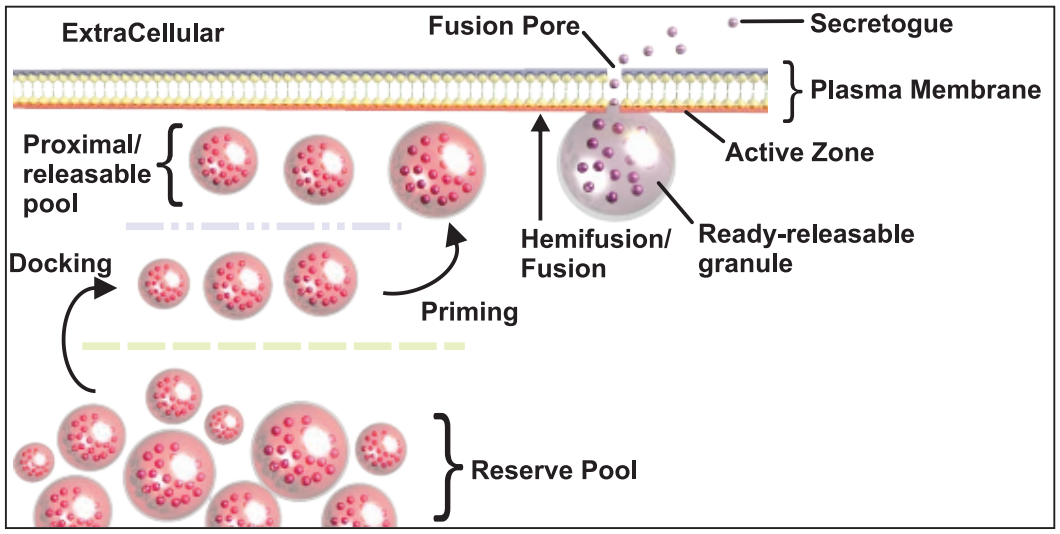

Figure 1.1: Transitional stages involving intra-cellular membrane fusion of a secretory granule with the plasma membrane during exocytosis.

1.2 Membrane Fusion

Fusion governs exocytotic transport and function by regulating the export of membrane-bound granules passing through intra-cellular compartments to the external medium via the plasma membrane. Fusion pores appear as nanometre wide openings on the cell membrane as a result of the aqueous connection between the lumen of an intra-cellular granule fusing with the plasma membrane. All exocytotic fusion reactions embody an elementary sequence of kinetic events governing membrane contact, merger and secretion. Prior to secretion, granules (vesicles) are progressively pre-prepared through slower maturation steps to a ready-releasable state. Only a small subset of granules form the ready-releasable pool at any given time and are deemed competent to undergo exocytosis with an immediate response. Those that are represent a pool of granules morphologically docked in close proximity to the plasma membrane and have fulfilled all requisite reactions to be primed for fusion. Reservoirs of releasable and then reserve granule pools serve as a refilling source for depleted ready-releasables completing exocytosis.

Exocytosis can be functionally dissected into a series of transitional steps accord-

ing to ***protein scaffold*** [3] and ***stalk hypothesi*** [4] - theories postulating the transitional states between two merging phospholipidic bilayers. The mechanics of the overall fusion reaction is illustrated schematically[1] (Fig. 1.1) and proceeds sequentially beginning with [6, 7]:

1. ***Tethering/Docking***

   After traversing the subcortical cytoskeleton barrier initial mergence occurs between proximal lipidic bilayers of the recruited granule and intra-cellular membrane target after overcoming counteracting electrostatic forces.

2. ***Priming***

   Activation of fusion machinery (t-/v-SNARES, etc.) by tethering triggers the assembly of protein complexes linking opposing granule and plasma membranes together. Initially a stalk is formed on the cell ultrastructure as a result of adjoining membranes, providing reactions bringing the membranes into proximity.

3. ***Hemifusion***

   Hemifusion is a natural transient intermediate reaction in exocytosis where the proximal phospholipid monolayers of the granule and plasma membrane are linked prior to the opening of a fusion pore - whether this remains obligatory in all fusion occurrences is yet to be proven.

4. ***Fusion***

   From an intermediary, fusion pores form and proceed to secrete granular contents according to transient and/or total exocytotic mechanisms.

In regulated exocytosis physiological function in a given cell type can define fusion pore attributes in terms of [6]; exocytosis rate, post stimulation lag-time, dura-

[1] Ongoing development in operative terms describing fusion stages including docking, priming and ready-releasables are derived from various observational methods, yet their certainty and true state remains indefinite [5].

tion, granule proportionality response, and the presence of single or multiple granule/fusion types. For instance there is considerable variation in the number of granules at an exocytotic-fused state during regulated exocytosis, and in certain cell types a solitary fusion pore may indicate a state of stimulation.

Although the many molecular components that comprise the fusion pore complex are well-defined the exact manner governing granular/vesicular release remain concealed. Common opinions accept secretory granule membranes are fully incorporated with the host cell plasma membrane during exocytosis, but studies over the last decade indicate otherwise [8]. Variation amongst different cell types now support opposing mechanisms describing the stages culminating in secretion as either ***total/full*** or ***transient fusion***. Classically ***'fuse-and-collapse'/'full-collapse' exocytosis*** have been pathways widely used to describe mechanisms completing total fusion, wherein full secretory release is followed by post-function dilatation and then continuity of the granule into the host cell membrane.

Fate of sites following mergence with the plasma membrane after termination of fusion is also much speculated. Shown in Fig. 1.2 one scenario frequently envisioned is the compensatory retrieval and internalisation of the plasma membrane back into the intra-cellular by ***endocytosis***. After complete fusion direct coupling of endocytosis with exocytosis is known to mediate the subsequent recapture of excess membrane by slow retrieval clathrin-assembly dependent and/or -independent endocytosis. In addition to providing a bidirectional mechanism of transport and communication, endocytosis is seen to act as a regulatory-balancing mechanism to satisfy the cell surface constancy requirement.

Whereas non-traditionally exocytosis is thought to form transiently, and is generically referred to as ***'kiss-and-run'*** [9]. Under this mechanism the fusion pore is predicted to temporarily connect and be recaptured intact without loss of identity from the plasma membrane by rapid endocytosis. The characteristic 'flickering' sequence as observed by capacitance measurements with patch-clamp techniques [10] allows limited vesicular release and process recycling. In regulated exocytosis spatial

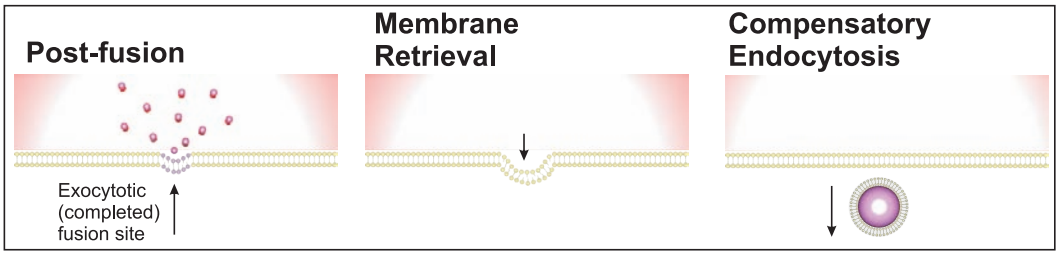

Figure 1.2: Compensatory Endocytosis: Animation showing compensatory retrieval of the plasma membrane post granular release at an exocytotic site.

and temporal coordination are hypothesised to be mediated by transient fusion and endocytotic vesicular membrane retrieval [2].

Figure 1.3 depicts the key transitional states describing the main intra-cellular membrane fusion mechanisms. Due to the interchangeable use of language in literature (i.e. fusion pore/depression, dimple/stalk, vesicle/granule, etc.), descriptive features incorporate elements encompassing a broad range of terminology according to models describing a secretory granule fusing with the plasma membrane.

Transient and full fusion are thought to coexist in many neurosecretory systems with the relative fraction of corresponding cell events dependent on regulation of molecular interactions within a cell type. In one instance a frequency ratio of kissed-to-collapsed vesicles of $\sim$ 2:1 was reported in favour of transient exocytosis [11]. While in other cell types it was established that rapid-recycling of granules through transient fusion was a rarity and the majority of secretory granules completely collapsed during exocytosis [12]. Nevertheless, general consensus now accepts the notion of rapid kinetics forming both total and transient fusion at a frequency unique to different neuroendocrine cell types.

Numerous classifications of kiss-and-run transient exocytosis exist based on retention or loss of vesicle shape, proteins or lipids [13]. One sub-category in particular supported by growing evidence describes a third regulating function coined ***'kiss-and-coat'*** exocytosis [14] from cells exhibiting functions unique to total and transient fusion. Kiss-and-coat entails the compartmental mixing and assembly of actin filaments around a steadily maintained dilated secretory vesicle, and subsequent

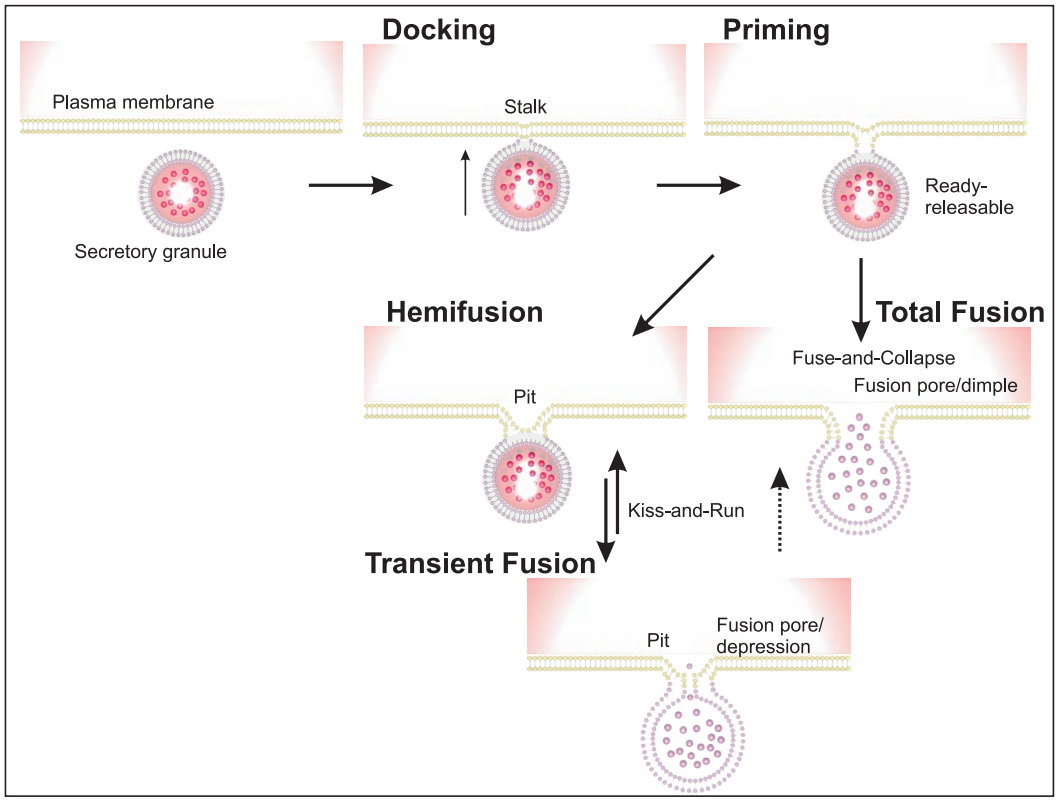

Figure 1.3: Transient and total fusion mechanisms: Illustration comparing the transitional stages for vesicle-granule exocytosis undergoing intra-cellular membrane fusion for different mechanisms.

fractionary retrieval of a direct proportion of the emptied body from the plasma membrane. Also supported with this mechanism are idealogies of intra-granule fusion by ***compound/piggy-back exocytosis*** [15] - where morphologically distinct secretory vesicles remain as empty and stable compartmental bodies beneath the plasma membrane undergoing fusion with each other. At the membrane a primary vesicle acts as 'ghost' or intermediary in order to maintain a gateway for linking deeper underlying vesicles in either a sequential or multi-vesicular cycle as shown in Fig. 1.4. Situations justifying a kiss-and-coat mechanism are warranted in the following circumstances [14]: discharge of less soluble contents from larger vesicles incapable of rapid secretion; guaranteeing complete secretion by extending release and dilation; and free transitional secretion from secondary/tertiary vesicles through the inward portal formed sequentially.

Despite a wealth of knowledge on exocytotic function, direct-visual verification of single fusion events has been limited due to the small magnitude, rapid function and often transient cycling of the fusion pore. Of particular relevance is the work performed by Jena *et al.* [16] demonstrating that in regulated exocytosis fusion pores form as stable and reversible intermediates whose openings are stimuli responsive and constant in frequency throughout. In this pioneering work the AFM was operated *in situ* on slow-secretory living pancreatic acinar cells, proving that fusion pores (referred to as 'porosomes') form as a result of secretory granules docking as ***depressions*** within larger-shallower ***pits*** on the plasma membrane.

The fusion debate ignites when advancements in technology and techniques fuel new perspectives and information on the functioning and construct of the fusion pore. At first the advent of the electron microscope allowed researchers to image biological structures at sub-micron scales and to qualitatively depict the fusion pore at high resolution. Since then, technologies such as fluorescence and scanning electron and probing microscopies, as well as patch-clamp, freeze-fracture and fixation have provided a diverse range of perspectives each contributing to the present-day understanding of fusion.

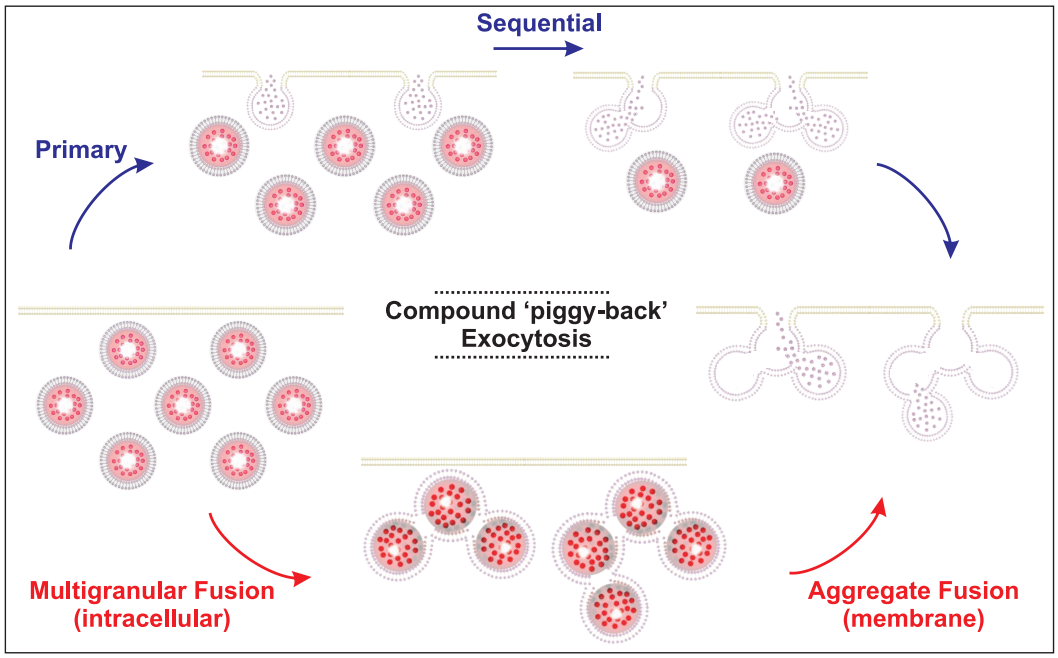

Figure 1.4: Compound Exocytosis: Animated illustration showing sequential and multigranular mechanisms of compound exocytosis [15] *with modifications*.

1.3 The Pituitary

The pituitary gland is part of the endocrine system responsible for regulating hormones critical for several physiological processes. Located at the base of the brain it consists of three separate sections; the anterior lobe, the posterior lobe and the intermediate lobe and is connected to the hypothalamus by the pituitary stalk, which mediates all lobes of the pituitary.

In comparison to other glandular exocrine systems (eg. the liver) the anterior lobe is far less accessible due to the small amount of tissue available (20-100 times less), multiple predominating cell types (at least 5), and microgram secretory output [17]. The anterior pituitary releases hormones packaged in the cell as granules in response to physiological signals received chemically from the hypothalamus. Cells in the anterior pituitary are classified according to their secretory hormones each unique in population and granular sizes [17, 18]:

1. ***Somatotrophs***;

   Responsible for the secretion of growth hormone (GH) it is by far the most abundant cell type representing 50 % of all cells in the anterior pituitary. Somatotrophs are readily identified as ovoid or polygonal in shape containing variable numbers of rounded granules ranging from 350-400 nm wide in a cytoplasm, which is evenly distributed around the nucleus.

2. ***Gonadotrophs***;

   Around 10-15 % of cells in the anterior pituitary are unique due to their bi-granular function - gonadotrophs are large rounded cells secreting both luteinising hormone (LH) and follicle-stimulating hormone (FSH) from distributed granules of varied sizes and irregular shapes, mostly 200-250 nm in diameter, but some also in sparse populations 400-500 nm wide.

3. ***Lactotrophs (Mammotrophs)***;

   Despite totalling only 10-20 % of cells in the anterior pituitary lactotrophs contain the largest secretory granules - approximately 600-900 nm in diameter, homogenously dense and elliptically shaped, granules of various sizes expel the hormone prolactin (PRL).

4. ***Thyrotrophs***;

   Typically angular shaped and small in size, thyrotrophs represent 10-20 % of cells in the anterior pituitary, and are responsible for secreting thyroid-stimulating hormone (TSH) from sparsely dense 140-200 nm wide granules.

5. ***Corticotrophs***;

   Corticotrophs synthesise and secrete adrenocorticotropic hormones (ACTH) from irregular shaped granules 200-250 nm wide. Overall cell shape is angular in profile, often containing numerous extrusions radiating from the main cell body, giving it a spider-like appearance.

While most of these cells are associated with one hormone and each regulated by different hypothalamic releasing hormones, gonadotrophs contain both LH and FSH. Gonadotropin-releasing hormone (GnRH) (also known as luteinising hormone-releasing hormone) is a hypothalamic hormone directly triggering LH release and synthesis in gonadotrophs [19]. In males, gonadotrophs are responsible for stimulating testosterone production, and in females for estradiol and progesterone production in the ovary. In absence of stimuli a basal level of secretion is detectable in almost all secretory cell types.

1.4 Research Objectives

In general, the manner in which neurosecretory vesicles release their contents is of considerable scientific interest - the ability to directly monitor and qualitatively visualise cellular response to stimuli will not only contribute to knowledge on fundamental physiology, but will potentially assist in drug development and understanding some diseases.

Much is still unknown about cellular function in the anterior pituitary lobe. The primary object of this thesis is to further advance the knowledge and understanding on anterior pituitary cells by developing tools and methodologies designed to facilitate the effective examination of cellular morphology *in vitro* using the AFM. Another primary goal of this research is to identify and characterise fusion pores in pituitary cells. More specifically, to analyse populations of single cells and record a direct stimuli response via the formation of the fusion pores on the membrane. Secondary aims include developing alternative tools and methods to allow the effective identification or evaluation of cellular response. One of the tools identified as beneficial for this task is the Biochip - a device designed to position cells into single-cell cavities using electrokinetic forces generated from microelectrodes.

1.5 Thesis Outline

The opening chapter of this thesis is dedicated to the *'The Atomic Force Microscope'*, focusing on the current state-of-the-art in AFM imaging, its application to biological systems and a comparison to other metrology tools. In the following chapter, *'Experimental Techniques & Equipment'*, a brief background provides an introduction to the semiconductor and biological experimental techniques and equipment applied in this research.

The following section entitled *'Direct Cellular Analysis'*, presents a detailed analysis of AFM imagery and discusses the range of fusion pores imaged in anterior pituitary cells. Initially, the AFM is applied to imaging cells directly *in situ*. From there, traditional chemical fixative techniques are explored as an alternative technique for evaluating cellular morphology and stimuli response. With the aid of immunohistochemistry identification of LH secreting gonadotrophs were attempted using functional quantum dots and peroxide staining.

This research focuses on techniques designed to overcome many of the issues and inherent difficulties of cellular analysis by AFMy. The subsequent chapter *'Bioimprint'* introduces a molecular imprinting replication process for recreating cell topography in a curable polymer, which is then scanned and digitally inverted to produce a positive replica image of the original cell. Imaging of molecular imprints presents a novel and alternative strategy designed to overcome the limitations associated with direct cellular analysis and chemical processing. In next chapter *'Bioimprint and Cancer Cells'* a preliminary investigation explores the benefits of applying Bioimprint to endometrial cancer cells with a focus on highlighting images with respect to morphological abnormalities and fusion pore characteristics.

In the following chapter, *'Biochip'*, another aspect of this work presents developments toward integrating an electrode array chip design as an electrically controllable method of positioning and trapping cells. This approach uses an electrokinetic force known as DEP to position cells within cavities fabricated above and around a series of interdigitated electrodes. Cavities act as single-cell incubators, holding

cells at known points of reference for addressing and analysis. Using these locations advanced microscopy tools are easily integrated for automated analysis or as a microscale positioning tool. Even though development of the Biochip occurred concurrently with previous investigations it is presented as the penultimate chapter in this thesis to illustrate the enhancements it makes toward cellular imaging techniques.

In the chapter *'Summary Remarks'* the key areas of this research are discussed and summarised with recommendations on future work and project directions. Finally, in the closing chapter *'Conclusions'* concise bullet-point statements are used to present the key findings of this project.

Chapter 2

The Atomic Force Microscope

The AFM was invented in 1986 by Binnig, Quate and Gerber [20, 21] at IBM's Zurich, Switzerland laboratory in collaboration with Stanford University, California. To-date it remains the most advanced and developed scanning probe technique, providing three-dimensional (3D) topographic mapping of surfaces with nanometre lateral and sub-angstrom vertical resolution. The field of AFMy is based on techniques which involve scanning a very sharp probe in proximity to, or in contact with, a sample and producing high resolution surface images from the resulting interactive forces.

2.1 Working Operation

A schematic illustration depicting the key components of the AFM during operation is shown in Fig. 2.1. Imaging is controlled by a fine-motion piezoelectric tube, which in response to an applied voltage travels a minute amount in a rastering sequence. During scanning a multiple-split photodiode detector known as a position sensitive detector (PSD) monitors the deflection of a laser beam from the backside-end of the cantilever. The reflected laser beam from the cantilever as it scans, and the change in direction are measured by the PSD and used to calculate the deflecting angle, which is dependent on the length of the cantilever. By detecting changes in the summation

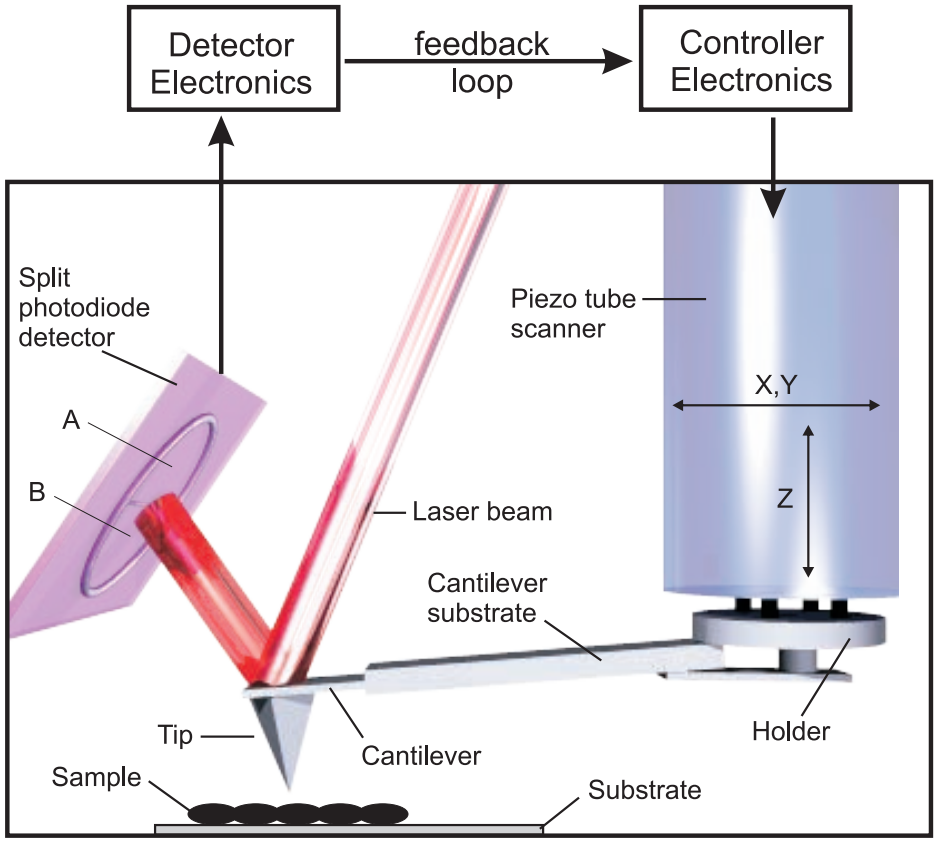

Figure 2.1: Key components of the AFM: A split photodiode detects the deflection of a laser beam off the backside of a sharp tip appended to the end of a cantilever and positioned by a piezo-electric scanner.

of output voltages at each photodiode in the PSD, the tip deflection or oscillation is calculated, and the signal to the piezoelectric scanner adjusted accordingly.

2.1.1 The Cantilever and Tip

Positioned at the end of the cantilever is a sharp micro-machined silicon tip designed to act as a nanoscopic force sensor. The single most important prerequisite for obtaining accurate AFM images is the quality of the tip. As the wavelength of light limits the resolution in optical microscopy so does the sharpness and geometric profile of the tip in AFMy. Primarily, the radius of curvature and the tip sidewall angles or 'tip apex' are the two most critical features for image resolution - a tip with a sharper/smaller apex will have a greater lateral resolving power than blunter

tips whose apex is greater. As the holder mounts the cantilever substrate at a 10 ° angle it is more suited to scan at 90 ° due to the front- and back-side sidewall gradients of the tip being askew by a similar degree. Properties of the cantilever are also crucial for regulating the manner and degree of interaction the tip is applied to the sample. Resolution critical parameters for the cantilever-probe include geometry and dimensions, mechanical properties (stiffness, hardness, quality factor), magnetic and electric properties and other factors including reflection or treatment coatings.

During extension of the tip to the surface it encounters a number of different forces influenced by separate boundary layers. The sequence of interactive forces at each boundary layer is defined by the tip height above the sample's surface plane, beginning with the far-ranging and ending with the near-ranging are [22]:

1. ***Fluid film damping***

   Fluid film damping is the initial boundary force exclusive to tapping mode, resulting from the dampened air film being squeezed between the oscillating probe and sample at a distance of $\sim 10\ \mu m$ from the surface.

2. ***Electrostatic forces***

   Electrostatic forces are present at a height between 0.1-1.0 μm and can be either attractive or repulsive depending on the sample and tip materials - conductors (eg. Gold) for instance have lower electrostatic forces than semiconductors (eg. Silicon).

3. ***Fluid surface tension forces***

   Condensed water vapour on the sample causes surface tension effects to attract the tip downwards at an amplitude of 10-200 nm from the sample.

4. ***Van der Waals forces***

   At an Angstrom's distance the tip will experience a weakly attractive van der Waals force from the atoms in the tip and sample.

5. ***Coulomb forces***

   At fractions of Angstroms electron shells repulse one another - by definition at this distance atoms from the tip and sample experience each others Coulombic forces and are said to be 'in contact'.

2.2 Imaging Modes

Depending on the imaging mode the AFM translates topography according to several different operator selected formats, commonly either in amplitude, height or phase (tapping mode only). The imaging mode defines the manner the tip is applied to the sample and the interactive forces used for sensing surface topography, the most common being:

2.2.1 Tapping Mode

One of the most popular imaging modes due to its low tip-sample forces and non-destructive imaging is tapping mode[1] [23, 24, 25] (also known as intermittent-contact mode or semi-contact mode). In tapping mode an oscillated cantilever is vibrated at an offset position on either side of its resonant frequency at an amplitude between 20-100 nm. The tip appended to the vibrated cantilever gently 'taps' the surface as it makes contact with the sample through the adsorbed fluid layer at the bottom of each cycle. In this mode the oscillation amplitude is used as a control signal to bring the tip in contact with the sample. The degree of interaction or contact, to the point of the tip either physically touching, or hovering at an Angstroms distance above the sample, depends on a number of parameters (eg. amplitude set-point and probe force constant). In some instances a frequency shift can occur at a distance far from the sample due to further dampening in the squeezed gas layer. Hence, tuning of the cantilever's frequency should be done very close to the sample's surface. Through the feedback loop from the PSD a constant oscillation amplitude

[1] Tapping mode is a trademark of Veeco Instruments Inc. (Santa Barbara, CA).

is maintained by adjusting the piezoelectric scanner at an average root-mean-square (RMS) amplitude. At each lateral step the necessary Z-positional compensation required to satisfy a constant amplitude set-point is recorded and a 3D topographic image compiled.

In most instances surfaces in air are covered by a minute absorbed layer of water condensate and contaminants, whose tension forces acts to attract the tip to the surface. Tapping mode alleviates any surface tension by penetrating the adsorbed fluid layer during the downstroke and breaking free on its upstroke. In ambient conditions adhesive and capillary forces from the tip-sample interface need to be overcome, therefore stiffer probes are used in tapping mode when compared to contact mode due to the forces required to withdraw the probe from the sample's surface during each cycle. An advantage of tapping mode is as the tip contacts the surface at cyclic intervals there are almost no shear forces. Consequently the damage from the impact of lateral forces on the surface by the tip is minimal, enabling non-destructive analysis of soft, delicate samples.

2.2.2 Contact Mode

In contact mode AFM the PSD electronics measure the laser's deflection off the tip, which is in contact with the adsorbed fluid layer. A steady cantilever deflection is maintained by the feedback loop dynamically positioning the vertical set-point of the piezo-tube to maintain a constant photodetector difference, and subsequently a constant force, during scanning. A topographic image is produced by recording the vertical distance traveled by the piezo-tube at each coordinate required to maintain a uniform deflection signal.

2.2.3 Non-Contact Mode

Due to strong tip-sample interactions fragile surfaces are easily damaged in contact mode. Non-contact mode alleviates this drawback by operating in the attractive

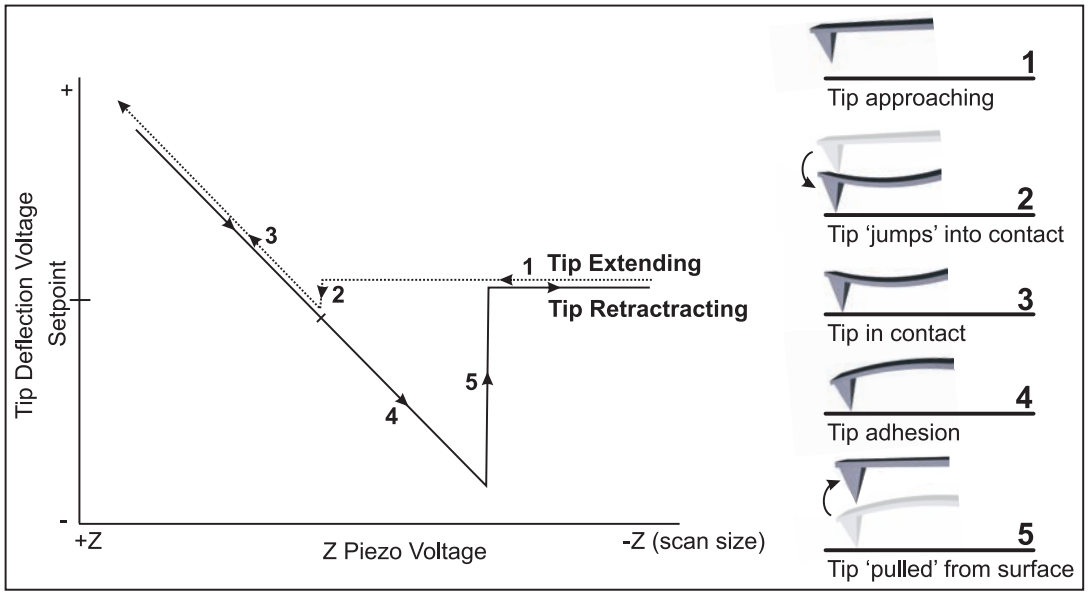

Figure 2.2: A force curve illustrating the key interaction points during tip approach and retraction.

force boundary region. Most surfaces in air are covered by a thin absorbed layer of water condensate whose tension attracts the tip. In contrast to tapping mode, which makes contact with the surface through the adsorbed fluid layer, in non-contact mode [24] the cantilever oscillates above the sample's adsorbed fluid layer at an amplitude of < 10 nm. The van der Waals forces present in short-range (1-10 nm) above the adsorbed fluid layer and other long range forces decreases the cantilever's resonant frequency and subsequently its oscillation amplitude. A constant amplitude or frequency set-point is maintained in non-contact mode by the feedback loop adjusting the vertical position of the scanner at each X and Y step.

2.2.4 Force Curve Mapping

Excessive or weak forces can reduce image resolution by introducing unwanted artifacts and damaging the sample and/or probe. Control of forces can improve the quality of images and minimise the attractive forces between the tip and the sample. The best method for viewing and calculating forces is by force curve mapping. This

technique is very useful for calibrating forces applied to the cantilever and measuring long range attractive or repulsive forces, which are critical for imaging soft materials. Figure 2.2 depicts a typical force curve illustrating the repulsive and attractive forces in the approach and retraction stages of the free end of the cantilever as the fixed end is brought vertically to, and away from the sample. Initially, an engaging tip (1) will suddenly jolt onto (2) a sample prior to contact (3) as a result of the attractive surface tension forces. Upon retraction (4) the tip proceeds to stick to the surface, wherein it is pulled from the surface (5) and runs clear.

A common misconception of the AFM is that data is purely topographic. In contact as well as tapping mode the probe is influenced by a sample's mechanical properties including stiffness, elasticity and friction. One technique for enhancing compositional differences is phase imaging - an operation performed while in tapping mode to monitor the phase lag between the oscillating drive signal applied to the cantilever and the oscillating detection signal from the photodiode detector. Using this signal, information on surface variations such as viscoelasticity and adhesive forces can be used to to detect differences in surface composition, or to enhance image contrast in a heterogenous system.

2.3 Fluid Imaging

In biology the AFM has proved a valuable tool, providing 3D topographical images of surface ultrastructure as well as functional-interactive investigations with nanoscale accuracy. Currently no other microscopy tool is capable of simultaneously delivering the structural and functional information with such high spatial resolution. While optical and electron microscopy rely on radiation scattered from a sample in liquid, results are often blurred from diffractive effects. Whereas the AFM uses interactive forces from the submersed probe scanned in fluid in proximity to, or in contact with a specimen, enabling visualisation of biological materials far beyond the resolution of optics [20, 21].

A unique advantage of the AFM is its ability to image living cells in fluid. With the aid of a fluid cell the sample is enclosed in a liquid environment enabling biological processes to be viewed *in situ*, mostly in tapping mode or contact mode. However, due to the destructive nature of contact mode on the plasma membrane imaging tapping mode is more suited. In fluids electrostatic forces between dissolved ions and other charged groups influence the forces sensed by the AFM probe. These interactions enable external tuning of the cantilever forces such that it is possible to create a situation where the attractive van der Waals forces are effectively negated by electrostatic repulsion. For biological applications this is important as tip-sample forces often damage soft samples if left uncontrolled. Factors such as medium pH are known [26] to have a strong effect on tip attraction at low values, with long-range repulsive forces dominating at higher pH.

A measure of a systems dampening is the quality or *'Q-factor'* - the minimal external vibrational force or noise applied to the probe to maintain a steady oscillation (i.e. the greater the Q-factor the greater the sensitivity). The Q-factor is largely governed by the mechanical properties and the damping conditions of the environment. In fluid there is a substantial reduction in adhesive capillary tip-sample forces and an increased hydrodynamic dampening[2], resulting in a Q-factor of $\sim$ 1-3, whereas the Q-factor in air is much higher ($\sim$ 13-21). Another influence compounding resolution is the tip drift caused by changes in thermo- and hydrodynamic forces, which frequently frustrate operators by the degrading resolution in the final stages of image capture.

There are numerous difficulties when imaging soft samples submersed in liquid. Firstly, the sharp probe can be destructive when the forces are unbalanced and blunter, more flexible probes made from silicon-nitride with low force constants are often required to reduce tip-sample impact. Another difficulty of AFM imaging when applied to investigate cellular dynamics and behaviour *in situ*, are the effects of the scanning cantilever in diminishing perturbation over time, and the environmental

[2]Rectangular cantilevers suffer less hydrodynamic dampening and thus an increased Q-factor when in fluid.

stabile conditions required (eg. temperature and pH). In addition, optimal imaging conditions require slow scan speeds with the time difference between image initiation to capture often lasting several minutes.

Creating higher temporal resolution for the AFM in fluid remains a challenge especially when cellular dynamics only last milliseconds. Given that full scan capture lasts minutes, at this rate there will be inconsistent and varying results across the image [27]. A 'quick-fix' method for achieving greater temporal resolution is to increase scan rate, but this will inevitably result in a trade-off to spatial resolution, or otherwise require greater forces for stability.

In most cells imaging is further challenged by the presence of glycocalix - a poorly defined coat covering the plasma membrane responsible for cell adhesion. This so-called 'carbohydrate cap', unless disrupted, hinders the resolution of AFM imaging in fluid and often treatment of cells with enzymes is required prior to imaging to enhance resolution [28]. Image contrast mechanisms and influences from sub-membrane and intra-cellular features also influence imaging even when in height-topography mode. Effects are most noticeable in contact mode where the underlying cytoskeleton can be imaged. Furthermore, deterioration of image quality in fluid is thought to be due to smearing and build-up of molecules or cell debris on the tip. Over time the loosely bound molecules can create aggregates, which act in a highly uncontrollable manner to diminish image clarity. [27]

Finally, loading forces if not damaging to the cell may reduce resolution when used too excessively by the tip's indentation into the cell surface, deteriorating the attainable resolution by the degree of the indentation profile. The range of suitable loading forces applied to the tip, considered to reduce tip-to-cell surface deformation and minimise contamination is between 1-10 pN [29]. This presents a challenge due to the difficulties of stable imaging with low forces and its affect on dictating low scanning speeds.

2.4 Limitations

For all its advantages the AFM has clear limitations. For one it is slow especially when imaging large samples or when in fluid. Secondly, the relationship between sensitivity and scan size of the piezoelectric scanner is non-linear and therefore the ratio of piezo voltage-to-movement is not constant. Scanners are known to exhibit greater sensitivity at the end of scan lines than at the beginning, resulting in variations and hysteresis between the forward and reverse scan directions. Furthermore, aging results in an exponential decrease in scanner sensitivity over time, requiring re-calibration or manual adjustment of imagery with calibration gratings.

Additional effects resulting from limitations in the piezoelectric scanner are *'creep'* and *'bow'*. Creep is the piezoelectric drift, which displaces the scanner after a DC voltage is applied from large lateral offsets. It is characterised by the elongation and stretching of features over a short-period after the offset and easily self-rectified after several scan passes. Bow is another scanner induced effect caused by the arching of the free-end of the scanner over its full range, resulting in edge-raising and a middle-depression particularly in large-scans where the intra-scan arch variation is at its greatest.

The travel range of the piezo-tube in the Z-direction and the surface area of the photodetector are fundamental limitations in cases where there are large and abrupt variations in topography. When operating in height or deflection acquisition mode the maximum sample corrugation that the piezoelectric scanner can travel in the Z-direction, or the maximum the deflection detectable by the photodetector, is limited to 6-18 μm (depending on the instrument). In situations where these constraints are breached, topographic features surpassing the Z-boundary are wasted, or worse, in situations of more excessive deviation a complete retraction or extension in travel range can result in loss of subsequent imagery.

2.4.1 Artifacts

Artifacts are inevitable in AFMy and are often caused by influences resulting in distorted translation from [30]; dull or dirty tips, double or multiple tips, sample contamination, optical interference, non-tracking, high frequency rings, and 2nd/3rd order bow. Tip artifacts caused by accumulation of debris can dull or even obscure imagery and result in double-tip effects or irregular translation of features. While these conditions are easily caught and corrected for more subtle artifacts include the influence of a sample's mechanical or underlying properties, as is a cell's cytoskeleton when translating membrane topography, are more difficult to detect and calculate.

Post capture there are various modifications that can be applied to enhance, modify or remove artifacts. One of the most common techniques is flattening - a filter used in off-line operation to remove artifacts caused by vertical drift, image bow, skips and other effects from inter-scan line Z-directional offsets. Flattening modifies the image on a line-by-line basis to remove the vertical offset by applying a 0-3rd polynomial least squares fit for each scan line and subtracting the polynomial fit from the original line value. With respect to a flat plane consisting of cells or biological features such as pits, depressions or fusion pores, flattening may often result in areas next to the object appearing lower with respect to surrounding area on the plane. This shadowing effect can be remedied by excluding raised areas from the flattening sequence. Scan lines caused by the tip skipping from the surface due to noise, vibrations or loose debris is another frequent modification, which is resolved by substituting the selected scan line with an average of the adjacent lines. [30]

2.5 Comparative Metrology and Microscopy Tools

When compared to other techniques the AFM differentiates with respect to the degree of contrast, speed, resolution and sample preparation of the following common microscopy tools:

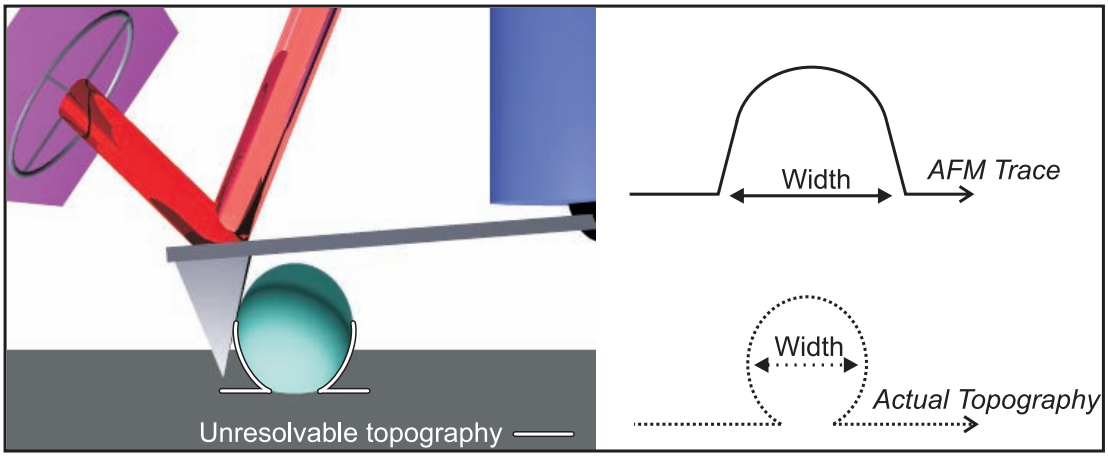

Figure 2.3: Unresolvable topography in atomic force microscopy.

- ***Scanning Tunneling Microscope (STM):***

  The STM [31, 32] preceded the AFM and in some instances its resolution is better due to the tunneling current's exponential dependence on distance. In contrast, the AFM's force-distance relationship is complex and dependant on tip shape and imaging mode, to name a few. The versatility of the AFM is by far superior due the STM requiring a conductive sample.

- ***Scanning Electron Microscope (SEM):***

  Compared with scanning electron microscopy [33] the AFM provides direct height measurements and unobscured views of surface features with extraordinary topographic contrast. In most instances the SEM requires a conductive sample or thin metallic coating but it can scan at a much faster rate than the AFM, providing real-time imagery regardless of image size. For the SEM samples need to withstand vacuum and electron bombardment and be capable of dissipating energy generated from a focused electron beam while preventing surface charge build-up. Nevertheless, this does not exclude the ability to analyse hydrated specimens at physiological conditions entirely, and tools such as the environmental SEM and fluid chambers enable analysis of living specimens.

  A comparison using standard equipment configurations and operating proce-

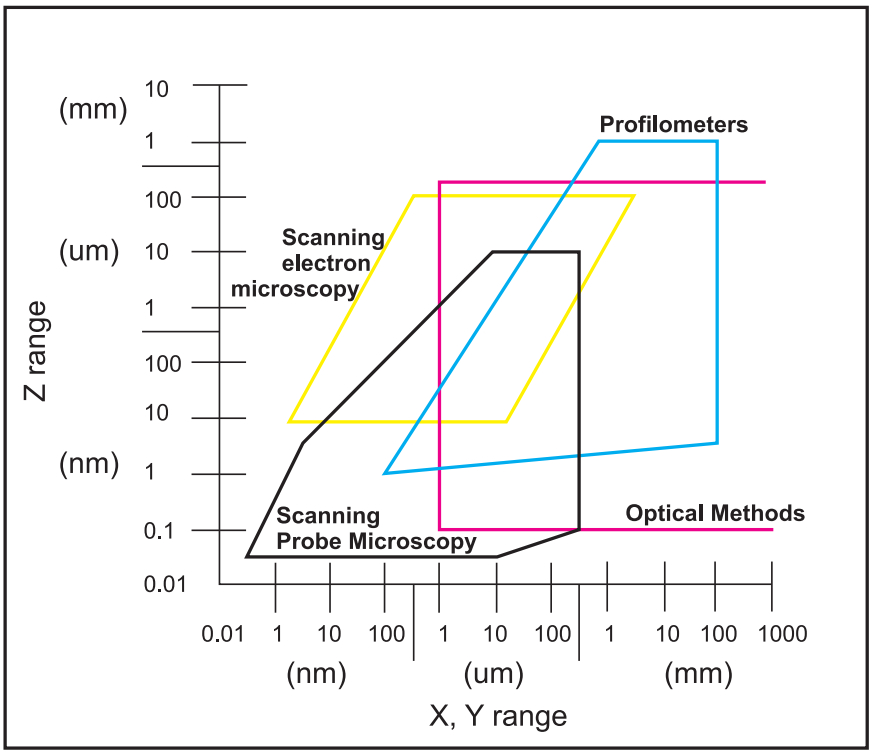

Figure 2.4: Resolvable ranges of common microscopy and metrology techniques used to analyse surface morphology, *reproduced with permission* [35]

dures of SEM and AFM can be made with respect to surface structure, composition and environment [34]. Principle differences between these devices is how changes in vertical information are processed. While both devices image with a similar lateral resolution, depending on circumstances there are instances where the AFM represents surface topography more accurately. Unlike the SEM, which has difficulty resolving subtle variations in height the AFM can accurately measure atomically smooth surfaces in 3D in a single scan pass. A further difference in vertical interpretation of a sample's height by scanning electron microscopy is the increase in electrons and the higher intensity that can result from changes in slope. Whereas an AFM image is essentially a data file containing a series of coordinates, enabling translating feature orientation (eg. a pit versus a bump) trivial.

On the other hand the SEM is able to image obtuse features or enclosed areas, which cannot be obtained with standard AFM's as shown in Fig. 2.3.

Common methods for obtaining dimensions of high aspect ratio structures with scanning electron microscopy consists of imaging the cross-sectional end of a cleaved sample. In contrast, the AFM provides non-destructive measurements of cross-sectional data as long as proper shaped tips are used to scan narrow openings, steep sidewalls and high aspect ratios. Even though similar qualitative images are obtained the AFM also provides quantified information directly (eg. surface roughness, line-edge roughness and step-heights).

One of the key advantages of the SEM is its ability to operate at a large depth of field enabling surfaces to be imaged with several millimetres of vertical freedom. Although the vertical resolution of the AFM is extremely accurate it is unable to image tall structures due to the vertical range imposed by the piezoelectric scanner. Standard scanners have limited vertical limits, and in circumstances where the sample contains significant height variation the SEM is more suited than the AFM. While the SEM offers similar resolution to the AFM, preparation and enhancing agents are often required for biological materials, which subject the sample to harsh denaturing processes, such as fixation, staining or cryogenic freezing.

- ***Transmission Electron Microscopy (TEM):***

  All instruments have specifications limiting the size of the samples able to be resolved. For the TEM these ranges are very stringent and space restraints around the objective lens require specimens to be mounted on a fine mesh grid 3 mm in diameter. While also limited by axial constraints the AFM needs no particular mounting substrate and provides complete information in comparison to the two-dimensional profiles generated from TEM cross-sectioned samples.

- ***Optical Microscopy:***

  In far-field focused light microscopy diffraction effects result in a half-wavelength dependent lateral resolution, which at its optimum imposes an attainable spatial limit of 180 nm in the focal plane and 500 nm along the optical axis

[36, 37]. On the other hand the AFM is independent from the reflectivity differences of the optical interferometric microscope, providing an unambiguous measurement of topography at a much finer scale. The AFM further offers a degree of contrast that is significantly higher than radiation-scattered tools.

Each tool has limitations and advantages making one more suitable for certain applications over another. The equipment X,Y,Z ranges for a selected range of microscopy techniques are highlighted in Fig. 2.4, reinforcing that the ability of the AFM is most suited to imaging microscale areas at high resolution.

2.6 Experimental Setup

A Digital Instruments (DI) 3100 Nanoscope III AFM, Veeco Instruments Inc. (Santa Barbara, CA) was used as the sole experimental device in this research. Illustrated in Fig. 2.5 (a) is the DI 3100 AFM system depicting the microscope mounted on a custom built water-bed and insulating box for vibrational isolation and sound proofing. An analog electronics controller and illuminator source are connected to a computer for digital signal processing, electronics interface and graphics, which is linked to a dual screen display monitor. Figure 2.5 (b) highlights the piezo-electric scanner system designed to scan overhead while keeping the sample stationary. The DI 3100 AFM has X/Y- and Z-axial limits of $\sim$ 110 μm and 6 μm, respectively. Calibration of the scanner was performed using calibration gratings with either the piezo-tube adjusted accordingly or the quantitative measurements restated correctly.

A fluid-cell tip holder was used for *in situ* imaging, performed primarily in tapping mode by modulating the piezo-tube. The fluid cell is a transparent glass assembly using a wire clip to hold the cantilever. An additional rubber skirting[3] is provided for fluid containment and as protective guard for the scanner. The fluid cell is used in an open environment and was submersed midway in a contained system (eg. 5 cm

[3]The rubber skirting was not used for fluid imaging and is only recommended when imaging in more than 3 mm of depth.

(a)

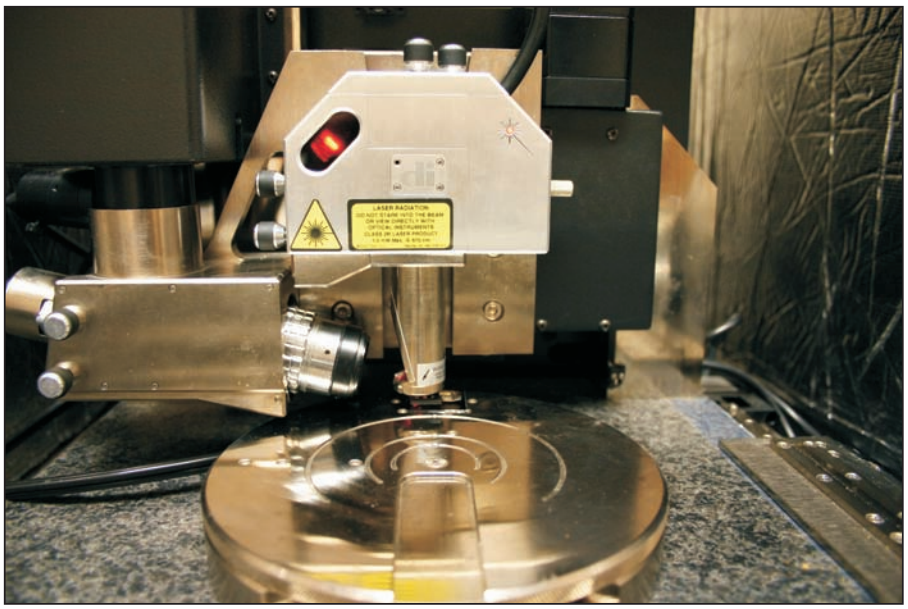

(b)

Figure 2.5: (a) Experimental setup of the DI 3100 AFM and the (b) piezo-electric scanner

Part #	**Type**	**Tip Radius** (nm)	**Force Constant** (N/m)	**Resonant Frequency** (kHz)
NSC18/AIBS[a]	Rectangular	< 10	3.5, 2.0-5.5	75, 60-90
DNP-S[b]	Triangular	~ 10	A-0.58 B-0.12	A-57 B-20
			C-0.32 D-0.06	C-56 D-18
BS-SiNi[c]	Triangular	< 15	short-0.27	short-30
			long-0.06	long-10

Table 2.1: Probe properties used for *in situ* AFM imaging.

[a]MikroMasch, Estonia.

[b]4 gold coated sharpened silicon nitride probes: A short-wide; B long-wide; C short-thin; D long-thin, Veeco Probes, USA.

[c]2 gold coated silicon nitride probes - short & long used for soft contact mode, Budget Sensors, Bulgaria.

Petri-dish). To prevent air bubbles from trapping between the cantilever and fluid-cell during submersion, after the tip was mounted a drop of PBS buffer solution was placed on the centre of the holder before submersion. In air the driving frequency is applied electrically to the cantilever, however, in fluid the piezoelectric scanner is frequency modulated in the Z-direction to resonant the cantilever. Hence, it is advantageous to match cantilevers that resonant at similar frequencies to the AFM fluid cell. The fluid cell has a resonant drive frequency of $\sim$ 10 kHz, which matches the equivalent vibrational resonance of cantilevers in air of $\sim$ 50-70 kHz. A list of the probes trialed for fluid imaging in this research are given in Table 2.1.

All imagery was presented in an amber colour-contrast scheme and processed using either the instrument's Nanoscope III v 5.12 or n-Surf v 1.0 3rd party application software. Where required the only 'manipulations' made to altering the original captured data files were flattening to remove background slope and erasing scan lines.

Chapter 3

Experimental Techniques & Equipment

This chapter introduces biological techniques and reagents for the preparation and culturing of cells from rat pituitary glands and human tissue at the Christchurch School of Medicine and Health Sciences. In addition, this section presents semiconductor equipment used at the University of Canterbury's Electrical Engineering Nanotechnology Laboratory for the fabrication of devices, substrates and the replication of cells. Several key processes are discussed including cell culture, reactive-ion etching, thin-film deposition, photolithography, mask-alignment and wet etching. Details and parameters specific to each technique are further elaborated in the respective chapters of this thesis.

3.1 Semiconductor Equipment & Processes

Photolithography is a pattern transfer process used predominantly in the semiconductor industry to pattern photosensitive resists using UV light. The following details a handful of photolithography techniques and devices investigated extensively in this research.

A common lithography tool known as a 'spinner' uses centrifugal forces generated

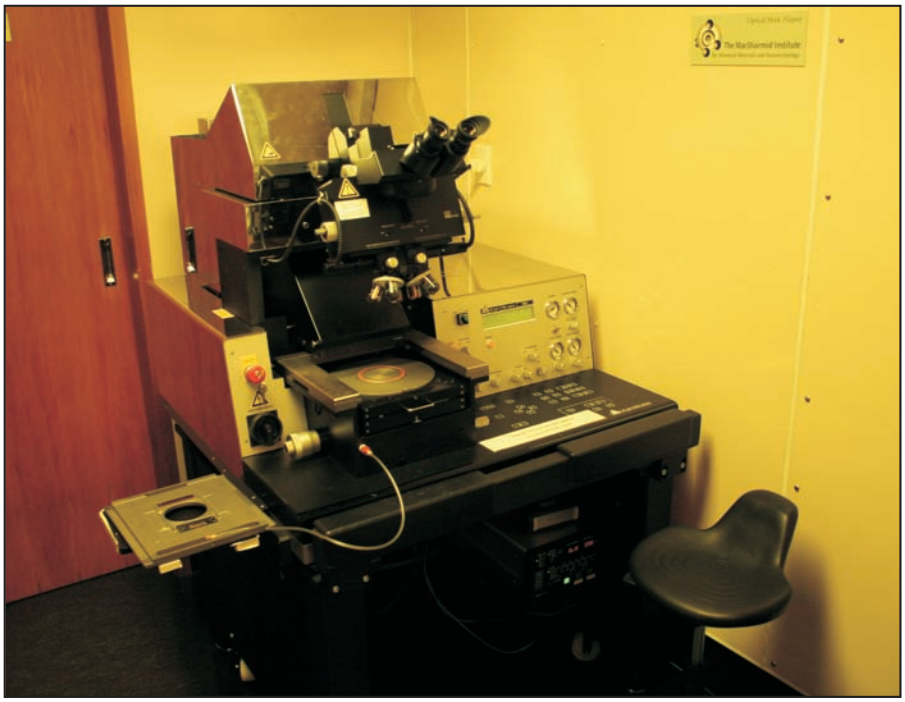

Figure 3.1: Mask alignment, imprinting and UV-exposure system.

by rotation to evenly distribute a liquified polymer into a thin layer over a substrate. Spinners are commonly used in photo or electron beam lithography to coat substrates with layers of radiation sensitive polymers with nanometre precision. Parameters critical in controlling film thicknesses include spin speed (rpm), spin time, acceleration, deceleration speed, material (eg. viscosity) and substrate properties (eg. size, surface). In this research a single wafer spin processor - Laurell Tech. Corp. (PA, USA) housed in a fume-hood was used to apply photoresists onto glass and semiconductor substrates prior to mask-alignment and exposure.

3.2 Mask Aligner

A mask aligner is a photolithography device primarily used to contact, align and transfer features from a patterned mask to a photosensitive material by UV radiation exposure. Figure 3.1 illustrates the MA-6 mask aligner - Karl Süss GmbH (Germany) used for precision alignment of micro-structures in Biochip fabrication, and as a contact imprinting system for Bioimprint replication. The exposure source

was a 350 W Mercury UV Lamp with an intensity at centre stage of 6.7 mW/cm^2. The mask aligner can perform mask-to-wafer front- or back-side alignment and photoresist UV-exposure in either proximity, hard- or soft-contact, or high and low vacuum contact mode. Initially, the MA-6 mask aligner brings an overlying mask and underlying substrate into the pre-set contact mode using a self-correcting vertical alignment mechanism known as wedge error compensation (WEC) - a procedure designed to align the bottom-side of the mask exactly parallel with the top-side of the substrate, guaranteeing a perfect gap setting and therefore a homogeneous exposure of structures across the entire substrate. This is achieved by detecting and correcting for the pressure variations distributed at different reference spacer locations during contact.

The mask-to-substrate contact mode is a critical setting for pattern transfer resolution and for methods exploiting the imprinting capabilities of the mask aligner. The contact mode and exposure settings available on the MA-6 mask aligner are:

1. *Proximity Contact mode*

   The most careful and least destructive setting for mask exposure, which sets an exposure proximity gap between the mask and substrate. Structural resolution is poor in contrast to other contact modes.

2. *Soft Contact*

   Mask and substrate are brought into contact only with the WEC force and the vacuum securing the substrate is maintained throughout exposure.

3. *Hard Contact*

   Similar to soft contact, instead after contact the vacuum securing the substrate is halted and nitrogen is purged against the substrate to guarantee closer contact.

4. *Vacuum Contact*

   Most accurate photolithography exposure setting. After WEC and alignment the mask and substrate are brought into contact with each other. A rubber seal

creates a mini vacuum chamber, which enables smooth contact and prevents gas bubbles forming by creating a vacuum in the chamber.

5. *Low-Vacuum Contact*

   Similar to vacuum contact mode with the difference that the vacuum level in the chamber is regulated.

6. *Flood Exposure (non-contact)*

   Non-contact mode exposes the whole substrate to UV light without requiring a mask.

3.3 Evaporator

Thermal evaporation is a heat deposition process used to deposit thin-films by applying a current across a resistive boat/crucible until high enough temperatures are reached for the material to melt and begin to evaporate. The depositing substrate is placed in direct line or sight above the boat and the thickness of the layer is calculated using a quartz crystal oscillator, which is positioned adjacent to the substrate and in line of sight of the boat. The thickness of the depositing film is calculated by monitoring the change in vibrational frequency of the crystal as the material deposits onto the crystal and the adjacent substrate. A given thickness will induce a change in frequency oscillation dependent on the depositing film thickness and material. A high vacuum evaporator - Balzers AG (Fürstentum, Liechtenstein) shown in Fig. 3.2 was used predominantly in this research to evaporate layers of NiCr and gold onto 10 cm quartz and silicon-nitride wafers with alumina-coated molybdenum boats.

3.4 Reactive-Ion Etching

In reactive-ion etching (RIE) a reactive gas species (eg. CHF_3, SF_6) is purged into a chamber and plasma ignited after application of an RF potential across the parallel

Figure 3.2: Evaporator for thermal deposition of thin-films.

Figure 3.3: Reactive-ion etcher.

plate chamber electrodes. A number of the fragmented and radical gas molecules become ionised and accelerate toward the electrode powered substrate on which the sample is placed. The exposure of the ion flux induced from the plasma results in ion bombardment and physical, as well as chemical etching of atoms on the sample, producing very anisotropic etch profiles. A PlasmaLab 80 Plus RIE system - Oxford Instruments (Oxon, UK) shown in Fig. 3.3 was used to etch silicon and nitride layers through patterned photoresist masks.

In addition to RIE, wet etching is an isotropic etching technique used to selectively remove metallic films by chemical dissolution. While acids can be classed as wet etchants, reactive solutions exist to target specific materials with high affectivity, while remaining largely inert to non-reactive species. In this research, gold and NiCr wet etchants were commonly used to remove exposed metallic material after UV irradiation and development of the overlying resist layer.

3.5 Cell Culture

All cells were prepared in accordance with institutional guidelines of the Christchurch School of Medicine and Health Sciences, University of Otago. Cells from the rat pituitary gland were collected according to protocols approved by the Animal Ethics Committee. Endometrial cancer tissue was collected according to protocols approved by the Human Ethics Committee and after patients provided informed consent.

3.5.1 Pituitary Cells

Rat pituitary cells were prepared at the Laboratory for Cell and Protein Regulation, Department of Obstetrics and Gynaecology, Christchurch School of Medicine and Health Sciences and dispersed according to protocols prepared by Prof. J.J. Evans and research fellow J. Nagase, for more details refer to Appendix A.1 - *Tissue Preparation/In Vitro (Static Incubation) and Stimulation of Dispersed Anterior*

Pituitaries with Gonadotrophin-Releasing Hormone [38]. Firstly, cells from the anterior pituitary gland were collected from adult female Sprague-Dawley or Wistar rats and cultured in dispersion medium consisting of 500 ml Dulbecco's modified Eagle medium (DMEM) that included GlutaMaxI with high glucose and 110 mg/l sodium pyruvate Gibco BRL Products (MD, USA) supplemented with 1.8 g HEPES, 1.5 g BSA, 800 U penicillin and 800 μg streptomycin Sigma-Aldrich (Sydney, Australia).

On average 2 million healthy cells were dispersed per pituitary and cells were typically diluted 10 fold to achieve a suitable density. For culturing, cells were resuspended in Medium 199 (M199) supplemented with 10 % fetal bovine serum (FBS) Gibo-Life Technologies (Auckland, New Zealand) and plated on Petri culture dishes - Nunc A/S (Roskilde, Denmark) or substrates (eg. Biochips, quartz or silicon-nitride) and incubated in a 5 % CO_2 incubator at 37 °C until experimentation. Cells were cultured for several days in order to 'reset' *in vivo* physiology so as to achieve an *in vitro* response regardless of the oestrous cycle of the rat beforehand. Another advantage of prolonging culture is to reduce the cell heights to work within the Z-limit of the AFM.

3.5.2 Stimulation of Gonadotrophs

Stimulation of gonadotrophs was done using GnRH - Sigma Aldrich (Sydney, Australia) at concentrations between 10^{-6} - 10^{-7} M in phosphate-buffered saline (PBS). Prior to stimulation the addition of oestradiol was used to sensitise the cells GnRH. Oestradiol stock diluted down to 300 pg/ml in incubation media was added to cells 2 days prior to stimulation in M199 with FCS. Immediately before stimulation cells were washed in incubated M199 for 1 hr and then in M199 with GnRH for periods lasting up to 1 hr.

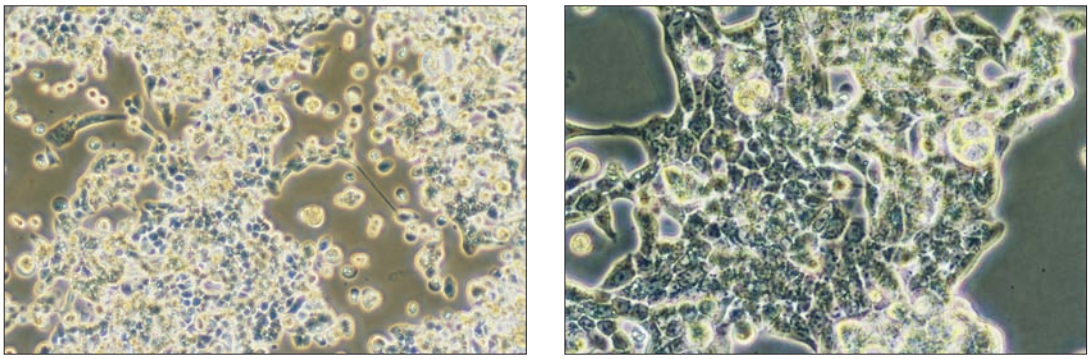

(a) 10 × magnification (b) 20 × magnification

Figure 3.4: Transmitted light microscopy images of a confluent population of endometrial cancer cells.

3.5.3 Endometrial Cancer Cells

Endometrial cancer is the most common gynecologic cancer in women and originates from malignancies in the inner lining of the uterus. In this research endometrial adenocarcinoma tissues were harvested from women undergoing hysterectomy, and non-myometrial biopsies were taken from the opened uterus tumour area by Dr P. Sykes with all primary cultures performed by J. Nagase. Tissues were digested in collagenase type 1A (Sigma, cat. no. C-2674) (1mg/ml) and cells dispersed and cultured in a solution consisting of minimum essential medium alpha medium (α-MEM) - Gibco (cat. no. 11900-024) containing 1 % penicillin/streptomycin, 0.1 % BSA and 10 % FBS. Figure 3.4 illustrates transmitted-light microscopy images of a fully confluent population of endometrial cancer cells grown in a plastic flask. For more details on reagents and protocols refer to Appendix A.2 - *Tissue Preparation and Dispersion of Endometrial Cancer Cells* [39].

3.6 Chemical Fixation

Structural studies on cells commonly involve several preservation stages for imaging in ambient-air conditions. Fixation is one technique used to arrest deterioration with chemical agents such as organic aldehydes applied at conditions (eg. time, concentration, temperature) dependent on the cell type, size and form. Fixatives

simultaneously stabilise and kill the cell rapidly by covalently cross-linking its protein structures and major biochemical constituents.

Critical factors for fixation include [40]:

1. ***Incubation temperature***

   For convenience fixation is performed at room temperature but for a more rapid effect higher temperatures can be used at the risk of introducing artifacts or distortions. Often to achieve a more life-like appearance the fixative temperature can be kept between 0-4 °C to slow autolysis and diffusion of cellular components.

2. ***Specimens size and fixative penetrability***

   Fixatives penetrate slowing according to the laws of diffusion and ideally tissues or cells should be thinly formed for optimal results.

3. ***Volumetric changes***

   Fixation and dehydration often cause changes in specimen volumes (eg. swelling or shrinking), which vary depending on the cellular constituents.

4. ***Buffer pH***

   The concentration of hydrogen ions should be kept to within a physiological pH range, which is achieved using buffer systems such as phosphate. To maintain buffer effectiveness and fixative function there should be no reaction between the two, and for histochemical analysis the buffer should not react with the incubation medium or inhibit enzymes.

5. ***Osmolarity***

   Another factor to consider during fixation is the change in osmotic pressure, which can cause the membrane to break, rupture or collapse. Fixative buffer osmolarity can alter the osmotic pressure of the fixative solution. Hypertonic solutions result in cell shrinkage whereas hypotonic solutions can cause swelling and poor fixation.

6. ***Concentration of fixatives***

   Providing pH is kept physiological, fixatives such as glutaraldehyde can remain effective at a high range of concentrations (0.25-4 %) but polymerisation with the buffer may decrease its concentration over time.

7. ***Incubation time***

   The duration of fixation is dependent largely on sample thickness and evidence suggests that over-fixation caused by extended incubation times may cause specimen shrinkage and hardening.

8. ***Fixation artifacts***

   Many artifacts are introduced by fixation and its poor penetration and latent effect can cause artifact responses. More obvious artifacts include swelling and shrinking but subtle changes relating to the movement of unfixed constituents, such as localisation of sub-cellular structures (eg. secretory granules) at false positions is of particular relevance to this research (eg. its distortion on fusion pores). One example is vesicles, which commonly fuse at the fibroblast cell membrane in fixation but not with freeze fracture (ie. frozen specimens). This suggests that vesicles form in the subjacent cytoplasm and are induced to fuse by fixation. Fixation can also cause loss of species from the specimen through molecular diffusion and denaturing of large molecules resulting in false histochemical reactions.

No singular fixative is suited for complete preservation of cellular substances and certain components are inevitably lost, degraded or removed during processing as a result of the unsuitability of the fixative on certain constituents. Ideally the fixative should insolubly coagulate cellular constituents, penetrate rapidly and protect tissue against distortion and shrinkage during dehydration. Glutaraldehyde (glutaric-dialdehyde) is a universal non-coagulative fixative with few negative effects. It is widely used in scanning electron microscopy and changes the cytoplasm's sol form into an electron transparent gel.

In this research cells were fixed in a 2.5 % glutaraldehyde - ProSciTech (QLD, Australia) in physiological PBS and incubated for 30-60 mins either at room temperature or in one instance at 37 °C. A solution comprising 4 % formaldehyde was also trialed (though only in a handful of experiments) with no visible difference or advantage over glutaraldehyde.

3.7 Dehydration & Drying

For further stabilisation a dehydration processes is applied after fixation to remove water in exchange for alcohol, which is achieved by submersing the sample in a graded series of increasing ethanol-water concentrations - 50, 70, 90, 95 % and then three steps of 100 % for between 3-5 mins.

After fixation and dehydration specimens are then dried in order to exchange ethanol for those solutions exerting lower surface tension forces. Critical point drying (CPD) is considered the preferred method for drying samples. However, the apparatus required for CPD was not immediately available and a good alternative, which has been proven by AFM, SEM and TEM to preserve cellular ultrastructure with similar quality is hexamethyldisilazane (HMDS) evaporation [41, 42]. The reduced surface tension of the HMDS meniscus and its ability to act as an agent for protein-protein crosslinking increases sample strength and reduces the likelihood of the cell fracturing or collapsing. Drying cells were immersed in HMDS - Microposit, Shipley Co. Inc. (MA, USA) for between 1-3 mins[1].

3.8 Cell Adhesives & Substrates

Substrate surface modifying agents were used to enhance cell attachment and to help anchor cells for AFM imaging *in situ*. Cell-tak[2] - BD Biosciences (MA, USA)

[1] After HMDS washing it is recommended that excess solvent be removed by blotting with filter paper and samples be transferred to a desiccator to avoid build-up of water condensation and contamination.

[2] Cell-tak is a registered trademark of BD Biosciences (MA, USA).

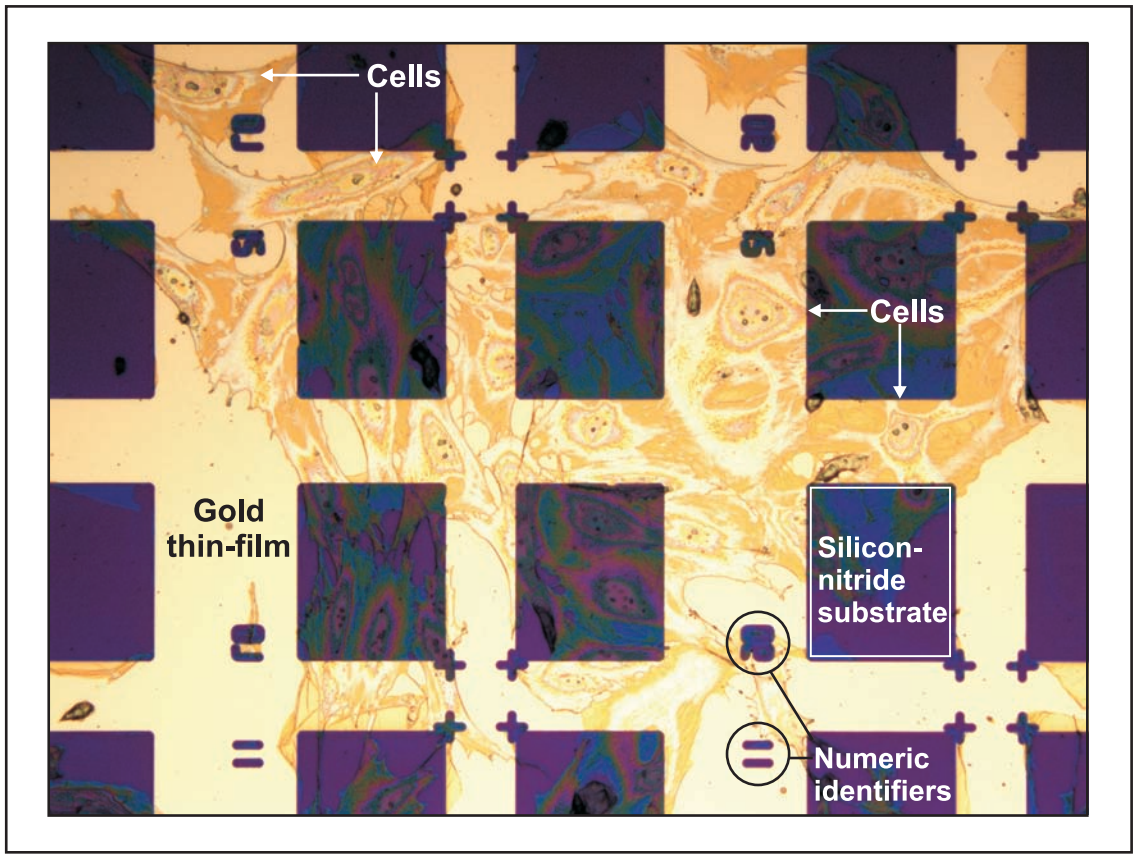

Figure 3.5: Optical image (20 ×) of a population of fixed, dehydrated and dried anterior pituitary cells cultured on a gold patterned silicon-nitride substrate.

and poly-L-lysine - Sigma Aldrich (MI, USA) were two solutions used to promote cell immobilisation and adhesion. Cell-tak is a specially-formulated polyphenolic protein solution - a family of proteins key to the anchoring and stabilisation of marine mussels to solid structures in nature. Treatment of coverslips and Petri-dishes were done using the adsorption method, which is based on the fact that Cell-tak is a neutral solution that spontaneously absorbs on to the first surface it contacts as the pH of the solution is raised. Upon treatment a thin coat closely resembling a protein monolayer is created on the substrate's surface. Alternatively, immersing substrates in poly-L-lysine creates a uniform net positive charge on the surface, which is used to enhance cell attachment and growth.

Surface modification of silicon or quartz substrates with either poly-L-lysine or Cell-tak were both effective in immobilising cells. However, the preferred substrate was thin-films (50 nm) of gold thermally evaporated onto an adhesive 20 nm nickel-chromium (NiCr) layer on quartz, silicon or silicon-nitride wafers. Apart from cells attaching well, gold has a low surface roughness and is easily wet-etched to form a patterned grid, which was useful for identifying individual cells. Figure 3.5 illustrates a population of fixed, dehydrated and dried anterior pituitary cells cultured on a silicon-nitride substrate with gold numeric grid identifiers used to assist in locating specific cells. This was particularly important when integrating optical and AFMy studies for the rapid identification and tracking of individual cells. Figure 3.6 (a) illustrates a reflected-light optical microscopy image (50 $\times$ magnification) taken of fixed (unstimulated) anterior pituitary cells after being cultured for seven days on a silicon-nitride substrate coated with a thin film of photolithography patterned and wet-etched gold ($\sim$ 100 nm including the underlying 25 nm of NiCr for adhesion). A specific cell (b) is identified as a good candidate for AFM analysis due to the presence of depressionary features thought to be fusion pores on the membrane. The cell's exact position is then recorded using the numeric co-ordinates visible on the thermally evaporated gold grid. (c) A high resolution AFM image is then taken of the exact cell identified optically (a), revealing fusion pores described as 'dilated craters', which are discussed in the subsequent Chapter - *Direct Cellular Analysis*.

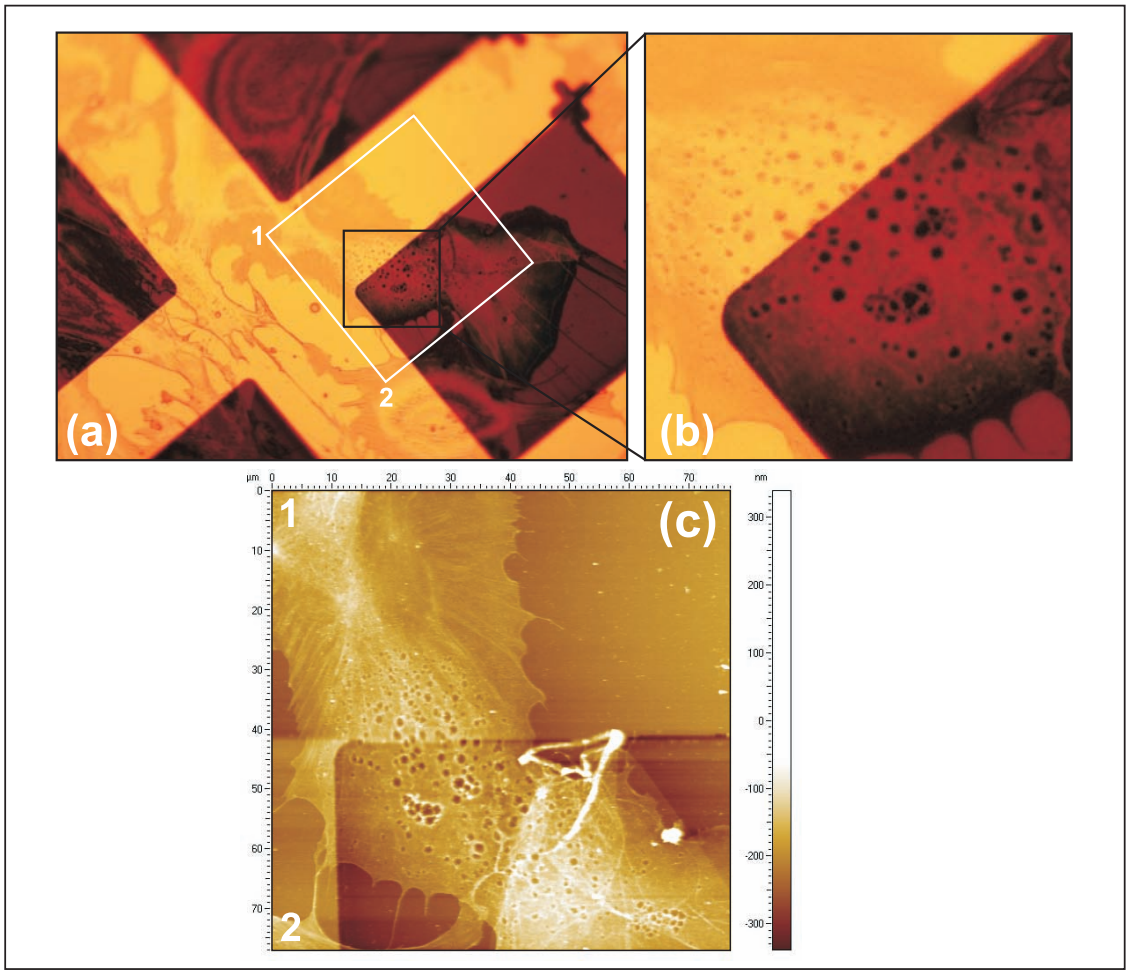

Figure 3.6: (a) Reflected-light microscopy image (50 ×) of a population of fixed, dehydrated and dried pituitary cells (unstimulated) cultured on a gold patterned silicon-nitride substrate for 7 days. (b) Initially, with aid of light microscopy a cell is targeted by its display of depressionary topography and subsequently (c) the AFM is used to image the same cell by noting its precise position on the substrate.

As well as providing a passive method for cell identification patterned substrates also indicated the resolution transfer for the Bioimprint cell replication technique - see Chapter 5. Replicas of cells were made over a large area (10 cm wafer) and inevitably one location was more suited than another, with respect to resolution transfer and cell integrity. It was difficult to predict these sites without imaging several locations and due to the various sizes and shapes of cells optical inspection was difficult. Whereas by fabricating a metallic thin-film pattern on the substrate it was easy to identify locations, which were obvious target areas to image cells due to there also being good replication of thin-film patterns in the polymer.

3.9 Immunohistochemistry

Immunohistochemistry is a family of techniques designed to label specific molecules using antibody-antigen binding reactions. In this research anti-LH antibodies targeted to LH antigens are used to identify and isolate the gonadotrophs (LH-synthesising cells) from other cells in the anterior pituitary. In one technique a peroxidase enzyme is conjugated to the LH-antibodies and a diaminobenzidine (DAB) enzyme used to produce a dye which is easily observed by optical microscopy. This technique is performed according to *Immunohistochemistry for LH/FSH...of Dispersed Anterior Pituitaries after Stimulation with GnRH and Oestradiol* compiled by Prof. J.J. Evans and J. Nagase [43].

After stimulation (optional) and fixing in glutaraldehyde for 1 hr cells were washed 3 times (10 mins each) in PBS - high NaCl consisting of 1.14 g Na_2HPO_4, 0.29 g $NaH_2PO_4.2H_2O$, 18 g NaCl in 1 L distilled of de-ionised water (DIW). For DAB peroxidase staining, cells were washed in H_2O_2 to quench residual peroxidase activity and washed again for 3 times (10 mins) in PBS (high NaCl) before blocking in tris-HCl containing 3 % bovine-serum albumin (BSA). Cells were incubated at 37 °C in primary antibody - anti-LH (rabbit) diluted to 1/1000 in 0.3 % BSA/PBS (physiological - 8 g NaCl, 0.2 g KCl, 1.44 g Na_2HPO_4, 0.24 g KH_2PO_4, 1 L DIW) for 1 hr. After washing for 3 times (10 mins) in PBS (high NaCl) cells were then

incubated at room temperature in the secondary antibody - anti-rabbit IgG diluted to 1/1000 in 0.3 % BSA/PBS (high NaCl) and cells were washed 3 times (10 mins) in PBS (high NaCl).

The Vector stain enzyme kit (Vector Labs - *Vectastain Elite ABC kit*) was prepared by mixing 5 ml PBS (high NaCl) with 2 drops each of reagents A and B supplied with the kit. Enough of the enzyme solution was applied to adequately cover all cells and incubated at room temperature for 30 mins, before washing for 3 times (10 mins) in PBS (high NaCl). The peroxidase substrate staining kit (Vector Labs DAB, cat. no. SK-4100) was prepared by mixing (in order) 5 ml DIW, 2 drops buffer, 4 drops DAB and 2 drops peroxide, which was applied to cells for 5 mins in darkened conditions at room temperature. Cells were washed in PBS (high NaCl) and then in DIW each for 10 mins, followed by graded ethanol dehydration and HMDS drying. Gonadotrophs were easily identifiable by the redish-brown staining on the cell membrane.

Chapter 4

Direct Cellular Analysis

Atomic force microscopy is used in biology for its ability to provide topographical information *in situ* at superior resolution to optical methods. However, cells are easily susceptible to structural movement and deformation caused by intermittent contact with the sharp AFM tip [44]. A determining factor influencing the degree of interaction between the cell and probe during imaging is the force applied to the probe [45]. The large scanning forces required for stable imaging can cause cell indentation, limiting lateral resolution and increasing the likelihood of deformation and damage [46, 47, 48, 49, 50]. Probe factors crucial in obtaining accurate images in fluid are; imaging force, image mode, tip sharpness, tip apex, cantilever force constant and scanning rate. Also critical are sample properties, including [50]; cell-surface adherence, cell type, topographic complexity, surface composition and tip indentation. Predictions on the attainable resolution when imaging cell surfaces regardless of whether they are living or fixed is considered in be in the order of 50-500 nm [51, 52, 53]. Tip sharpness is crucial in AFM investigations but for cellular analysis it is desirable to image with blunter probes because of the likelihood of membrane penetration [54].

Attempts to image cells in fluid proved challenging and arduous due to the aforementioned complications and influencing factors. Forces often damaged or pulled the cell from its surface, requiring excessive extension of culture time to promote

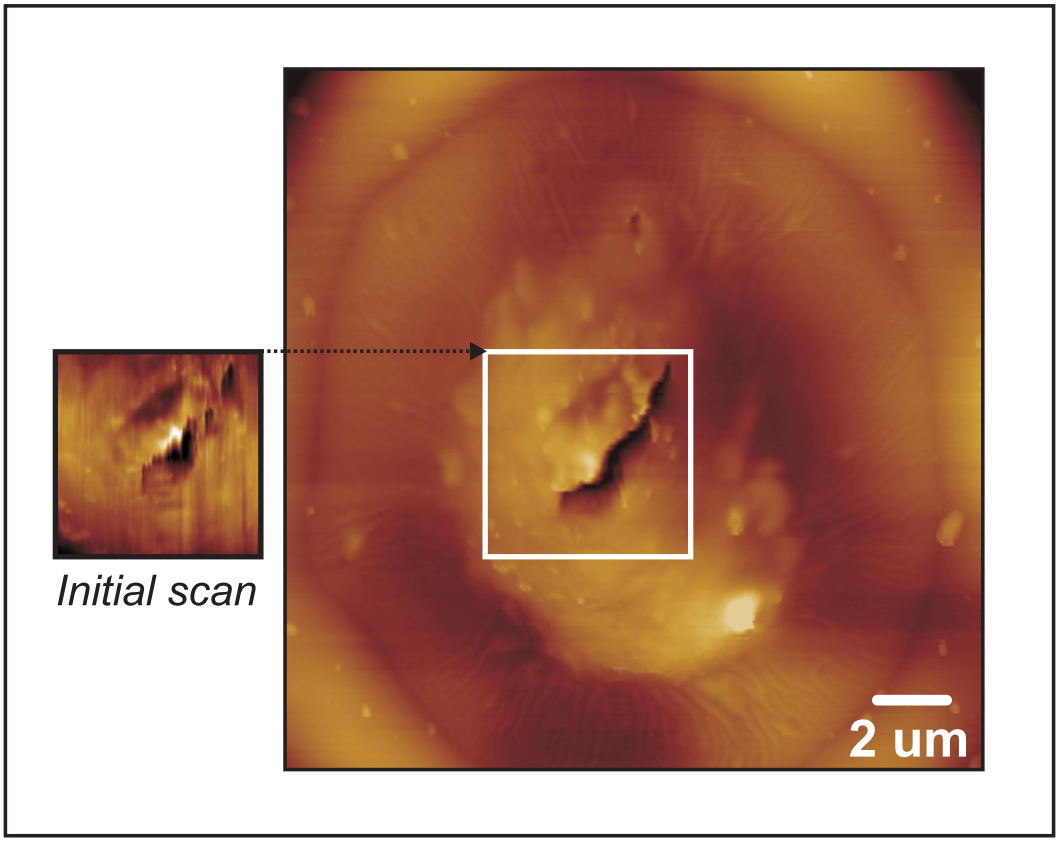

Figure 4.1: Time-lapsed AFM fluid-tapping image illustrating the tip perturbing effect caused to the membrane of a pituitary cell after several scan passes.

adhesion and reduce Z-height variations. Despite efforts to immobilise cells using specialised substrates and coatings (Chapter 3) they were still too unstable for force imaging making it difficult to achieve quality images while guaranteeing ultrastructural integrity and cell viability. An example of the invasive and interactive forces caused from the tip are shown in Fig. 4.1 - the continual damage of the sharp AFM tip on a pituitary cell using a silicon-nitride cantilever DNP-S Series (D probe) Veeco Probes (CA, USA) in fluid tapping mode, after initial and repeated scanning is illustrated by the large gash seen extending deep within the cell. Otherwise when using reduced loading forces image clarity is severely diminished to an unusable standard.

In addition, time resolution inequalities questioned the AFM's ability to capture exocytotic events in anterior pituitary cells. Axial and time dimensional response of the AFM occurs at millisecond pace in the fast scan lateral-X and Z-height direction,

but in the slow scan Y-direction resolution is measured in intervals lasting seconds [55]. In living cells dynamic events during this time would be represented over a sequential period comprised of several hundred scan line intervals making it difficult to correlate an accurate state or stimuli response. When compared to other secretory cells exocytosis in neuroendocrine cells is especially brief, lasting only milliseconds to seconds [56]. This time frame seriously impacts on the time-resolution limits of the AFM and the slow scanning times in combination with rapid exocytosis puts doubt on whether images could accurately capture reliable exocytotic events.

Lack of success and difficulty in obtaining high quality AFM images led to the exploration of more effective imaging techniques and methodologies to extract membrane topography. One of those methods is the use of chemicals to preserve and condition cells for imaging in an ambient-air environment.

4.1 Chemical Fixation

The first step and foundation to a sequence of events designed to prepare biological specimens for ambient examination is fixation. Fixation is a standard methodology used in biology to rapidly link and lock-in cellular architecture. Techniques commonly involve treating cells with chemicals selected based on a balance between two characteristics [57]; preservation of cellular 3D structure and the ability to label antigenic sites. Ultimately, fixatives aim to preserve sufficient cellular organisation to allow identification of features yet retain the antigenicity of the target. Fixation preserves cellular constituents at a near life-like condition by arresting autolysis[1] and bacterial decomposition, stabilising the cell to withstand further processing [58].

Fixatives crosslink protein membranes increasing cell rigidity, stiffness, mechanical properties and facilitating visualisation of fine surface details such as bumps, indentations and surface invaginations, which remain loosely attached *in situ* [59]. More specifically, aldehyde fixatives are good preservatives of secretory granules

[1] Autolysis is the self-destruction of a cell after its death by its own enzymes, which act to break down its structural molecules.

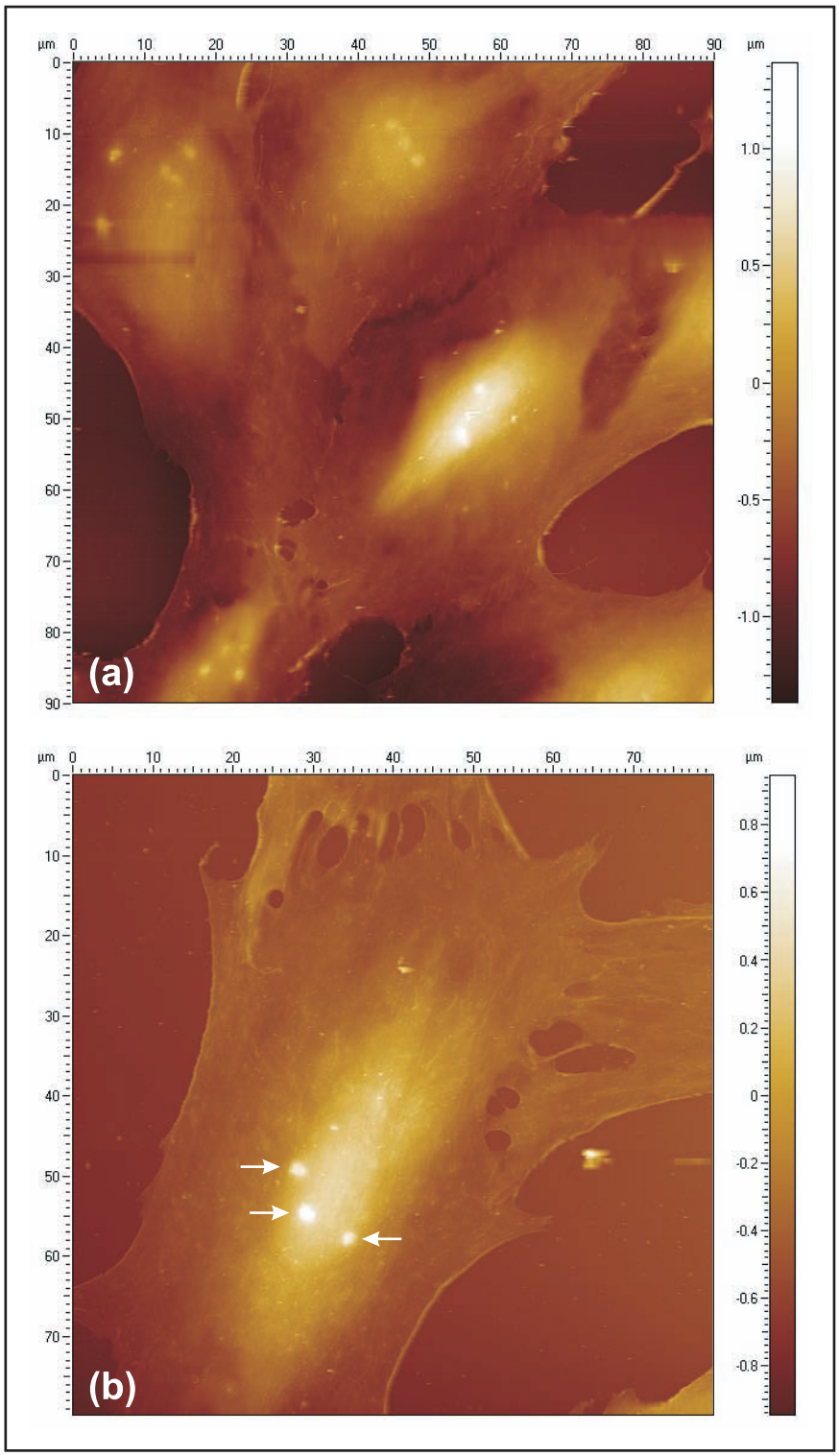

Figure 4.2: (a,b) AFM images of pituitary cells from Sprague-Dawley rats cultured for 4 days and prepared by glutaraldehyde-fixation, graded ethanol-dehydration and HMDS-drying, with arrows highlighting 'mound' artifacts in (b).

in gonadotrophs [17] but in general can produce dramatic changes in cellular surface structure including increasing membrane roughness and corrugation - thought to originate from mechanical stabilisation of microvilli [55]. Examples of anterior pituitary cells dispersed from Sprague-Dawley rats and prepared by glutaraldehyde-fixation, graded ethanol-dehydration and HMDS-drying according to protocols given in Chapter 3 are shown in Fig. 4.2. Highlighted in (b) are a handful of surface bulges, referred to as *'mounds'*, which were seen in the majority of fixed cells and appeared as aggregated particulates of varying width protruding above the membrane most distinctly at heightened points associated with nuclear locations. These features typically measured 0.5-1.5 μm tall and 1-3 μm wide, and while not immediately identifiable in literature they possibly represent rigid subapical structures in transition, or membraneous constituents distorted by the inability of glutaraldehyde to penetrate thicker areas on the cell. Further analysis discussing their origin is evaluated in the following Chapter 5 - *Bioimprint*.

Excessive amounts of loosely attached particles and debris on and around the cell made scan-free analysis very difficult and frequently imagery required scan line corrections - a result seemingly reinforced in AFM images of endothelial cells presented by Braet *et al.* [41]. Nevertheless, on the surface cells appeared well rounded with no visible signs of dehydration.

4.2 Cytoskeleton & Molecular Ultrastructure

As well as surface topography, influences from sub-cellular components impact AFM imagery via the membrane's conformation around rigid submembraneous structures. Impeding exocytosis is a dense barrier of actin filaments between the plasma membrane and the various releasable pools and surrounding granules. Figure 4.3(a) depicts elements in the form of fine fibres arranged in parallel, most evident in those cells having sub-micron heights from 6-7 days culture - cells *in vitro* for short periods are more rounded in shape often concealing these structures. Most likely molecules represent intermediate cytoplasm filaments or stress fibres in the cytoskeletal, and

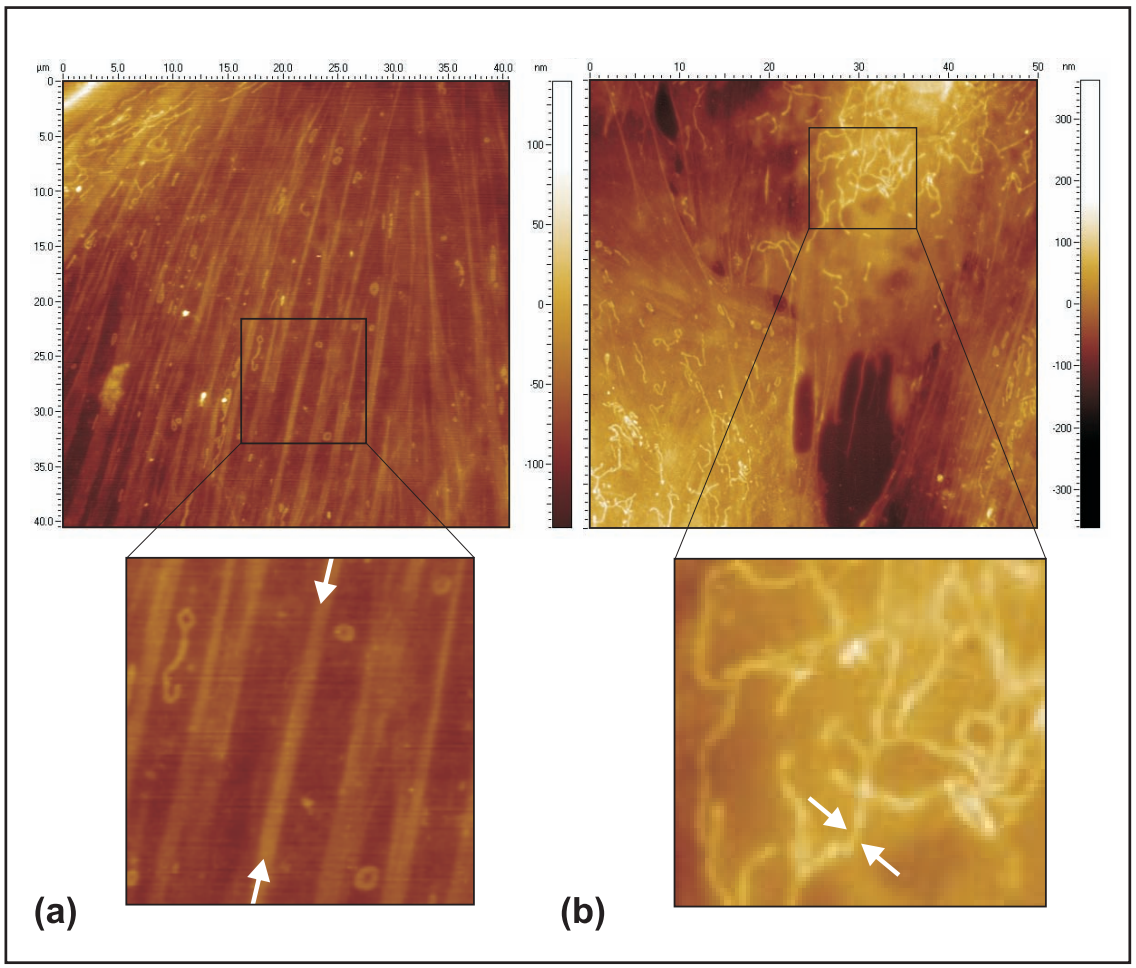

Figure 4.3: AFM images of the (a) cytoskeleton in a glutaraldehyde fixed, dehydrated, and dried pituitary cell cultured for 7 days - stress fibres are readily discernable in cells cultured for prolonged periods due to the development of cytoskeletal 'tracks' and the conformation of the membrane to the underlying structure. (b) In cells cultured for several days molecular strands are also visible on the membrane.

form part of the cortical actin network located beneath the plasma membrane. The cytoskeletal 'cell-web' is predicted to have an active, but not controlling role in modulating secretory granule motility in regulated exocytosis, as substantiated in many secretory cell types including those in the anterior pituitary [6]. The cytoskeleton is critical to intra-cellular transport [60, 61] but likely indirectly coupled to regulated exocytosis in events proceeding fusion such as supplying the readily releasable pool rather than directly regulating it [62]. By acting as a fusion barrier gateway assembling and disassembling depending on regulatory function the cytoskeleton has a dual role in facilitating and inhibiting exocytosis.

After cell stimulation regulated exocytosis commences through dynamic cytoskeletal events including removal of the barrier by actin filament disassembly, which are critical to events leading to secretion. This structurally stable network impedes fusion pore formation, potentially one reason explaining the absence of any sign of fusion activity in Fig. 4.3(a). The cytoskeleton also governs the mechanical stability of cells, which plays an integral part in intra-cellular transport and dynamics.

Additional filament-like organelles observed in Fig. 4.3(b) were seen distinctly protruding or forming on the membrane in various shapes. These are likely cytoskeletal filaments or molecules such as mitochondria which, again, were most noticeable in cells cultured for several days. Seemingly, as observed in the proceeding imagery they also acted as a barrier to exocytosis as indicated by observations depicting fusion pore formation around these molecules (see for example - Fig. 4.13). It is also possible these molecules constitute, in part, fibres of the extra-cellular matrix - an intricate network of inanimate macromolecules composed of a variety of proteins and polysaccharides (eg. collagen) produced and orientated locally by cells and abundant in connective tissue. A substantial volume of tissue is constituted by this matrix and interestingly its meshwork is closely associated with the orientation of the internal cytoskeleton. The secretion and establishment of the matrix assembly is most likely re-constituted over time after enzymic digestion and dispersion. Variations in the organisation of different macromolecules supplying the matrix result in a diverse range of forms, depending on the functional requirements of cells.

Previously the function of the extra-cellular matrix was thought to primarily serve as an inert scaffold for physical stabilisation. However, its function is now known to be far more active and complex in regulating cell behaviour with roles influencing; survival, development, migration, proliferation, function and shape. [63]

4.3 Exo-/Endocytotic Fusion Pores

A variety of exocytotic but potentially endocytotic, hereafter '*exo-/endocytotic*', fusion pores were observed in pituitary cells, demonstrating considerable diversity in size, shape, depth, construct, frequency, locality and proximity to associate structures. Fusion pores were grouped according to the following characteristics[2]:

1. **Major Openings**

   Uniform spherical openings of symmetric depth often seen grouped at localised regions on the outer membrane - analogous to *total fusion* or *endocytotic pores*.

2. **Channels**

   Seen infrequently, most likely due to their small sizes, 'channels' measuring $\sim$ 6.5/60 nm - deep/wide were frequently observed in proximity to 'major opening' fusion pores - analogous to *stalks* or *hemichannels*.

3. **Dilated Craters**

   Spherically regular in shape and measuring 0.6-2 μm/200-600 nm wide/deep. As depicted in Fig. 4.4, 'dilated craters' frequently saturated the entire membrane in cells absent of stimuli and were visible with optical microscopy.

   Containing Openings

   Selected craters infrequently contained a small narrow fusion pore opening(s) extending further within the cell.

[2]Generic descriptions are accompanied with analogies to forms previously presented (Chapter 1 - *Introduction*) to maintain non-exclusivity.

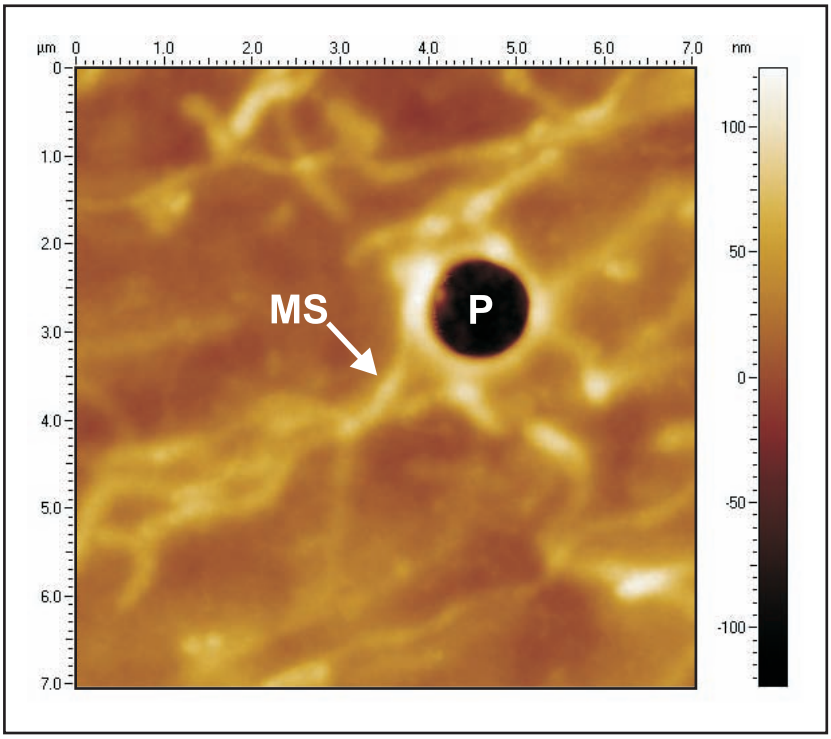

Figure 4.4: Solitary 'dilated crater' fusion pore (P) surrounded by molecular strands (MS) observed in a 7 day cultured pituitary cell subjected to GnRH for 4 mins.

4. **Molecular Craters**

   A small proportion of craters were seemingly inhibited from complete dilatation with the membrane by a molecular mesh-like scaffold which contain asymmetric openings - analogous to *depressions* (irregular openings) forming in *pits* (craters).

One of the most common formations imaged were spherically-rounded, uniformly-indented invaginations (Figs. 4.6, 4.13), referred to herein generically as 'major openings' and often seen localised on the outer regions of the membrane. One possibility is they are one of an interconnected series of transitional structures that constitute either an endocytotic or exocytotic process as hypothesised in Fig. 4.5. Nevertheless, the possibility of these structures being independent from each other cannot be ruled out.

In proximity to major openings were much smaller open 'channel' fusion pores as observed in the magnified image (1) displayed in Fig. 4.5, which measured 60 nm

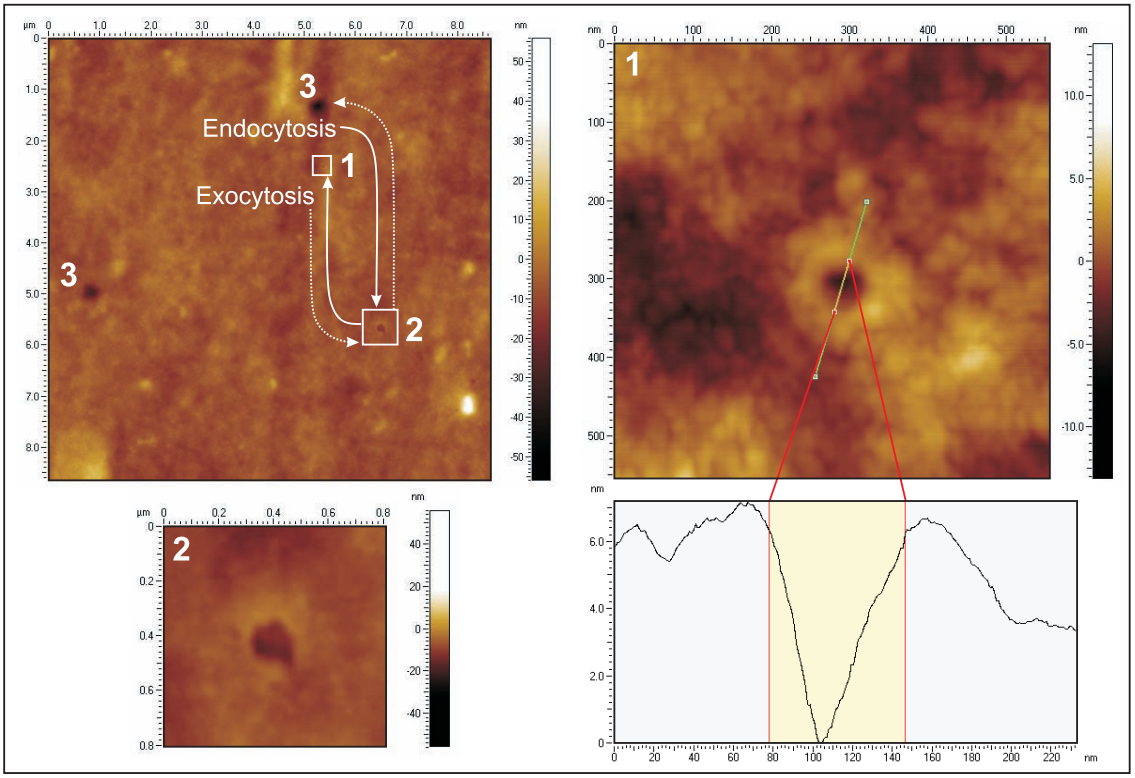

Figure 4.5: Postulating ultrastructural forms as transitional states, either by exocytosis (ie. stalk formation to fusion pore (*sequence 1,2,3*) or membrane retrieval (*sequence 3,2,1*) by endocytosis in a 7 day cultured pituitary cell.

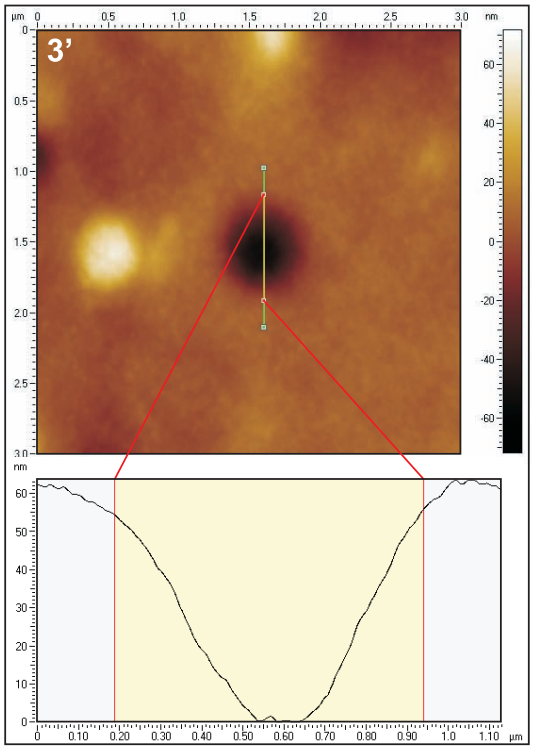

Figure 4.6: AFM image of major fusion pore opening on the membrane of a pituitary cell cultured for 7 days.

wide and at least 6.5 nm deep. From the scope trace it is apparent the fusion pore dimensions exceed the resolving limits of the probe, resulting in a profile reflecting tip geometry rather than of true pore construct. Pore depth fits within approximate ranges accepted for mammalian cell plasma membranes (6-11 nm) and if associated with exocytosis would likely represent a rapid transitional stalk phase - a stage defining initial contact of the underlying granule with the plasma membrane, and followed by a total fusion or hemifusion event (refer to Chapter 1 - *Introduction*, 1.1).

Similar pores termed *'hemichannels'* have been observed by Prof. Lal's group [64] and are critical in providing an interface between the external milieu and cell interior. Hemichannels are linked to mechanisms controlling normal physiological state such as regulating cell volume and mechanics, with hemichannels designed to act as a self-destruct mechanism by opening under oxidative stresses (eg. the presence of free radicals). This in turn disturbs cell homeostasis and results in cell death. [65]

Predominantly cells absent of stimuli contained large-shallow invaginations referred to as *'dilated craters'* (Fig. 4.4), which frequently saturated entire areas on the membrane surrounding the nucleus and were bordered by elevated ring-like assemblies. Figure 4.7(a) highlights an unstimulated cell progressively focused at an area on its membrane (b) showing a range of depressionary features centred at areas on the membrane surrounding the nucleus. Upon further magnification (c) 6 crater-pore formations grouped in close proximity are measured using a cross-sectional scope trace (d) as having widths and depths ranging from 0.7-2.1 μm and 150-250 nm, respectively. These forms are thought to represent granules dilated with the membrane post-secretion.

In addition, a small proportion of dilated craters contained further openings as evident in Fig. 4.8 - a scope trace taken across one crater and an opening in (a) measured 1.75 μm wide/250 nm deep, and 700 nm wide/100 nm deep, respectively. Likewise in (b) amongst several empty craters one contained a solitary fusion-pore in the form of a 550 nm-wide, 125 nm-deep opening visibly centred within a 1.6

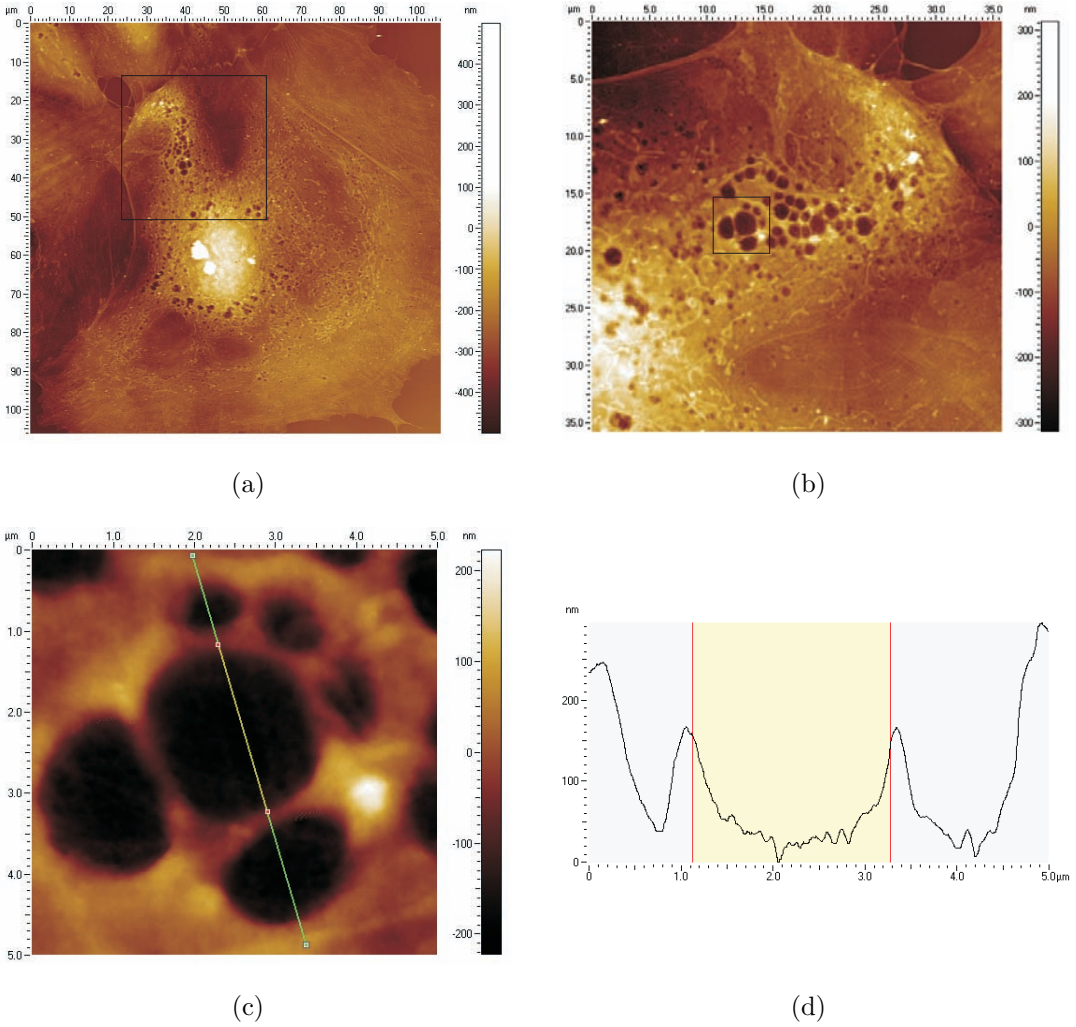

(a) (b)

(c) (d)

Figure 4.7: AFM images highlighting 'crater' fusion pores in an unstimulated pituitary cell cultured for 7 days, fixed in 2.5 % glutaraldehyde for 1 hr at room temperature before being dehydrated in an increasing grade of ethanol solutions (70,80,90,100,100%) for 3 mins each.

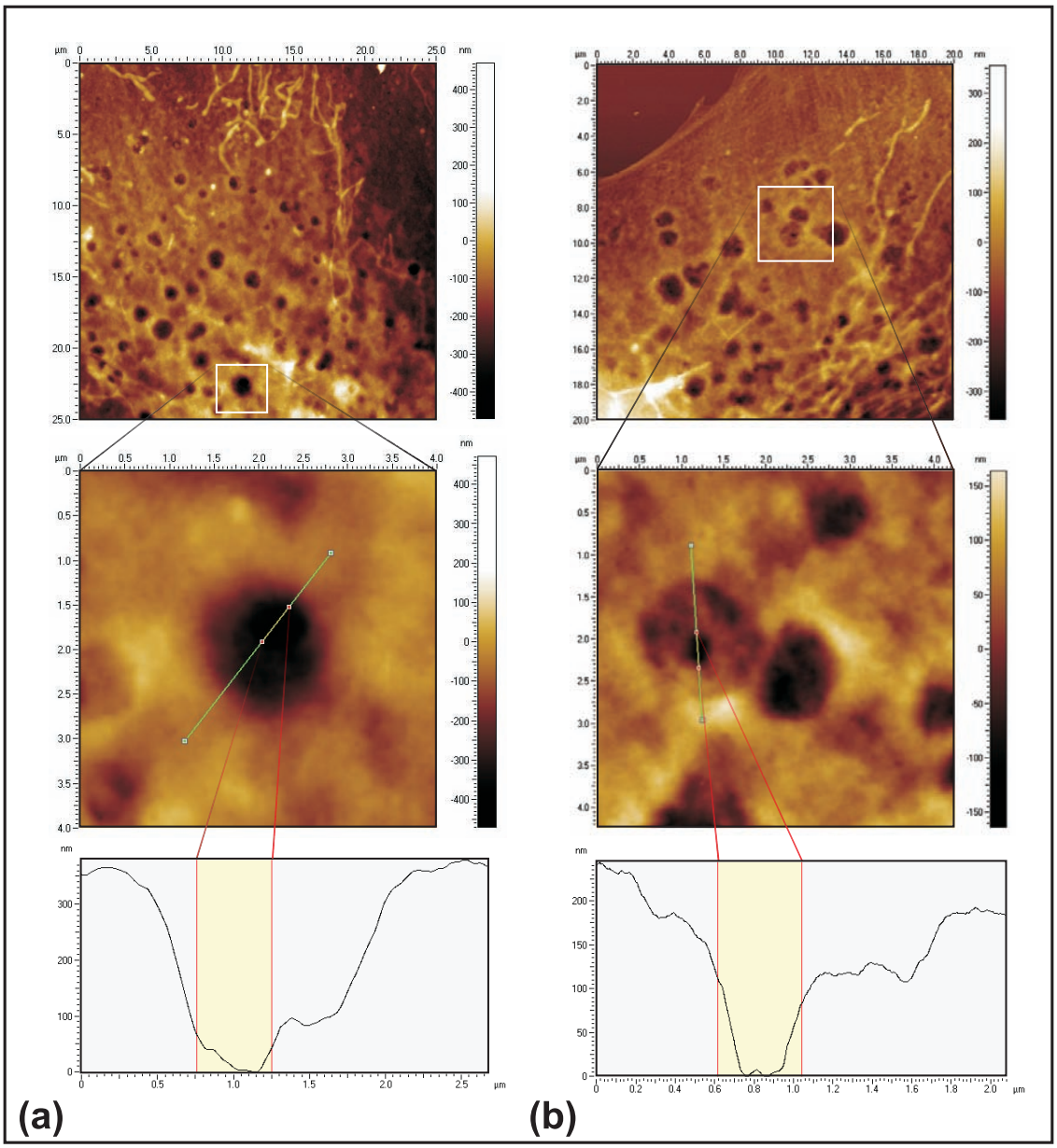

Figure 4.8: AFM imagery highlighting selected areas on fixed, dehydrated, pituitary cells (cultured for 7 days) displaying fusion pore openings within dilated craters.

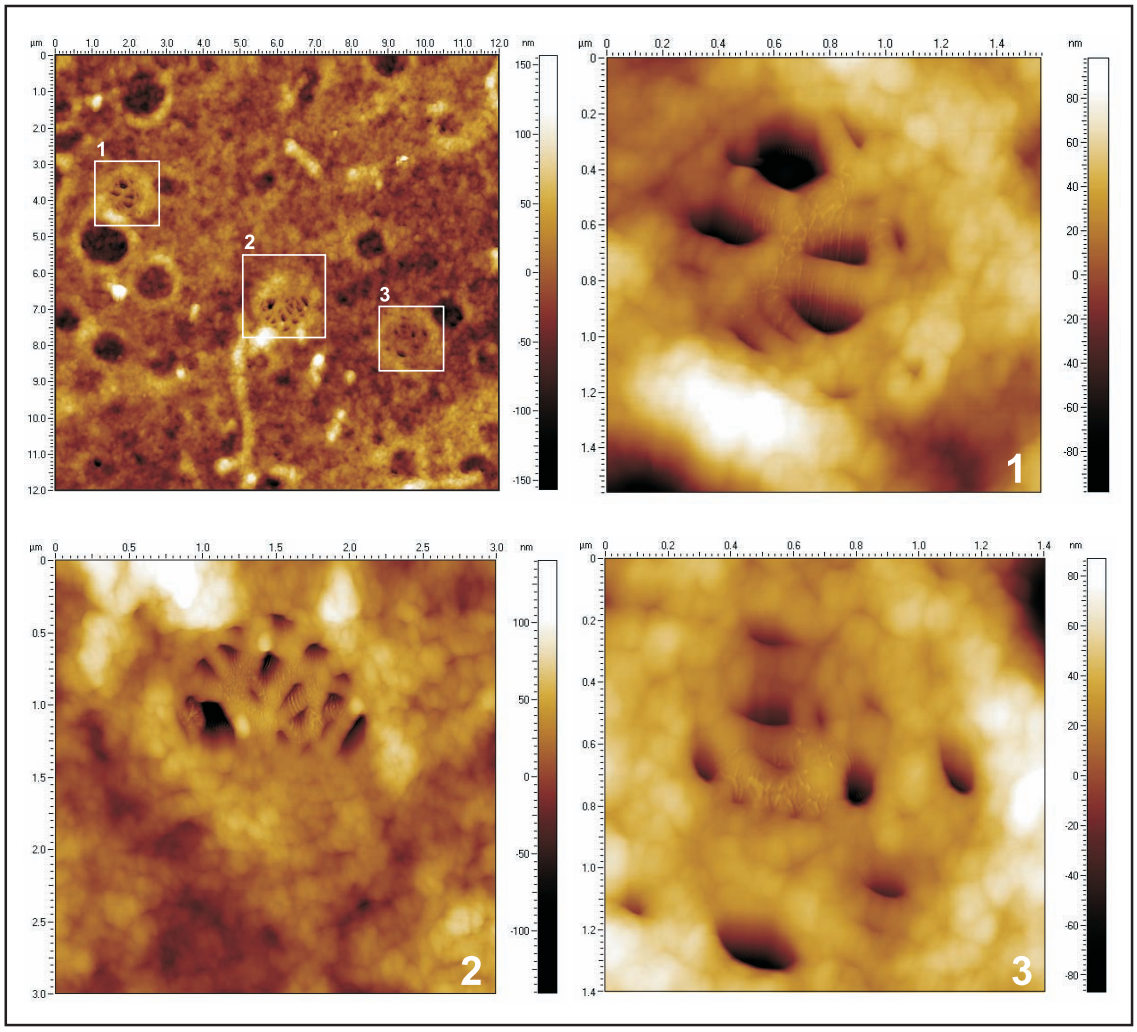

Figure 4.9: Transitional states of dilated craters highlighted by molecular craters (1,2,3) seen in unstimulated pituitary cells cultured over 6 days.

μm-wide, 85 nm-deep crater. These openings are thought to represent fusion pores formed from sequential docking of underlying granules at previous dilated granule sites by compound exocytosis (refer to Chapter 1 - *Introduction*, Fig. 1.4). Even though it was evident craters contained openings thought to signify fusion pores it remained unclear if their formation was preceded by an intermediary structure, or even still, if they were cell permeation artifacts resulting from inadequacies from fixation, dehydration, drying processing.

Illustrating the range of membrane topography and variation in forms resembling fusion pores is continued in Fig. 4.9 - highlighted are *'molecular craters'* thought to

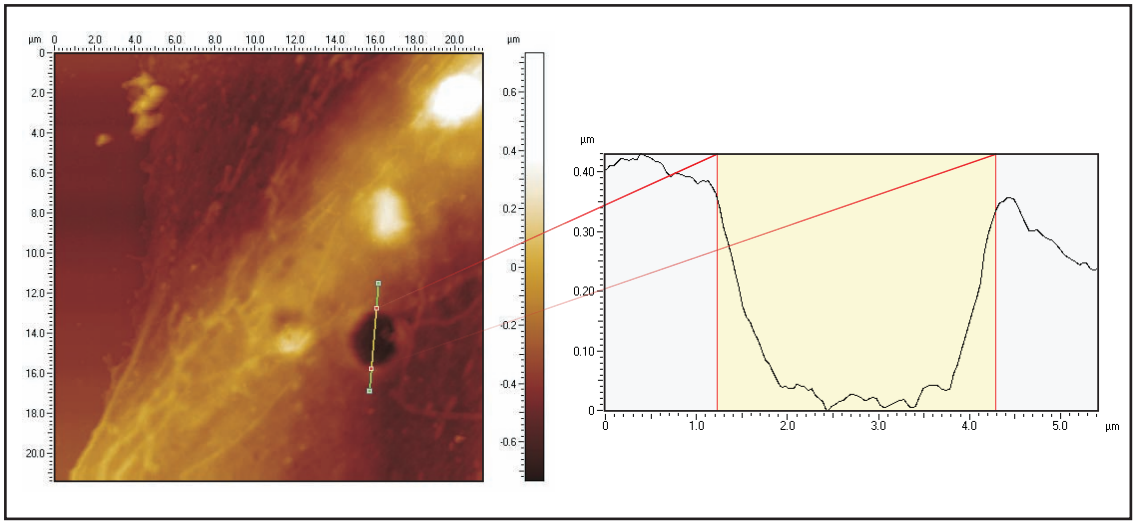

Figure 4.10: Single large invagination measuring 3 μm wide and 400 nm deep from an unstimulated pituitary cell cultured for 6 days.

resemble fusion pores forming on the membrane by underlying granules. This form is most similar to the *'depression and pit'* model, which to-date has only been observed by Jena's group [66], and is interpreted here to signify the transient-regulatory state of a craters pre-dilation. At higher magnification **(1,2,3)** molecules built into the membrane are seen to form a mesh-like structure predicted to regulate exocytosis from the underlying granule(s). One hypothesis is that molecular craters are sites of primary fusion, where granules initially dock in a sequential exocytosis mechanism (refer to Chapter 1 - *Introduction*, Fig. 1.4), which undergoes transient exocytosis from initial docking at the plasma membrane not previously occupied by dilated sites. Whereas dilated openings forming within craters are a result of sequential docking at primary fused crater sites. However, it is also likely that these sites represent differential effects caused by processing resulting in the delicate meshwork above the granule collapsing. While mostly it was obvious to differentiate different fusion pore types, in certain instances there appeared to be an infinite number of uncharacteristic and different fusion pores on a given membrane perhaps caused by process induced distortions.

In previous work [67, 68], ultrastructural evidence confirmed compound exocytosis in stimulated anterior pituitary cells as well as in a number of other neuroendocrine

cells [69]. Its existence occurs under different control mechanisms and is predicted to involve only a small proportion of the granule availability pool. An effect caused by multigranular docking initially occurring intracellularly by homotypic fusion, followed by membrane fusion of the multigranular aggregate at a single fused site as predicted with compound exocytosis (refer to Chapter 1 - *Introduction*, Fig. 1.4). One possible effect of this fusion mechanism on the membrane is illustrated in Fig. 4.10 - depicted is an unusually large 3 μm wide, 400 nm deep invagination entering within the cell interior likely caused by focused fusion of several granules, each time widening the initial fusion site. While difficult to conclude ultrastructurally, in the past granule-to-granule fusion has been highly controversial and possibly signifies an eventful form of exocytosis or a certain cell type. In the case of pituitary cells this mechanism could provide an alternative pathway for increased secretion in response to stimuli. [6]

4.4 Stimulation Studies

At first, attempts utilised known morphological characteristics to identify gonadotrophs, within the mixed populations in the anterior pituitary gland, based on granule sizes, cell shape, and characteristic features (eg. extrusions). This proved difficult due to cells appearing alike and while optical and AFM images displayed repetitive characteristics for different cells they deviated with matching descriptions in literature, making morphological identification inaccurate [17]. Another technique to identify LH-secreting gonadotrophs was through fusion pore response in cells subjected to GnRH stimuli - a peptide hormone that would specifically stimulate exocytosis in gonadotrophs. For the most part attempts to conclude either a morphological or fusion pore response from fusion pore topology by comparing overall populations proved challenging. Changes in pore numbers, density, size, shape, position or construct were often alike and quantification was inconclusive regardless of whether cells were treated with stimuli or not.

Radioimmunoassay results from Prof. J.J. Evans' group investigating the effects

of GnRH response in anterior pituitary cells exhibited LH surges approximately 5 minutes after stimulation [70]. It is reasonable to assume a similar, if not faster LH response in cells cultured over several days due to a greater surface area and potential for stimuli uptake. In an attempt to investigate transitional fusion states and determine the fate of the fusion pore and membrane morphology, stimuli conditions were trialed in assays experimenting shorter time periods (30 secs - 5 mins), GnRH concentrations (10^{-6}-10^{-7} M) and incubation temperature (37 °C - room temperature), with no indication of increased pore formation in any of the different cells imaged. While extending culture times was assumed to re-set *in vivo* physiology, one explanation for the non-responsive nature of certain cell populations is potentially related to the dispersion of pituitaries from non-cycling or irregular cycling rats. Nevertheless, there were specific instances where the effects of GnRH did induce an aggressive change in fusion pore characteristics.

Due to the considerable variation in sizes and types of exo-/endocytotic features, cells were characterised based on the display of fusion pores per square area on the membrane. Hence, using randomised selection, cells were classified as being above or below a threshold frequency regarding the number of pores within an area defined by a fixed scan size centred on the nucleus (heightened cell location). Initial assumptions predicted that GnRH exposure would increase fusion pore frequency due to the triggering of regulated exocytosis, thereby increasing the likelihood of visualising openings formed on the membrane, at least in the proportion of cells representing gonadotrophs.

On one occasion cells derived from one anterior pituitary showed a marked difference in membrane topography when exposed to GnRH compared to cells incubated in parallel basal conditions. In this experiment the membrane displayed high numbers of exo-/endocytotic features in pituitary cells incubated in the absence of GnRH prior to fixation and dehydration. In fact instead of a dominant population of cells portraying bland morphology devoid of fusion pores, approximately 55 % (20/36) displayed a large number of exocytotic features ($> 15/50\ \mu m^2$) indicative of cells depicted in Fig. 4.11, which illustrates hundreds of exo-/endocytotic features. Such

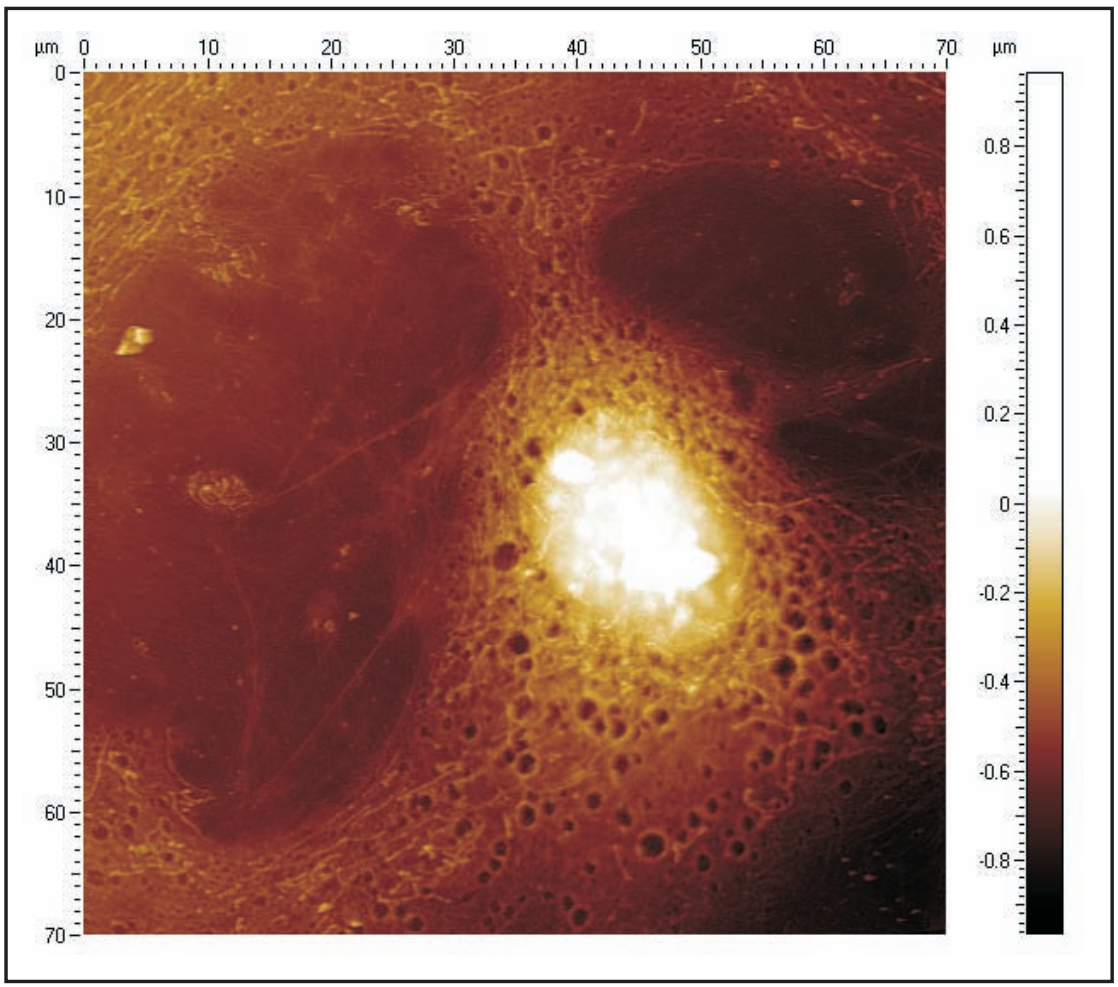

Figure 4.11: Picture of the topology of the apical cell surface of an unstimulated pituitary cell cultured for 7 days (fixed, dehydration and dried) seen saturated with dilated fusion pore 'craters'.

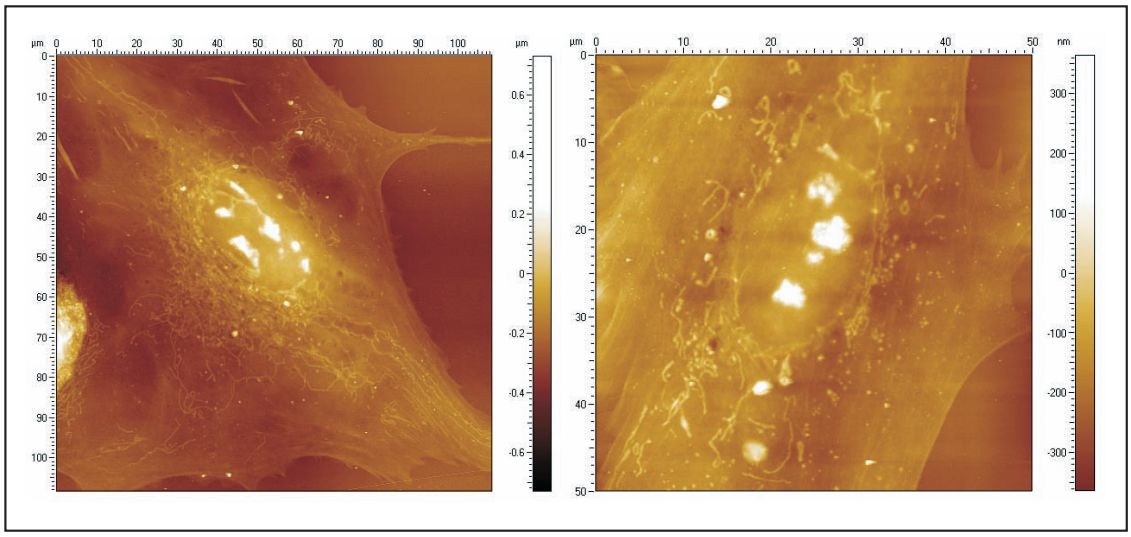

Figure 4.12: Pituitary cells cultured for 7 days prior to submersion in 10^{-7} M GnRH:M199 for 10 mins, followed by fixation, dehydration and drying.

features were sparse in corresponding GnRH stimuli-subjected cells.

Figure 4.12 illustrates 2 fixed/dehydrated/dried cells with the low numbers of fusion pores numbers, which were typical of the majority (80 %) of cells exposed to GnRH for 10 mins in this experiment. The remaining 20 % (7/35) of cells had more than 15 exo-/endocytotic features within a 50 μm square area. Hence cells displaying some form of fusion characteristics, be it craters or openings, were infrequent in this group. Figure 4.13 illustrates one of those cells, which at high focus, on the membrane surrounding the nucleus, depicts a fusion pore lying adjacent to a molecular strand.

These observations although not regularly observed suggest the disappearance of fusion pores on the membrane in cells subjected to GnRH, but the fate of the fusion pores post secretion is still unclear. However, the technique employed to monitor the cellular response based on counting pore numbers is largely unsuited to measure stimulation state due to its dependence on an arbitrary threshold level, set as the approximate average of fusion pore frequency in stimulated and unstimulated cells. As an indication, the difference between cells exposed to, or restricted from GnRH in the percent of cells displaying more than a threshold of 15 pores was 35 $\pm$ 11 % standard error (SE) (ie. 35 % of the pituitary cells apparently responded to GnRH and lost pore structures). Put into perspective 35 % is more than double the

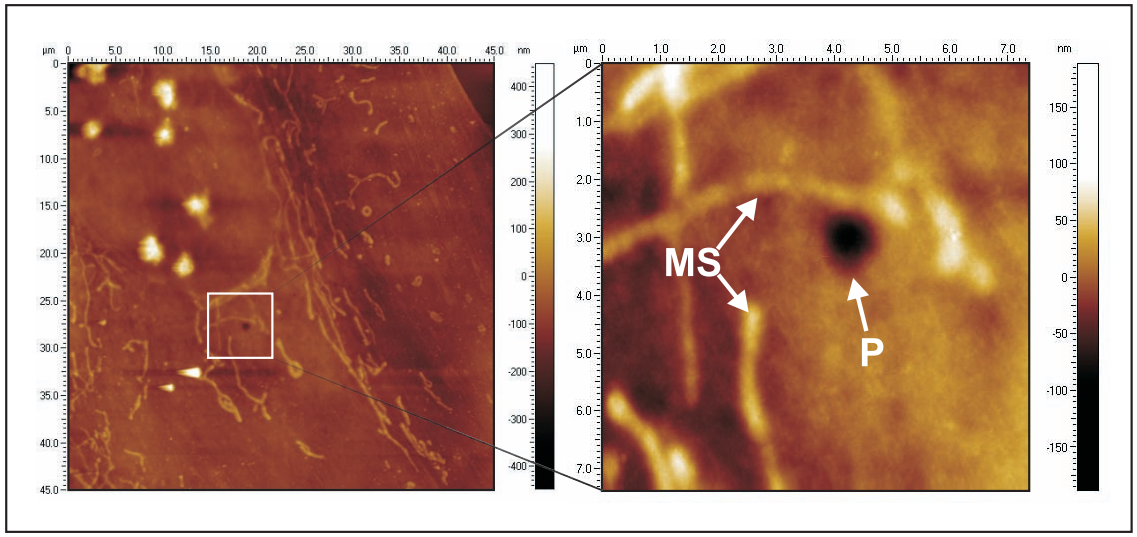

Figure 4.13: A solitary major fusion pore opening (P) observed between molecular strands (MS) in a 7 day pituitary cells stimulated with 10^{-7} M GnRH for 10 mins (fixed, dehydrated and dried).

total estimated gonadotroph cell population - the cell type principally responsive to GnRH, which consists of approximately 10-16 % of the anterior pituitary population. Nevertheless, it should be emphasised that these results represented one experiment in many that failed to show a definitive fusion pore response to GnRH.

According to previous observations by Jena [66] and Anderson *et al.* [8], the frequency of fusion pores ('porosomes') and pits remains constant during stimulation, only the pore openings ('depressions') widen. One explanation for observances showing the decrease in fusion pores in cells subjected to GnRH is the notion that the ready-releasable granules primed at docking positions at the plasma membrane fuse and blend rapidly with the membrane at a rate too fast for fixation to capture. In the meantime the transitional lag time for secondary granules to become primed and ready-releasable, results in the membrane being absent of fusion pore activity.

Despite having considerable stockpiles of granules with long half-lives, in the event of an action potential granular release can function with a variety of responses. A reserved effect might witness a handful of fusion pores forming, on the other hand, a vigourous reaction would result in a flurry of granules being released from the ready-made pool. In endocrine cells only a small percentage ($\sim$ 1 %) of granules

are actually readily and rapidly releasable, with rate limiting steps in the process being synthesis and recruitment of subsequent granules to the membrane. However, for gonadotrophs hormone release might not warrant an instantaneous response due to the systemic effect of LH release on the reproductive system through blood circulation in the body [6]. Temporary absence of fusion pores after stimulation is possibly explained by the inability of exocytosis to persist for prolonged periods. The initial rapid (milliseconds) exocytotic burst is likely followed by a subsiding depletion of ready-releasable granules at the membrane [71]. In the following phases, lower secretion results from a sustaining balance of the subsiding group of ready-releasable granules and arrival of reserve granules progressing through slow maturation steps. In most instances radioimmunoassay predicts LH to peak at approximately 5 mins post-GnRH stimulation. Even at this time the lag in fixation prevented cells from being preserved at this state.

Despite wide use of chemical fixatives there remains significant technical shortcomings in their application for studying dynamic events. Fixatives are too slow to definitively capture rapid exocytotic events [72] and cells were rarely halted after stimulation and in time to represent heightened states of fusion. From evidence showing the decay of exo-/endocytotic sites on the membrane it was concluded that granular release not only occurred rapidly but was short-lived and more rapid than the process of chemical fixation.

4.5 Immunohistochemistry

A link between fusion pore construct and function was required to confirm an association with exo- and/or endocytosis. To accurately determine basal fusion pore topology and cellular response, isolation or identification of gonadotroph cells types were required. Immunohistochemical methods are frequently employed in biology to label specific molecules using antibody-antigen affinities - in this case LH antibodies to target the LH antigen. In one technique, immunohistochemical staining enables visualisation of this interaction by conjugating a peroxidase enzyme to the antibody,

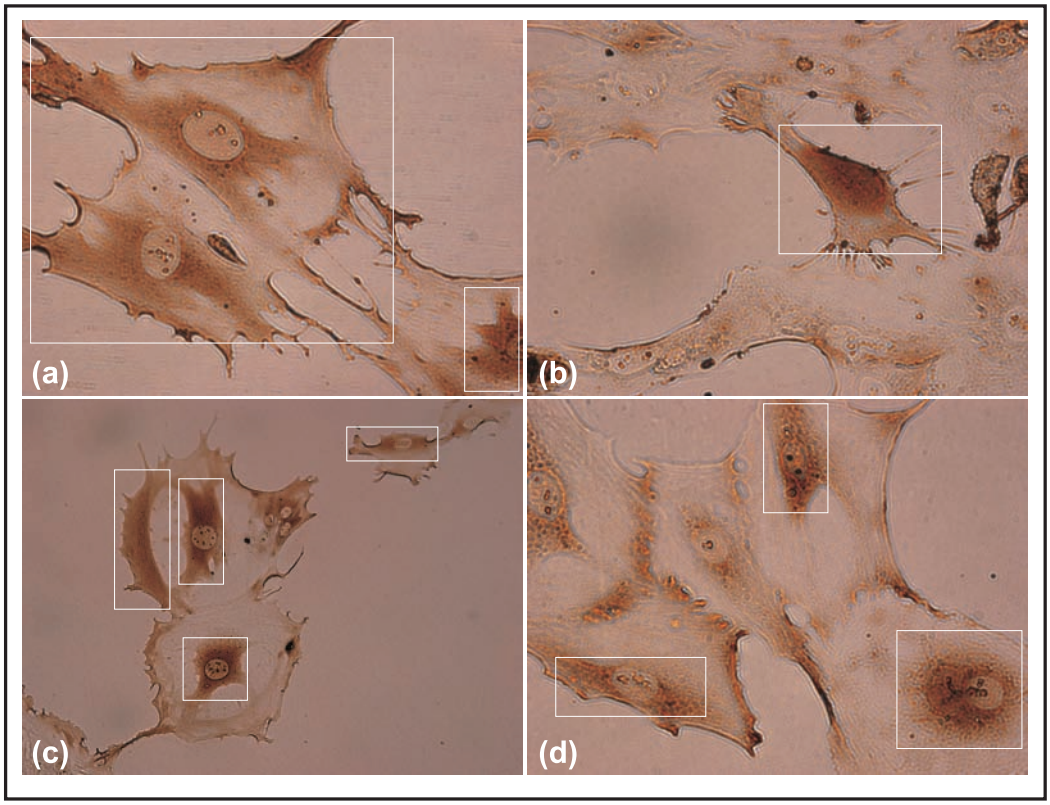

Figure 4.14: Transmitted-light microscopy images of anterior pituitary cells (6 days culture without GnRH) after immunohistochemistry staining for LH - sites are dyed red on the cell and are highlighted (white boxes).

which catalyses to produce a staining reaction.

Figure 4.14 illustrates 4 (a,b,c,d) transmitted-light microscopy images of unstimulated anterior pituitary cells (6 days culture) after immunoperoxidase staining for LH before ethanol dehydration and HMDS drying. The redish-brown or darkened coloured areas on cells as highlighted by white boxes is an optical stain for signalling the presence of LH secreting gonadotrophs using primary anti-LH antibodies coupled to peroxidase dye markers on protein IgG (see Chapter 3.9 - *Immunohistochemistry*). The intensity and degree of staining indicates LH concentration and while some cells (b) stained almost completely in others (a,c,d) only specific areas on the membrane stained possibly due to the localised secretion of LH. Despite this, AFM images targeting stained locations revealed no obvious sign of fusion pores or characteristics indicative of exocytosis. Even though LH antigenic sites remained permanently stained after peroxidase labeling fusion pores seemingly dissipated during processing or otherwise were never completely halted during fixation.

For higher accuracy and specificity rather than attaching the antibody to an enzyme it can be tagged to an organic fluorescent dye or stain (eg. fluorophores) allowing visualisation of single molecular interactions and proteins when under confocal or fluorescent microscopy. Quantum dots are fluorescent nanoparticles becoming a popular alternative to fluorophores due to their superior optical luminescence, narrow emission band and conjugative stability. Another technique for identifying fusion pore locations with a high degree of precision made use of water-soluble quantum dots pre-conjugated to LH antibodies. To begin with lyophilised anti-rat-LH beta IgG (0.43 mg/ml)[3] purchased from Prof. A.F. Parlow, National Hormone and Peptide Program (CA, USA) was conjugated to quantum dots using a Qdot® antibody conjugation kit (605 Qdot® Invitrogen CA, USA) [73]. The quantum dots had a peak luminescent emission intensity of 595-605 nm and were observed by fluorescence microscopy using a Texas Red® Molecular Probes Inc. (OR, USA) filter set. In addition to non-stimulated cells, pituitary cells were subjected to GnRH at 10^{-7}

[3]For quantum dot-antibody bioconjugation it is recommended primary antibodies are pure ($\sim$ 1 mg/ml) and free from serum and BSA to avoid unspecific conjugation.

M concentration between 3-16 minutes and incubated at room temperature with quantum dot anti-LH bioconjugates of concentrations of 1/10 and 1/50 in PBS after fixation for 1 hr. Subsequently, cells were dehydrated and dried but unfortunately fluorescence was not specific to a certain proportion of cells and there was a high degree of cell auto/background fluorescence.

Other functional nanoparticles also trialed included gold nanoparticles ($\sim$ 13 nm) and magnetic beads ($\sim$ 50 nm) (MACS) Miltenyi Biotec GmbH (Gladbach, Germany) conjugated to LH antibodies but in both cases their small sizes made AFM detection and differentiation from the granularity of the cell membrane difficult.

Chapter 5

Bioimprint

It is of interest to determine the impact of chemical preservatives on cell morphology to gain an insight into artifacts introduced during processing. Fixation, dehydration and drying often requires treatment of cells with aldehydes and solvents, which can result in morphological distortions. In itself, fixation constitutes a major artifact, where a living cell in a semi-fluid state is altered to represent a coagulation of constituents - essential to prevent their loss, rearrangement or diffusion during processing [40]. For faithful acquisition of images reflecting living cells it is ideal to eliminate as many of the potential artifact producing preparation steps as possible. Ideally, samples are fixed in a time and at conditions such that there is no molecular displacement at a distance greater than the resolution limit imposed by the imaging tool [74]. Despite previous studies confirming their satisfactory equivalence, of particular concern was the impact of glutaraldehyde-fixation and HMDS-drying.

To explore these possible effects a Bioimprint replication technique was developed to recreate cell topography without requiring fixation. An animated illustration describing the process of imaging cell replicas is shown in 5.1 - (a) using transparent elastomers, controlled conditions are applied to set a replica cell impression, (b) after separating the cell and replica (c) the mould is imaged with the AFM and digitally inverted to yield a positive replica. Motivation for Bioimprint derives from deficiencies in current air and vacuum nanoscale imaging devices that require harsh

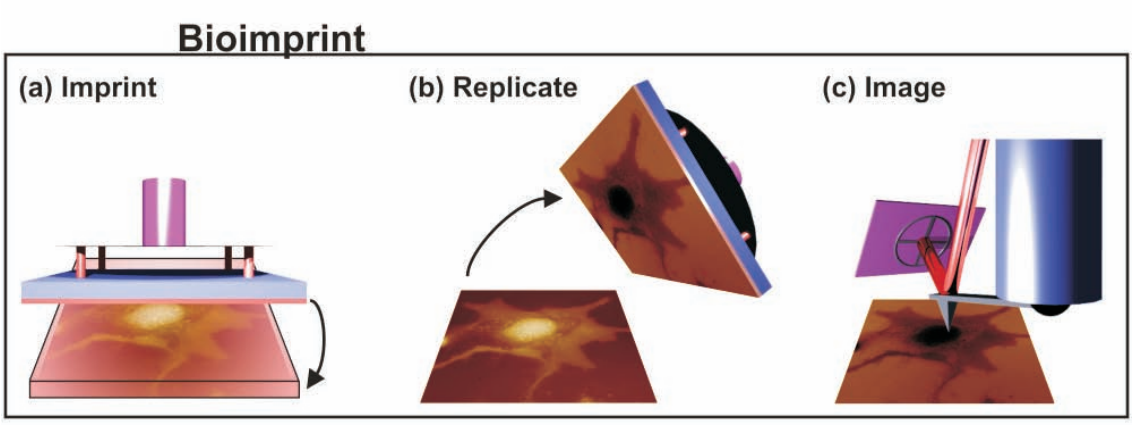

Figure 5.1: Artistic depiction of the Bioimprint replication process.

drying and modification techniques for sample preservation, possibly deforming and misrepresenting the true cellular structure. Bioimprint also overcomes many of the difficulties associated with *in vitro* cellular analysis, which results from the impact of the sharp scanning probe on the soft cell membrane, thereby facilitating the integration of the AFM as a non-destructive tool in biology.

5.1 Background

Replication has long been a popular technique for the indirect analysis of biological surfaces in scanning electron microscopy, especially in situations arising from the following circumstances [75]:

1. Sample sizes are too large for the microscope and are unable to be easily divided.

2. Excessive distortion in the SEM's topographical secondary electron emission mode from orientation effects or atomic number contrast.

3. Sensitive organic materials are damaged by the SEM's electron beam and vacuum environment.

4. Fixation, dehydration or drying induces artifacts.

5. Sample contamination of the vacuum chamber (eg. from hydrated biological materials).

6. Inability to directly resolve internal structures (eg. field depth or charging).

The initial replica of a sample's surface is also known as a cast, impression or negative mould, where submersions (eg. fusion pores) in the original surface appear as protrusions in the impression. The advantage of the AFM over the SEM with respect to imaging replicas is the ability to directly convert the negative topographic image/data to an inverted contrast model without positive replication (ie. replicating the negative mould). In addition, for the SEM replicas must be electrically conductive and require sputter coating or evaporation of metallic or carbon thin-films in vacuum.[75]

Established bio-replication methods generally begin with physical fixation of a living specimen by rapid cryogenic freezing (eg. freeze-fracture [76]). The result is instantaneous halting of biological function while at the same time preventing any process-induced reaction or distortion [77]. Subsequently the specimen is sliced at low temperature to reveal its internal surfaces and shadow replicas are taken by carbon evaporation and platinum coating, using strong acids to dissolve any organic material from the replica. In 'freeze-etching' [78] the added step of applying a short burst of radiant heat to sublime ice formed on the sample's surface is introduced prior to replication and shadowing to set non-volatile components in sharper relief. These techniques have produced some of the most accurate images of living morphology to-date, but they are notoriously difficult to create. Expensive equipment is required to rapidly cryogenically freeze samples in order to systematically 'freeze-slam' them against a metal slab, or plunge them into a super-cool environment. Simpler approaches to replication [79, 80, 81] have also demonstrated the ability to recreate a range of moist surfaces in polymers for examination by light microscopy. More recently, replicas of hydrated biological surfaces have been used to investigate nanometre variations in surface topography by AFMy [81].

Reference to Bioimprint is made with respect to 'molecular imprinting' [82] - the process of using soft materials to transfer selective recognition and catalytic sites into synthetic polymers and macromolecules through the use of bio-molecular templates [83, 84, 85]. Additionally, a completely unrelated process to Bioimprint but known similarly as *'Bioimprinting'* [86], refers to molecular imprints made in proteins rather than organic monomers. In the past molecular imprinting has been used in far-ranging applications from viral detection [87] to imaging hydrated biological samples [88]. However, its ability for recreating cells for applications investigating cell topography at high resolution using the AFM remains relatively unexplored.

The quality of replicas can be judged with respect to; 3D specimen reproducibility, material resolution, certainty of being able to replicate surface features, stability of the hardened replicas, the ability to recognise artifacts or inclusions (eg. air bubbles, replica damage during peeling) and the degree of damage to the specimen during replication. There are also factors related to the ease of replication including; the ability to separate the replica from the sample completely, reactivity of replica material with the specimen, compatibility of the replica with the microscopy tool (eg. conductivity, hardness, vacuum suitability), replication time and the response of the specimen during that time. [75]

In this chapter two Bioimprint methodologies are introduced. The first technique utilises a conventional replica-moulding method with a heat curable elastomer, and the second, a UV-curable polymer applied to cells using an imprint technique. The first technique is used to analyse cancer cell morphologies, which is discussed separately in the following chapter. Whereas the latter technique is applied to investigate the molecular structure of fusion pores in anterior pituitary cells, which are a particular interest due to their comparison to those previously imaged in chemically fixed cells.

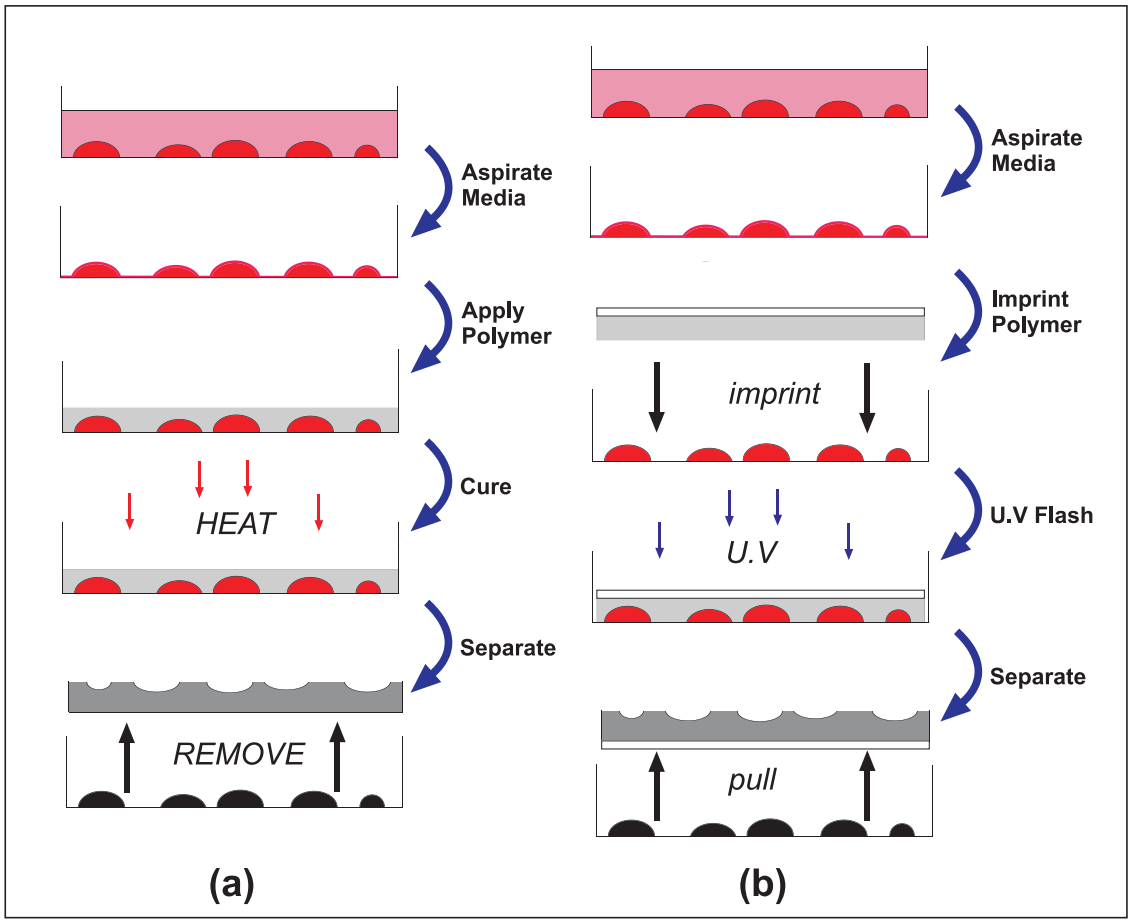

Figure 5.2: Bioimprint (a) PDMS replica moulding and (b) UV-imprinting pattern transfer schemes - cells are replicated either with (a) thermal- or (b) photo-initiated polymer curing agents with heat or UV light, respectively. The resulting negative replica or topographic 'impression' of the cell is subsequently scanned by the AFM and digitally inverted to form a positive image.

5.2 Materials & Methods

For Bioimprint it is advantageous to analyse cells cultured for several days to reduce cell variations, but more so to promote cell-to-surface attachment on culture dishes or substrates (eg. quartz) through an increased surface area flattening. This ensures cells remain sufficiently attached to the substrate during replication and clean polymer separation after mould hardening.

5.2.1 PDMS Replica Moulding

Replica moulding is a soft lithography [89] process whereby a master object is submersed in a liquified polymer material and curing conditions are applied to permanently transfer complete topography. Initial experiments verifying the ability to replicate cells employed a heat-curable poly(dimethylsiloxane) (PDMS) - Dow Corning (MI, USA) elastomer using standard replica moulding techniques as illustrated by the pattern transfer scheme shown in Fig. 5.2 (a). Prior to polymer application all incubation media was aspirated and samples were washed twice in physiological PBS to remove any debris or loose material. Fabrication began by mixing the PDMS composite at a 10:2-3 ratio of base polymer to curing agent, and expelling any trapped air bubbles using a vacuum-desiccator or leaving the solution overnight, followed by pre-curing for 2 mins at 95 °C. As much of the PBS solution as possible was removed without completely drying the substrate and approximately 3-5 grams of composite was applied above the cells attached on a 5 cm plastic Petri-dish, and immediately incubated in a 37 °C oven for 2 hours. The thickness of the resulting polymer above the cells was typically 5 mm. Attachment of cells to the substrate prevented features from being submersed completely within the polymer material, enabling fabrication of an impression of the exposed cellular surface. The hardened polymer mould was then peeled off, ultrasonically washed in detergent-DIW and if required submersed in strong acids to remove any attached biological material. A final polymerisation stage in a 95 °C oven for 30-60 mins ensured complete polymer curing and stabilisation.

As well as PDMS other thermal replicating materials also investigated by replica moulding included hydrogels; c-plaque agarose low melting temperature Cambrex Corp. (East Rutherford, NJ) and high gel strength DNA/RNA agarose # AHGS0250, The Nest Group, Inc. (MA, USA). While natural polymers showed enormous promise for future investigations, these specific formulas were insufficient either in resolution or curability requirements.

All hardened cell impressions were analysed in air tapping mode using triangular or

rectangular non-contact cantilevers (MikroMasch, Estonia) with sub-10 nm curvature radii and force constants of 48 N/m, typically operated between 0.6-1 Hz at a resonant frequency of $\sim$ 315 kHz. To recover the original cell orientation positive replicas are made by digitally inverting the AFM images of the impression (also referred to as the mould or negative replica) taken of the cells following hardening of the polymer.

Figure 5.3 illustrates a 40 μm AFM image made from a rat pituitary cell[1] replicated in PDMS. Most noticeably are the distribution of large pores on the cell membrane and their clustering around a nucleus centred within the cell. Submersions had mean widths and depths of 953 $\pm$ 173 nm SE and 200 $\pm$ 26 nm SE (calibrated), respectively, and are assumed to be distorted fusion pores or permeation artifacts resulting from prolonged curing. Evidently their formation is limited to locations on the membrane immediately around an area centred on the cell, assumed to be the underlying nucleus. One main difficulty of thermal curing as observed in Fig. 5.3 is the dehydration effects [90], which results in an indentation profile across the cell surface from collapse of the nucleus or of its dematerialisation. At first indentation effects were thought to be formed as a result of the pressure of the polymer on the nuclei. However, they proved to be more profound with longer polymer curing times and temperatures, and thus were linked to dehydration effects.

5.2.2 UV-Imprinting

Because of the deficiencies with moulding of cells in PDMS modifications were undertaken to develop an imprinting methodology that used photo-initiated elastomers. Photo-initiators convert absorbed light into chemical energy providing temperature-independent polymerisation and easy control of a variety of composites. Ideally, for efficient curability the emission spectrum of the excitation light source should overlap with the absorption band of the photo-initiator and there must be minimal absorption competition by the formulation components at the photo-initiator ex-

[1] All anterior pituitary cell imagery presented in this chapter are from female Sprague-Dawley rats.

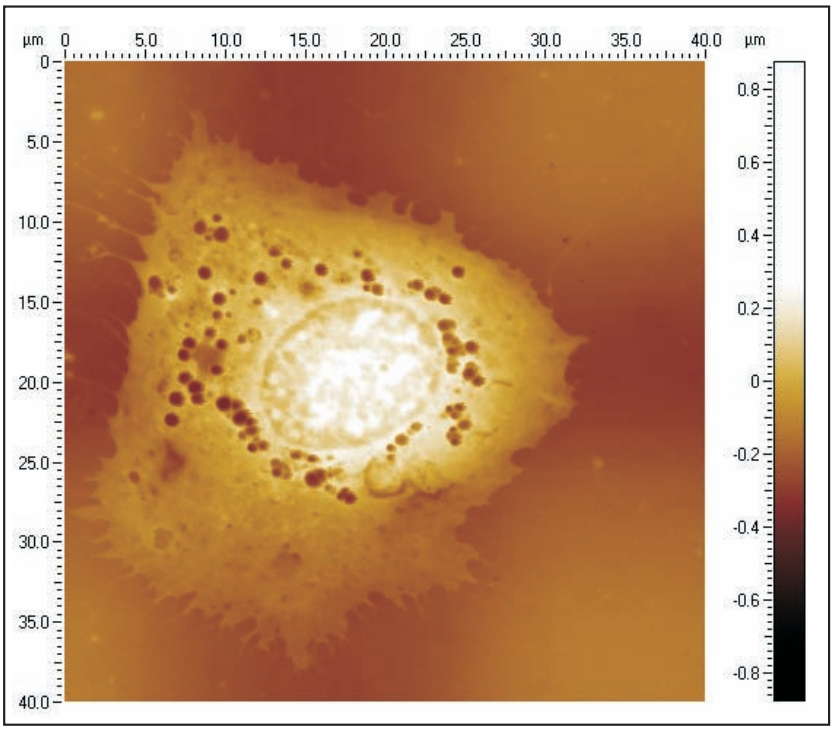

Figure 5.3: AFM image of an anterior pituitary cell replica fabricated in PDMS displaying nuclei dehydration effects.

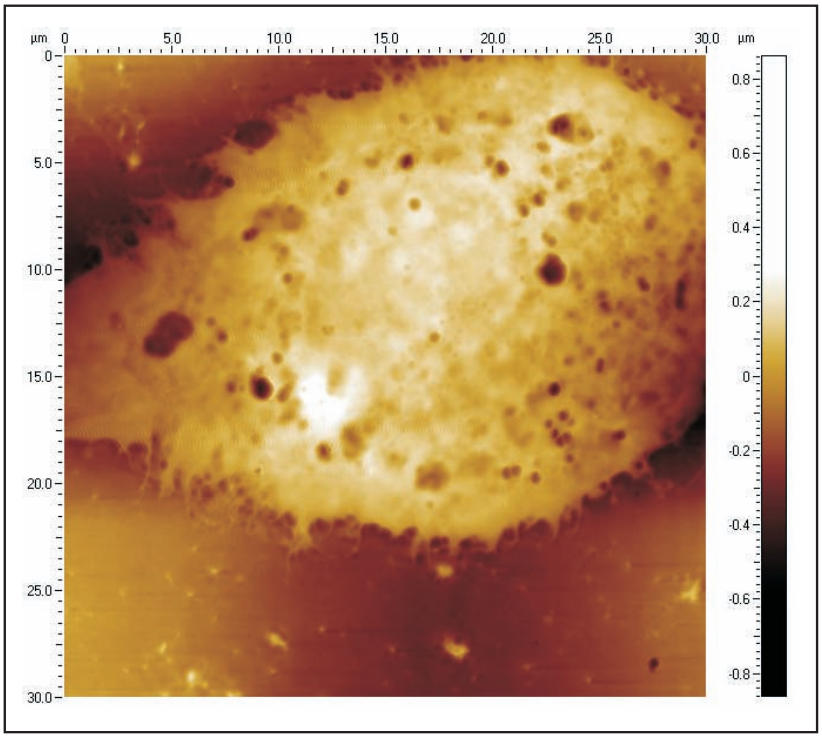

Figure 5.4: Replica of a pituitary cell fabricated in a photo-curable elastomer after 3 days culture displaying varying sized intrusions on the surface.

citation wavelengths. 2,2-Dimethoxy-2-phenylacetophenone (DMAP) is a free radical (type 1) photo-initiator (molecular -formula $C_6H_5COC(OCH_3)_2C_6H_5$, -weight 256.30) with an absorbance spectra [91] responsive to the broadband source generated by the mask-aligner's 350 W mercury lamp.[2]

By virtue of its similarity to PDMS and photo-curability speed (Methacryloxypropyl) methylsiloxane (2-4%)-dimethylsiloxane copolymer (MAPMS) RMS-033 ABCR GmbH (Karlsruhe, Germany) was selected as the UV-imprinting elastomer. Prior to imprinting all suspension medium was aspirated and samples were washed in physiological PBS. Initially, 200 mg of 99% DMAP Acros Organics (Geel, Belgium) photo-initiator was dissolved in 400 mg xylene, mixed with 10 g of MAPMS and placed in a desiccator or left overnight to remove air bubbles.

The photo-initiated MAPMS-elastomer was unable to cure in open air because of the inhibitive effects of oxygen on polymerisation. To minimise oxygen inhibition, anaerobic conditions were created by sealing the system using a transparent mask plate, which acted as an oxygen barrier as well as creating a level layer during imprinting. Alternatively, reducing agents such as amine synergists may also be used in conjunction with the photo-initiator to increase the UV polymerisation rate by acting as an oxygen scavenger in free radical formation. Otherwise, surface curing can be enhanced with nitrogen blanketing conditions.

Rather than pouring the polymer onto cells an imprinting technique was investigated. Figure 5.2 (b) illustrates the preferred pattern transfer scheme, referred to as *'UV-Bioimprint'* and used alternatively to replica moulding. Initially 1-2 g of photo-activated elastomer composite was centred on a UV-transparent mask plate and left to settle for 1-2 hrs. A mask alignment system (Karl Süss, Germany) operated in its proximity exposure setting was used as the controlled contact and leveling system. A double layer of silver tape applied to the mask acted as a spacer between the substrate and mask during WEC and contact. The mask was inverted, inserted into the mask aligner and imprinted on top of the cells. A thin layer ($\sim 150\ \mu m$) of polymer formed and was polymerised in UV-light for 2-5 mins. Advantages of

[2]DMAP photo-initiator has a low response to the I-line (365nm) node.

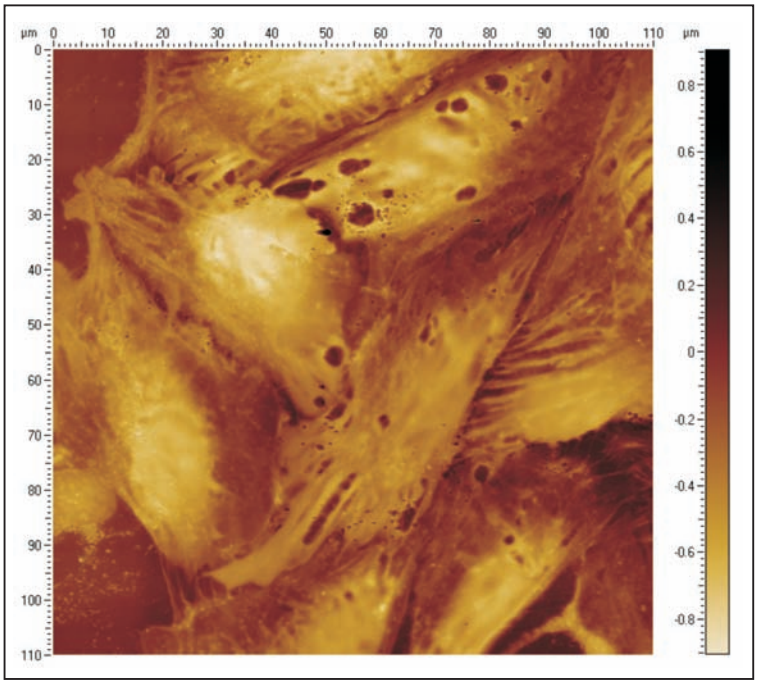

Figure 5.5: A 110 μm AFM image of a replica showing a population of untreated pituitary cells grown into confluence over a period of 5 days.

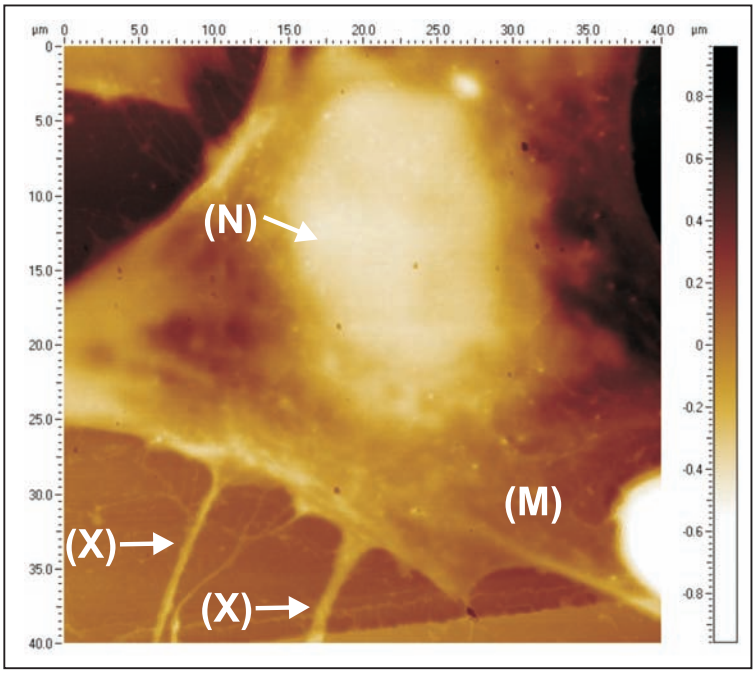

Figure 5.6: An AFM image of a single pituitary cell with extrusions (X) radiating from the cell membrane (M) and its nucleus (N) visible at the cell centre.

this technique were in the rapid curing of the polymer, and though the polymer was exposed to UV light for up to 5 mins, solidification time was significantly less ($\sim$ 30-45 secs).

In engineering the term 'imprinting', by definition is used to refer to the process of transferring a topographic pattern featured on a template to a soft polymer using pressure. However, in this case pressure driven forces act solely to form a uniform polymer layer rather than to press features upon imprint contact. When compared to PDMS, pituitary cell replicas fabricated in photo-curable elastomer as illustrated in Fig. 5.4 show improved hydration and more rounded structures.

After replication, cell impressions were imaged and checked for material transfer artifacts (eg. biological residue). If visible material transferred to the mould during imprinting, the polymer was submersed in a warm water bath solution with a non-ionic Triton X-100 detergent and ultra-sonified for 10 mins and re-checked using the AFM. If the cellular residue remained a more aggressive approach whereby the mould was submersed in acid (eg. 33 % HCl or concentrated HNO_3 acid) for 5-15 mins and if excessive material still remained the sample was either discarded or the process repeated.

Many derivations from mechanised imprinting were developed, and utilisation of the mask-aligner depended on the substrate and its compatibility with the system. It was assumed that cell viabilities diminished upon UV-irradiation but an precise moment of fatality was uncertain. In any one imprint, depending on the cell concentration, thousands of cells are replicated at once. So as to provide a proper account for but not an exhaustive number of cell images, imprints reflecting the overall cell population are provided for each experiment.

5.3 AFM Images of Bioimprints

The usefulness of UV-Bioimprint was investigated for its ability to rapidly replicate cells with nanoscale precision at a state closely reflecting a living entity. Figure 5.5

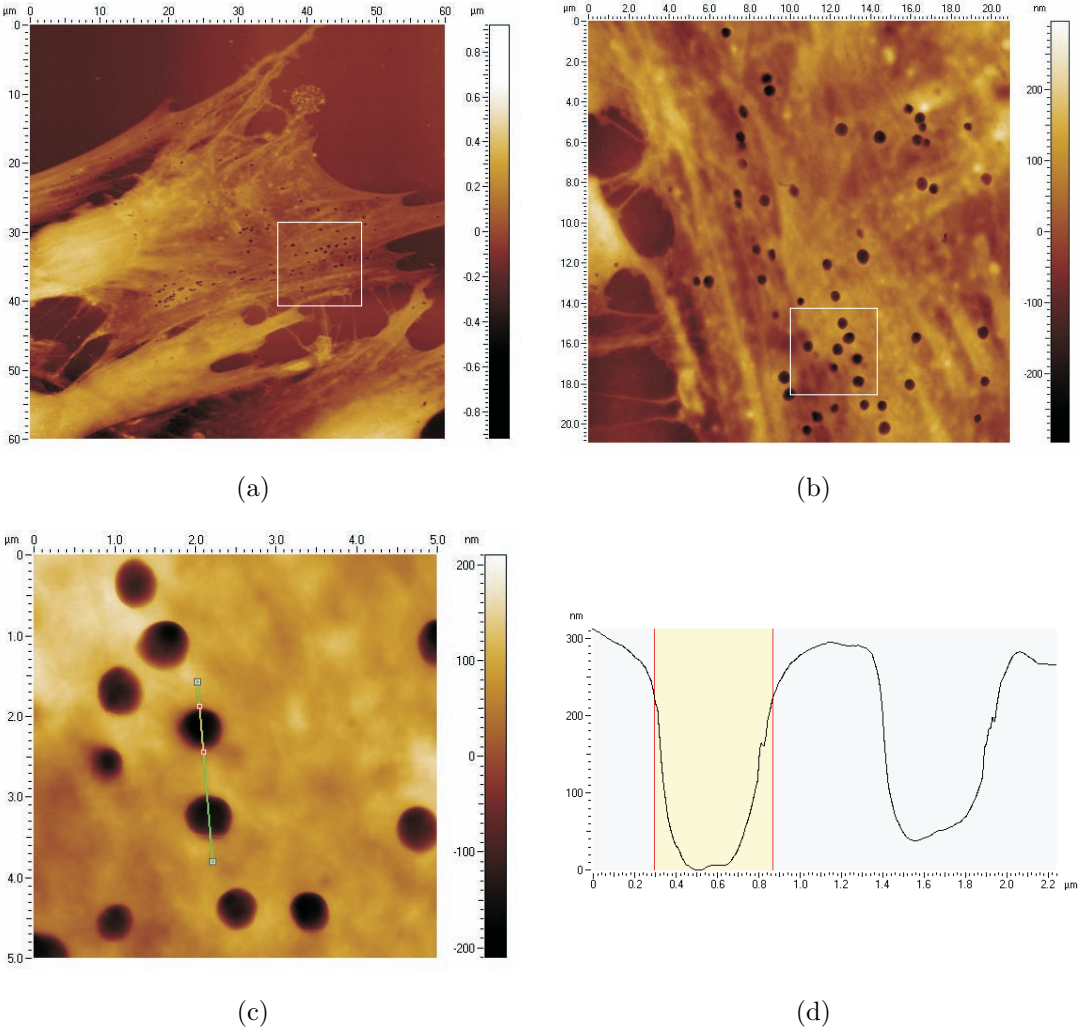

Figure 5.7: (a) UV-Bioimprints of unstimulated pituitary cells, (b) where one displays numerous fusion pores aggregated on the membrane periphery and (c,d) measuring 635/144 nm - wide/deep (calibrated).

depicts a large-area (110 μm) AFM image of a replica illustrating the close packing of an anterior pituitary cell population when cultured after 5 days. Over time cells spread out and grow flatter resulting in very small height variations at the boundaries demarcating adjacent cells. In situations of tight-packing normal/healthy cells will stop spreading when bordered by adjacent cells through contact inhibition, whereas as discussed in the following Chapter - *Bioimprint and Cancer Cells*, malignant cells will proliferate beyond boundaries into a chaotic, multi-tiered organisation.

Figure 5.6 illustrates a 40 μm AFM image of a single pituitary cell with extrusions (X) extending from the membrane (M), with a nucleus (N) form seen at the heightened point on the cell. When compared to heat curable techniques [92, 93] the membrane appears intact and well structured having no indentation profile across the cell body.

One of the motives for developing a replication methodology was to investigate the response of membrane morphology to stimuli in comparison to chemically fixed cells. Figure 5.7 illustrates a non-stimulated cell displaying numerous fusion pores, similar to those described in Chapter 4 as *'major openings'*. At higher magnification (b,c) the localisation of fusion pores on the membrane periphery are seen uniformly distributed with a scope trace (d) quantifying 3 of the pores having calibrated mean widths and depths of 635 $\pm$ 82 nm SE and 144 $\pm$ 17 nm nm SE, respectively. The number of exo-/endocytotic sites present in this particular cell were much higher compared to those adjacent, which only contained a handful of pores sporadically distributed on the membrane.

In comparison to chemically fixed cells the reduction in frequency of exo-/endocytotic structures present on the membrane in replicas is potentially explained by the controlling function of aldehydes in determining the rate of transmitter release. The effect of aldehydes may increase the rate of synaptic vesicle transmitter release [94], which could have a similar result for secretory granule exocytosis. Thus the number of pores due to basal secretion together with stimulation and fixation could be much higher than without fixation. It is additionally observed that exo-/endcytotic struc-

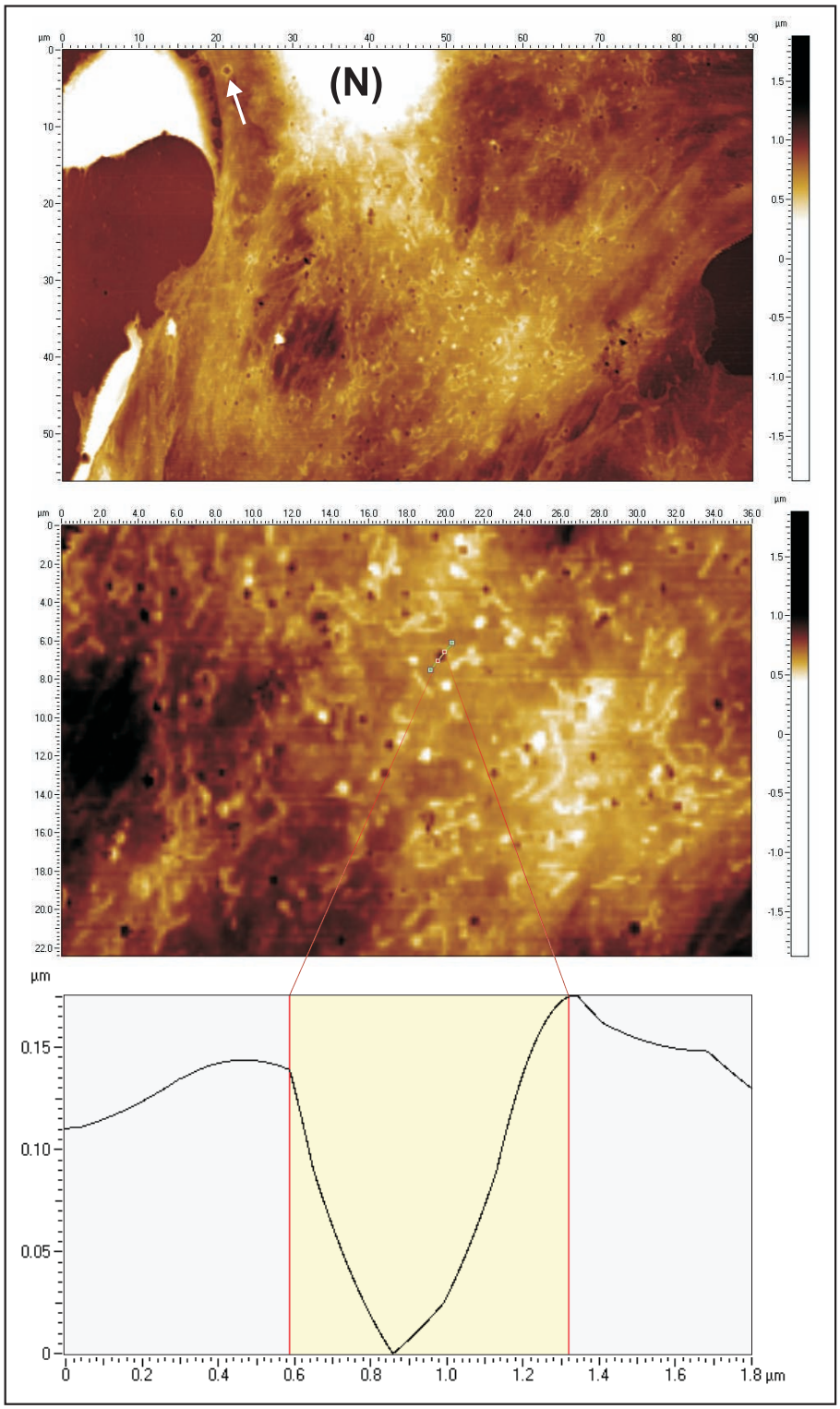

Figure 5.8: AFM image of a pituitary cell replica after treatment with GnRH-stimuli for 1 hr and fixation. Highlighted is the nuclei (N) and numerous fusion major fusion pores, one of which is depicted in the scope trace, ranging from 500-850/70-120 nm wide/deep (calibrated) and observed evenly distributed on the membrane. An arrow (top-left) points to one pore appearing like those described previously as dilated craters.

tures were slightly smaller ($\sim$ 10-20 %) and narrower in replicated cells than they were otherwise in fixed cells, which could be due to the distortion by the fixative or to the inability of the fixative to halt dynamic events at a unique transitional stage, or otherwise related to the Bioimprint replication process (eg. polymer shrinkage).

5.3.1 Bioimprint replicas of fixed cells

From the sensitivity of cells to UV light [95] it is of interest to examine the effects of UV-Bioimprint on biologically stable cells. As presented previously (Chapter 4), processing of many biological samples begins with fixation to preserve morphology and ultrastructure, which are traditional protocols used to prepare cells for analysis by scanning probe and electron microscopy. Chemical fixation was incorporated prior to replication to test if the cellular state could be frozen in time without inducing a response, which may occur during physical replication. For fixation, cells were submersed in glutaraldehyde-buffered physiological PBS solution, either at room temperature (22-24 °C) or 37 °C incubation. While fixation prior to replication is not mandatory replicas of both fixed and non-fixed cells were studied.

Stimulation studies investigating the ability of UV-Bioimprint to record a fusion pore response to GnRH stimuli were inconclusive - overall fusion pore frequencies were alike regardless of stimuli conditions. To examine if the UV-imprinting replication methodology was rapid enough to capture a fusion pore response to GnRH, with the assistance of fixation, cells were subjected to GnRH and submersed in glutaraldehyde for 1 hr prior to replication. Figure 5.8 illustrates an AFM image of an anterior pituitary cell cultured for 4 days prior to application of GnRH stimuli and fixation at 37 °C incubation for 30 mins. Major fusion pore openings, similar to those in unstimulated cells (Fig. 5.7) 300-700 nm wide saturated entire areas on the membrane, with a solitary pore highlighted using an arrow (top-left) appearing like those described previously as ‘dilated craters’ - potentially indicating an interconnection between these two different pore types, or otherwise pores regulated by different mechanisms. While this image illustrates significantly more fusion pores

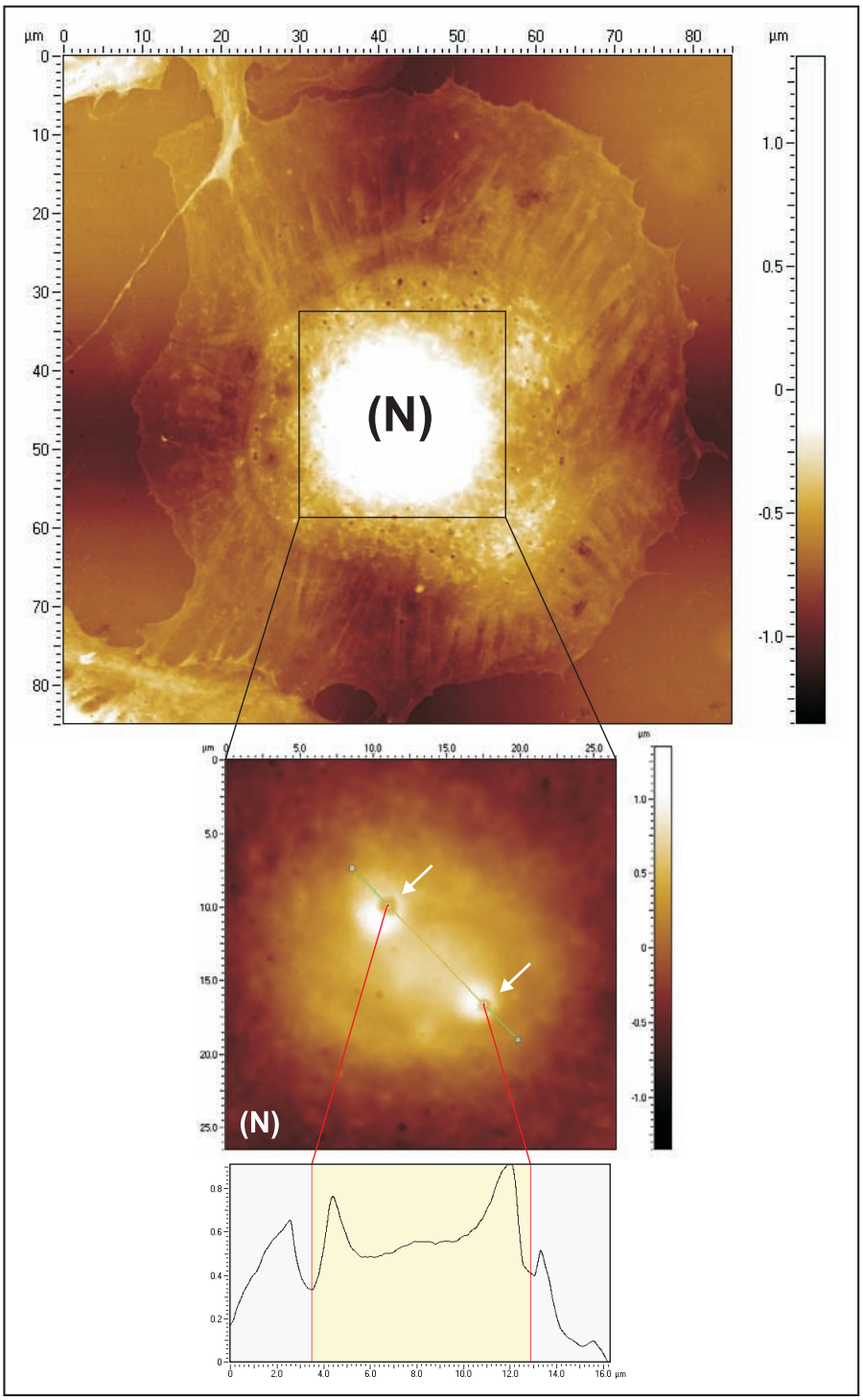

Figure 5.9: Replica (AFM flattened) of a pituitary cell cultured for 4 days and chemically fixed (30 mins at 37 °C incubation) in glutaraldehyde post GnRH-stimulation (1 hr) prior to replication. Visible features show the membrane spread over the surface and mounded-invaginations (arrows) positioned above the nuclei (N), with their cross-sectioned profiles illustrated by a scope trace (un-flattened).

compared to non-stimulated cells, even with the aid of fixation, on average, fusion pores failed to display an overwhelming response. However, it should be mentioned that the frequency of fusion pores is not necessarily indicative of a cell's state of stimulation. Only a small proportion of cells representing gonadotrophs are ever likely to respond to GnRH, which makes concluding stimulation from taking an average count of fusion pores across all cells difficult given the likeliness of pores in other cell types to fluctuate.

At these fixative conditions (ie. 37 °C incubation for 30 mins) distinct structures best described as *'mounded invaginations'* (previously referred to as 'mounded-channels' in [96]) were observed in a number of cells. These features appeared as protrusions with a single deep invagination present at each summit and are highlighted by arrows in the 85 μm AFM image shown in Fig. 5.9. Mounded invaginations were localised on the membrane at heightened points on the cell, which appeared to be at positions on the membrane overlying the cell nucleus. Mounds similar to those introduced in Chapter 4, without any invaginations were also frequently seen in the majority of fixed cells. In this instance invaginations appeared most distinctly in replicas of cells subjected to GnRH prior to being fixed at 37 °C for 30 mins as shown in Fig. 5.10 - arrows highlight the more obvious mounded invaginations in the majority of cells captured in the four 110 μm AFM scans. Mounds were distinguishable by several characteristics; their formation on the membrane above the nuclei, only a handful ever present on any given cell, large sizes (1-3 μm), evenly distributed above the nuclei, and when they contained invaginations, they extended deep within the cell. However, as shown by the replicas in Fig. 5.11, studies testing the effect of glutaraldehyde at 2.25 % concentration at different incubation temperatures and time revealed no such features, either at (a) 37 °C for 30 mins or at (b) room temperature for 1 hr. Similarly, replicas (not shown) also confirmed the absence of mounded invaginations in cells subjected to GnRH, indicating that the degree and severity of the mounds and the presence of invaginations are highly correlated to fixative conditions.

For the preservation of most microscale features chemical fixatives are considered to

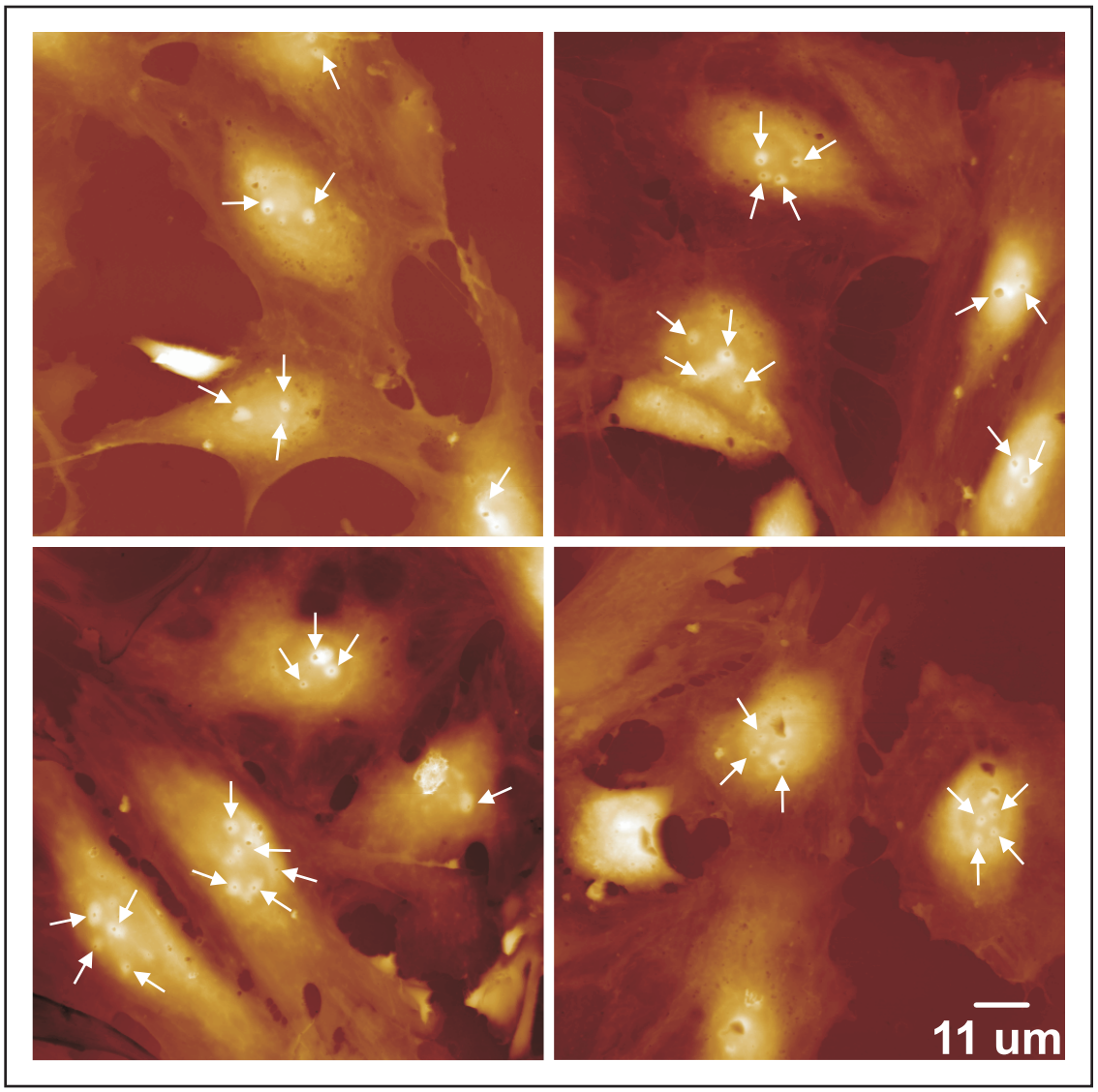

Figure 5.10: Four large-area (110 μm) AFM replica images of pituitary cells cultured for 4 days and subjected to GnRH-stimuli for 1 hr prior to being fixed in glutaraldehyde for 30 mins at 37 °C incubation. Arrows highlight the mounded invaginations, which frequently appeared ruptured at heightened positions on the membrane.

adequately preserve cellular structure, and at the surface appeared to be relatively quick acting in crosslinking membrane proteins into permanent stasis. However, glutaraldehyde penetrates tissues slowly, which possibly explains the continuing function of cells at thicker-nuclei locations. In circumstances where chemical fixation conditions resulted in mounds and invaginations forming, there is no evidence to suggest that these are not natural structures with a physiological role, or that invaginations are a fine structure representing an entity that may have a channel-like function. Yet their absence from *in vitro* studies performed by transmitted-light optical microscopy and their selective appearance at certain fixative conditions meant they are most likely artifactual occurrences. One of many possible explanations for their origin is that they are due to a pressure imbalance from within the cell created against the fixed membrane from higher incubation temperatures.

Generally fixation agents such as glutaraldehyde are thought to rapidly kill and stabilise the cell, though they are not without consequence and inevitably produce structural changes and effects [97]. In histology, these alterations are often referred to generally as fixation artifacts. The fixative may distort the cell and its components in manners ranging from cell enlargement or swelling to a complicated mix of intra-cellular responses and effects. Several fixation artifacts have also been reported during granule fusion with the plasma membrane [98], such as intra-membrane clearing of particles on the membrane overlying secretory granules prior to exocytosis. Artifacts have also been reported post-fixation, where glutaraldehyde was either unable to halt fusion components or fusion was induced after fixation. More specifically, aldehyde fixation in cells is known to cause cytoplasmic tubules and membranes to fragment and vesiculate [99, 100] as well as the outward ballooning of blister-like blebs extending from the plasma membrane. Though often named interchangeably, there are subtle differences between blebs and blisters [76] formed as artifacts from fixation, namely that blebs are bounded by a membrane containing inter-membrane particles [101].

A further possibility is that mounded-invaginations are formed by a highly localised increase in membrane mobility at sites withstanding fixation - a combination of fix-

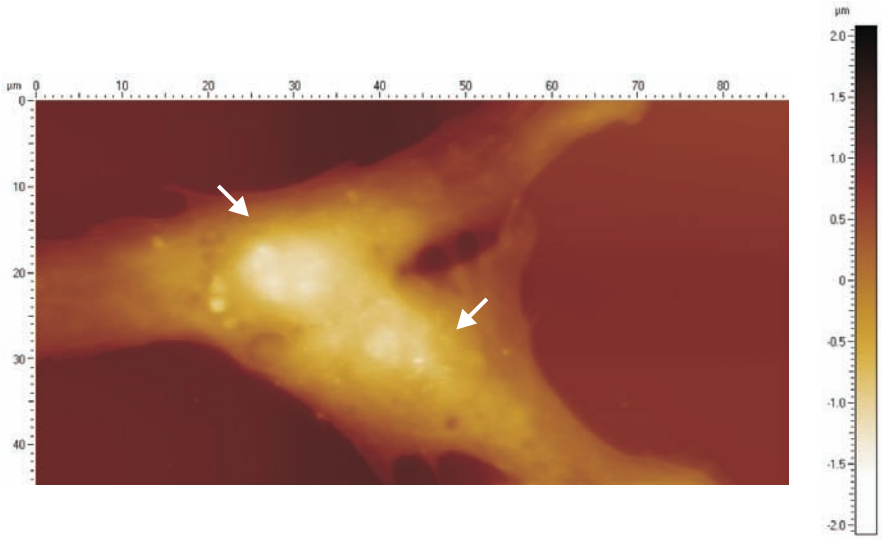

(a)

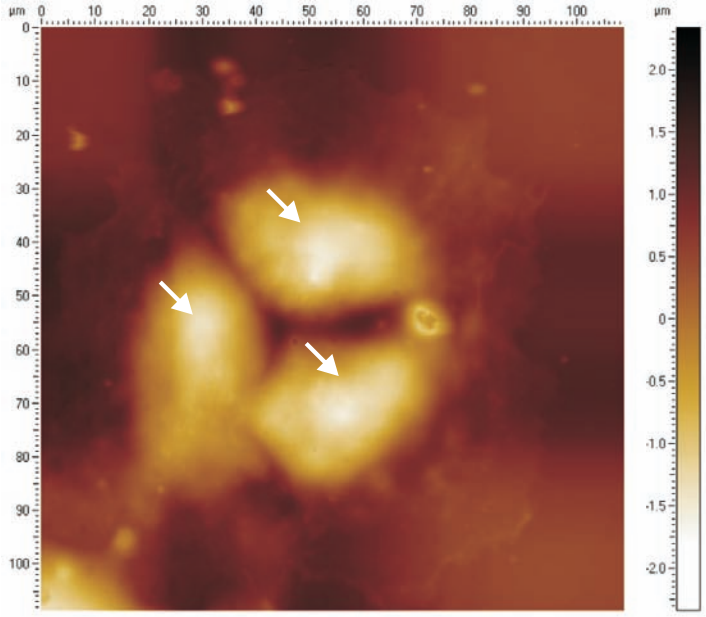

(b)

Figure 5.11: AFM image of pituitary cell replicas where arrows are used to highlight (a) 2 cells cultured over 3 days and fixed in glutaraldehyde at 2.25 % concentration for 30 mins at 37 °C incubation, and (b) a grouping of 3 cells treated in glutaraldehyde of the same concentration for 1 hr at room temperature.

ative effects and dynamic cellular mechanics acting on cross-linked membrane by GnRH stimulation. The readiness of glutaraldehyde to cross-link proteins combined with its inability to effectively react and preserve phospholipids [102, 103] abundant in the plasma membrane means it is a poor fixative for exocytotic fusion sites undergoing rapid changes. One reason for the varying effects of fixatives were thought to be related to the differential modes of action at the membrane. Another explanation for the unusual forms can also be explained by fixation conditions such as incubation temperature, which may cause over-fixation, likely resulting in the expulsion of nuclear constituents transported through mounds that have ruptured at the invagination [104].

5.4 Discussion

This research reports the detection of morphologically distinct fusion pores similar in shape, dimensions and characteristics to those described as major openings in direct imaging of fixed cells - Chapter 4. Significant aggregation of fusion pores appeared to be dependent partly on nuclear location, which had a significant effect on their distribution. Upon UV-irradiation it is thought replication is able to lock cellular processes within 20-40 secs during which the polymer is able to sufficiently harden. However, depending on cell type and whether the exocytotic mechanisms maybe transient or total, fusion may last only milliseconds. Failure to image other varieties of fusion pores (eg. craters, channels) described previously in Chapter 4 is possibly explained by their transient or rapid response to the polymer, their existence as permeation artifacts from dehydration and drying or lack of replica resolution.

Freeze fracture studies [105] in mast cells have shown time sequences for various stages of exocytosis lasting 15 seconds after stimulation. However, it still remains a challenge for the Bioimprint process to rapidly replicate cells at physiological conditions within such periods. Compared to methods with heat-curable polymers UV-Bioimprint presents a remarkable improvement in replication time but further testing is required to establish if the impression accurately represents a living cell.

A trade-off in conditions suited for replica fabrication while maintaining physiology relates to the amount of fluid in the layer between the cell and the polymer. Removal of too much culture medium inevitably exposes the cell surface to high water tension forces and causes aridity, resulting in dehydration in both unfixed and fixed cells. On the other hand, the interfacial fluid layer remaining after aspiration and its inhibitory effect in the resolution transfer of cell topography into the polymer was equally an issue.

It is reasonable to suspect that routine interpretations of living cells by replication or fixative treatments may produce significant changes in morphology. The impact of fixative chemicals on cell topology enforces the need to develop alternative stand-alone methods and techniques that do not require prior treatment, and facilitate integration with high resolution imagery tools. Evidently there were several drawbacks associated with the current replication conditions. Issues such as subjecting cells to a preservative environment while applying UV light outside of physiological conditions undoubtedly causes harm to cellular structure. In order to reduce the impact caused by the harmful UV rays on cells selecting a non-destructive polymer reactive at physiological conditions, which retains its structural resolution remains to be discovered. Producing reliable and accurate replicas offer many advantages over direct imaging but there remains several issues, such as dehydration during replication, and matching optimal conditions for replica fabrication while maintaining physiology, which need to be addressed before widespread acceptance. Though doubt remains whether replicas reflect true biology they are nevertheless an accurate representation of chemically fixed cells.

When compared to direct-ambient cellular imaging (Chapter 4), replicas demonstrated a low surface roughness and displayed good fidelity in resolution and ultrastructure. In terms of scan lines Bioimprint produced cleaner AFM images, perhaps, in part due to the stabilisation and removal of loose extra-cellular particles and structures (eg. microvilli) into the polymer. In the absence of chemical fixation replicas showed no evidence of artifacts forming on the membrane over the nuclei, presenting researchers with an alternative choice for preparation of cells for microscopy. In

order to capture the physiological form an optimal process for fabrication of true-to-life imprints may include a combined chemical and physical replication technique. Otherwise, incorporating a cryogenic freezing method to the replication process may offer more reliable results.

Advantages of cellular replication extend beyond its primary application of being a non-destructive solution for AFM imaging, providing both a suitable and reproducible medium for examination of cell topography for a range of analytical tools. It is also possible to completely analyse, over a long period of time, large sample populations treated in similar conditions offering savings in materials and resources that are copiously wasted as a result of disintegration of biological material. It is envisioned that with further development Bioimprint will facilitate the integration of nano-imagery tools to the enhancement and understanding of biological mechanisms at the molecular level.

Chapter 6

Bioimprint and Cancer Cells

Each year around 40,000 women learn they have endometrial (uterine) cancer in the USA alone, making it the fourth most common cancer in women. Despite recent headway in understanding pathological changes in cancer cells, verification still requires biopsy inspection by optical microscopy such as when screening for malignant and premalignant changes of the cervix by Pap smear [106]. A tumour in a specific progressive state can have distinct structural changes - nucleus size, shape and cell morphology texture, to name a few, are related to the functional alterations in cancer cells and may offer crucial information to a particular tumour type and hold the key to successful treatment. For over a century identifying these changes has been the benchmark for cancer diagnosis but it has been difficult to correlate a relationship between morphology and malignant phenotype, in part due to the poor understanding of the functional significance of many of these features.

Currently, optical microscopy techniques are the primary method for cell surface visualisation, with microscopic characteristics such as those illustrated in Fig. 6.1 traditionally used for diagnosis and classification of cancers. However, because these differences can be subtle, accurate detection can be challenging and ambiguous [107] due to the diffraction limit of light preventing nanoscale markers from furthering the potential for visual diagnosis. The AFM's superior resolution enables exploration of new topographic identities, which when combined with fusion pore attributes are

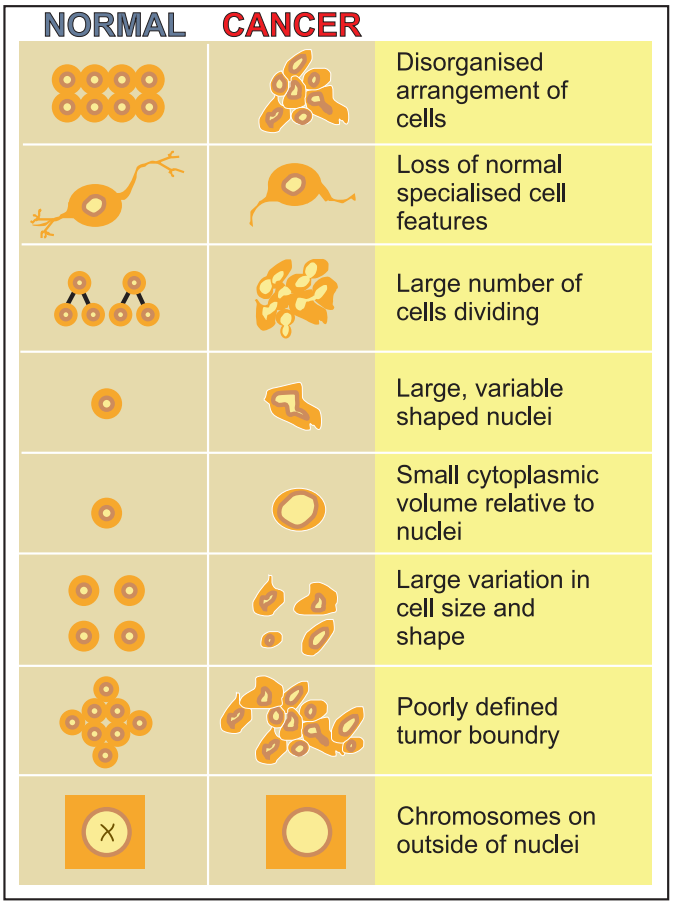

Figure 6.1: Generic mutations and abnormalities in many cancer cell types [108].

potential methods for cancer cell identification.

This chapter presents an investigation on the ability for Bioimprint to recreate cancer cell topography in PDMS using the replica moulding method previously described in Chapter 5. As non-malignant endometrial cells were not immediately available to be used as controls this work represents a preliminary study.

6.1 Fusion Pores

A limitation of the PDMS replica moulding methodology was its lack of precision in fabricating accurate and consistent living cell moulds. Curing conditions were too slow and a large proportion of the cells inevitably failed to be accurately replicated due to severe dehydration. Figure 6.2 depicts a malignant endometrial cell replica

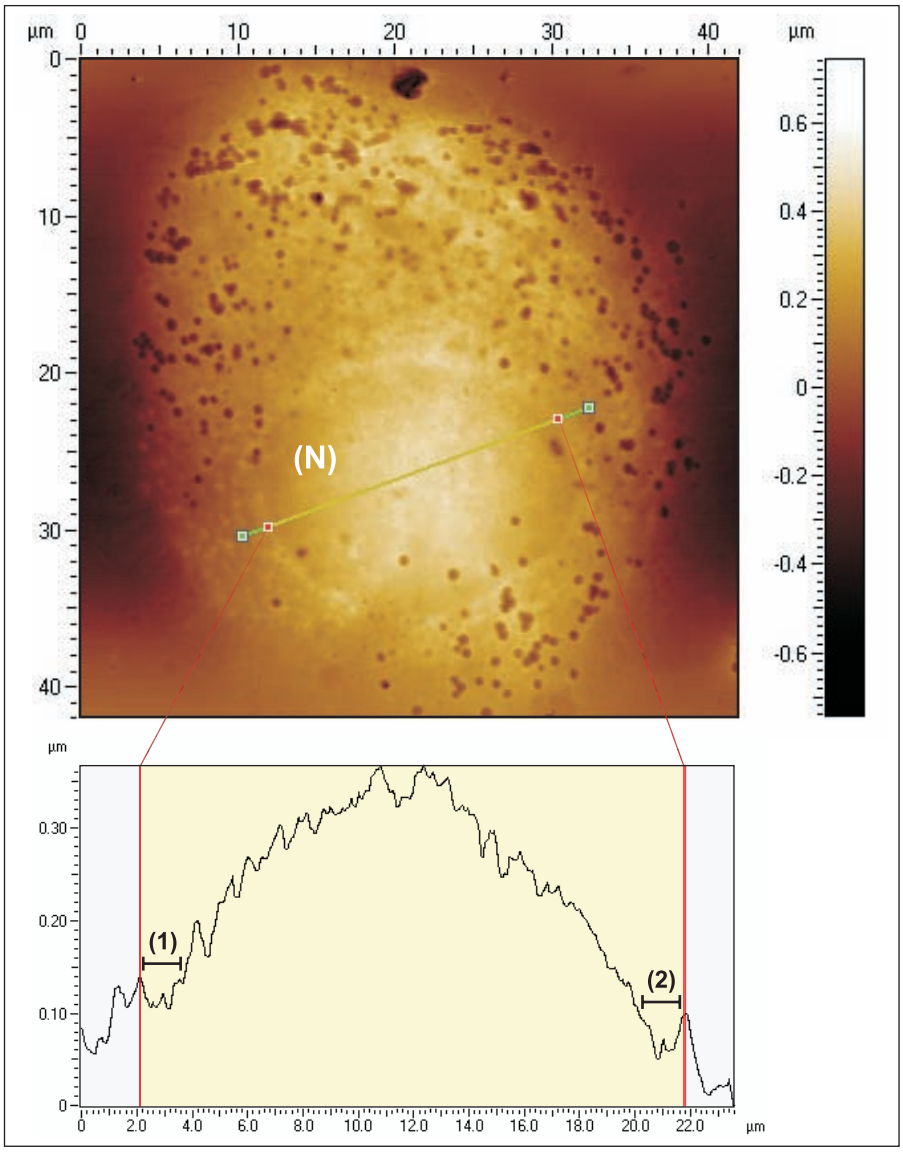

Figure 6.2: AFM image of a 40 μm endometrial cancer cell replica showing numerous pores scattered on the membrane. A scope trace focused on the membrane above the nucleus highlights the dehydration-indentation profile beginning and ending at locations (1),(2) on the membrane at the edge of the nucleus.

displaying distinct features at both micro and nanoscales. Scattered on the membrane are numerous pores with mean widths and depths of 820 nm and 360 nm, respectively. Though they appear relatively large they are potentially associated with exocytosis and bear similarity to *'major openings'* described in Chapter 4. In this investigation references to elements appearing similar to fusion elements are termed 'pores' due to the potential impact of the PDMS replica moulding process, and the influence of permeation artifacts in causing cell deformities. A spherical form underlying the cell membrane is assumed to be the nucleus (N), and its outline is shown in a scope trace revealing the impact and distortion on the cell membrane beginning and ending at points (1),(2) on the membrane. Collapse or dematerialisation of the nuclear structure is a feature resulting from cell dehydration and was relatively widespread in the cells imaged. When investigating the dehydration effects on malignant mesothelioma cells using the AFM Weyn et al. [90] also reported a much harder and uniform indentation profile over the entire cell, compared to hydrated cells, which displayed more rounded and smooth surfaces.

The impact of the nucleus location on the formation of pores is further evident in Fig. 6.2, where pores are seen predominantly concentrated at surrounding areas. This is reinforced in the AFM image shown in Fig. 6.3, where the majority of pores are scattered around the nucleus (N). Here in contrast to Fig. 6.2, the nucleus appears well hydrated and as a uniform rounded structure with no indentation features across the nucleus. Locations on the membrane surrounding the nucleus are seen saturated by various sized spherical pores.

In Fig. 6.4 a 10 μm image focused on an area of the membrane from Fig. 6.3 illustrates the variation in the size of pores on the membrane. Collectively visible are larger and smaller pores shown by points (1) and (2), which are analogous to *'craters'* and *'major openings'* (see Chapter 4), respectively. Absence of a ring-like structure appearing around larger pores meant they were not entirely identical to craters and perhaps represented a unique structure in their own right. One hypothesis speculates their association to sites of repeated fusion in compound exocytosis, with smaller pores being primary fused granule-pores (refer to Chapter 1 - *Introduction*). One of

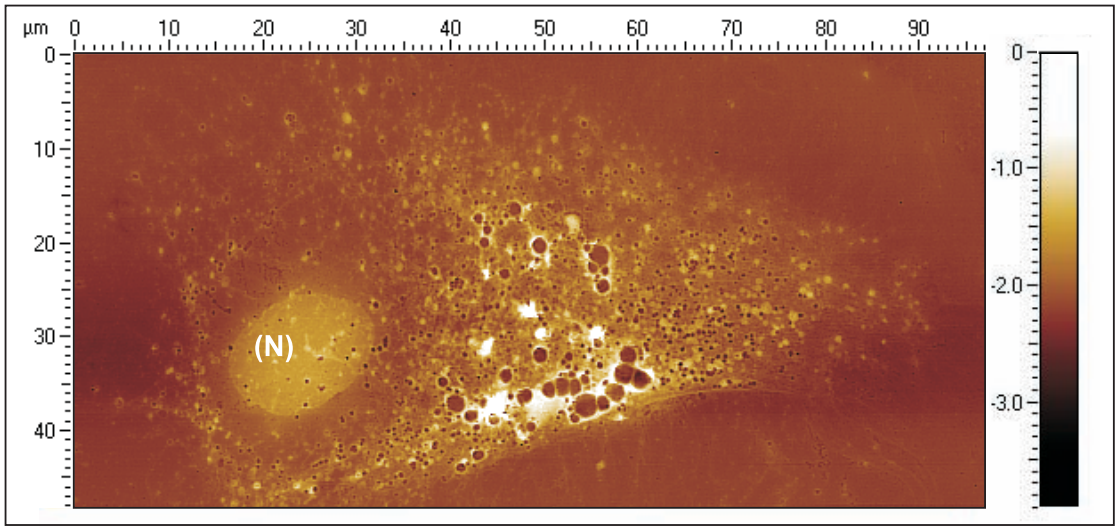

Figure 6.3: Large-area (100 μm wide) AFM scan of a replica made from an endometrial cancer cell, illustrating a rounded nucleus (N) beneath a membrane containing numerous pores of varying sizes.

the advantages of the AFM is its ability to accurately produce 3D topography with a high degree of contrast, whereas with radiation scattered devices the contrast is weak and the Z-dimension is often disregarded as diagnostic evidence. Demonstrating the AFM's advantage for measuring small Z-variations is shown by the scope trace in Fig. 6.4, which quantifies the cross-sectional dimensions of 3 smaller pores having an average diameter of 600 nm and depth of 80 nm.

6.2 Tumour Cells

Observations in this study suggest that cells had diverse morphologies potentially caused by cancer mutations, which act to deform and distort the cell [109, 110] resulting in complex and varying forms. Even considering the potential artifacts introduced during replication cells demonstrated a large variability in the shape and locations of specific features, namely the nucleus and membrane. Figure 6.5 reinforces this observation through an endometrial cancer cell replica bearing a different nuclear appearance and cellular arrangement from those presented previously. A

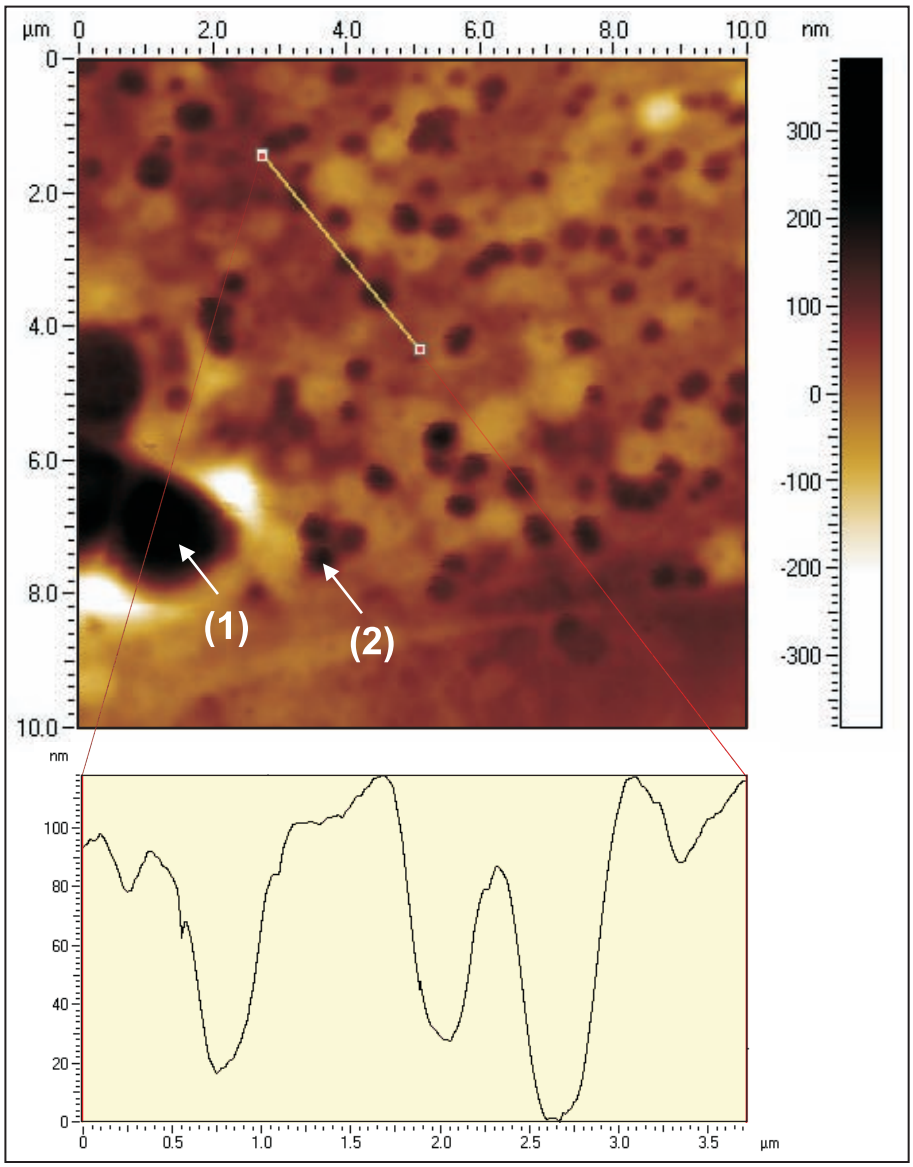

Figure 6.4: A 10 μm AFM height image taken from a replica showing two types of pores scattered on the membrane of a malignant endometrial cell - deep and wide (1) as well as more abundant smaller and shallower (2) depressions. A scope trace taken across the membrane illustrates three smaller pores with opening widths of approximately 600 nm and 100 nm deep and formed as concave submersions.

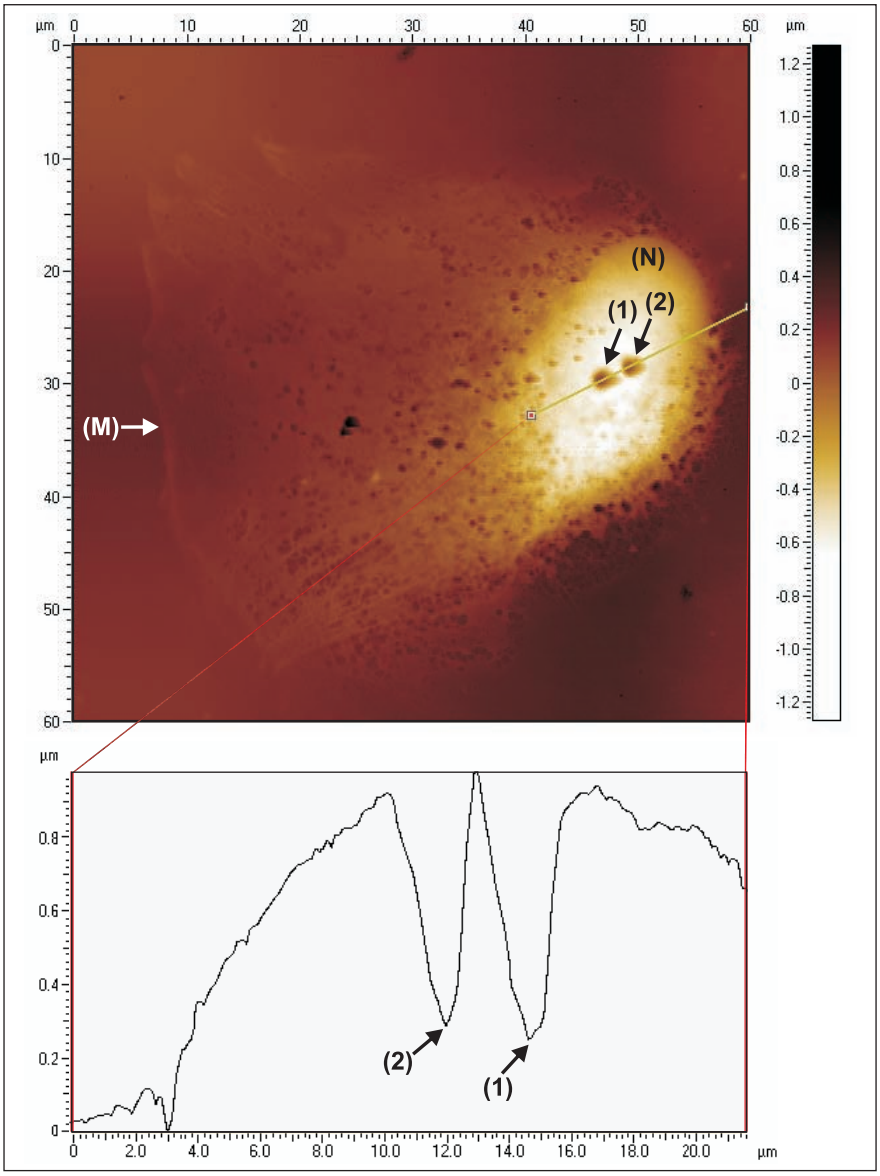

Figure 6.5: A replica from a 50 μm endometrial cancer cell, showing the membrane extending leftwards from a 1 μm tall rounded nucleus (N) body, which is seen to contain two large ruptured depressions (1),(2). A scope trace examining these ruptures (1),(2) depicts them being approximately 3 μm wide and submersing deep within the cell.

rounded nucleus (N) is seen clearly offset to the right of the cell, with the membrane extending leftwards. Again, numerous pores are seen located on the membrane around the nucleus, but especially apparent are two large invaginations above the nucleus. The scope trace in Fig. 6.5 quantifies the invaginations being approximately 3 μm wide and extending at least 700 nm deep within the cell. However, their true shape and depth are difficult to accurately measure due to limitations associated with the imaging tip, which has resulted in a scope trace distorted by tip geometry.

Further illustrating the range and variation of cell morphologies, and the potential effect of prolonged replication in PDMS has in generating nuclei artifacts is illustrated in Fig. 6.6 (a) - an AFM image of a replica from a 40 μm malignant endometrial cell contains a distinct nucleus (N) form appearing to protrude above the surrounding membrane. The scope trace in (b) quantifies the nucleus to be 18 μm wide, which is seen extending sharply $\sim$ 300 nm above the surrounding cell body. While other cells imaged also displayed large variations in nuclei and membrane forms, without non-malignant controls it remains uncertain whether they are artifacts induced from the Bioimprint process or are characteristics of tumour cells.

6.3 Discussion

Much remains unknown about the morphological characteristics of endometrial cancer cells and there are few methods designed to visualise cell topography in air and at high resolution without chemical fixation. Only a select number of cells depicting diverse morphologies were chosen to illustrate examples of malignant identities. On a larger scale, the ability to directly view an established catalogue describing a wide-range of potential cancer marker identities using the AFM could assist pathologists in cancer diagnosis. As well as morphology, considerable variation in the presence and sizes of pores, as well as their dynamic formation and grouping, illustrates that they in their own right are possible bio-marker candidates.

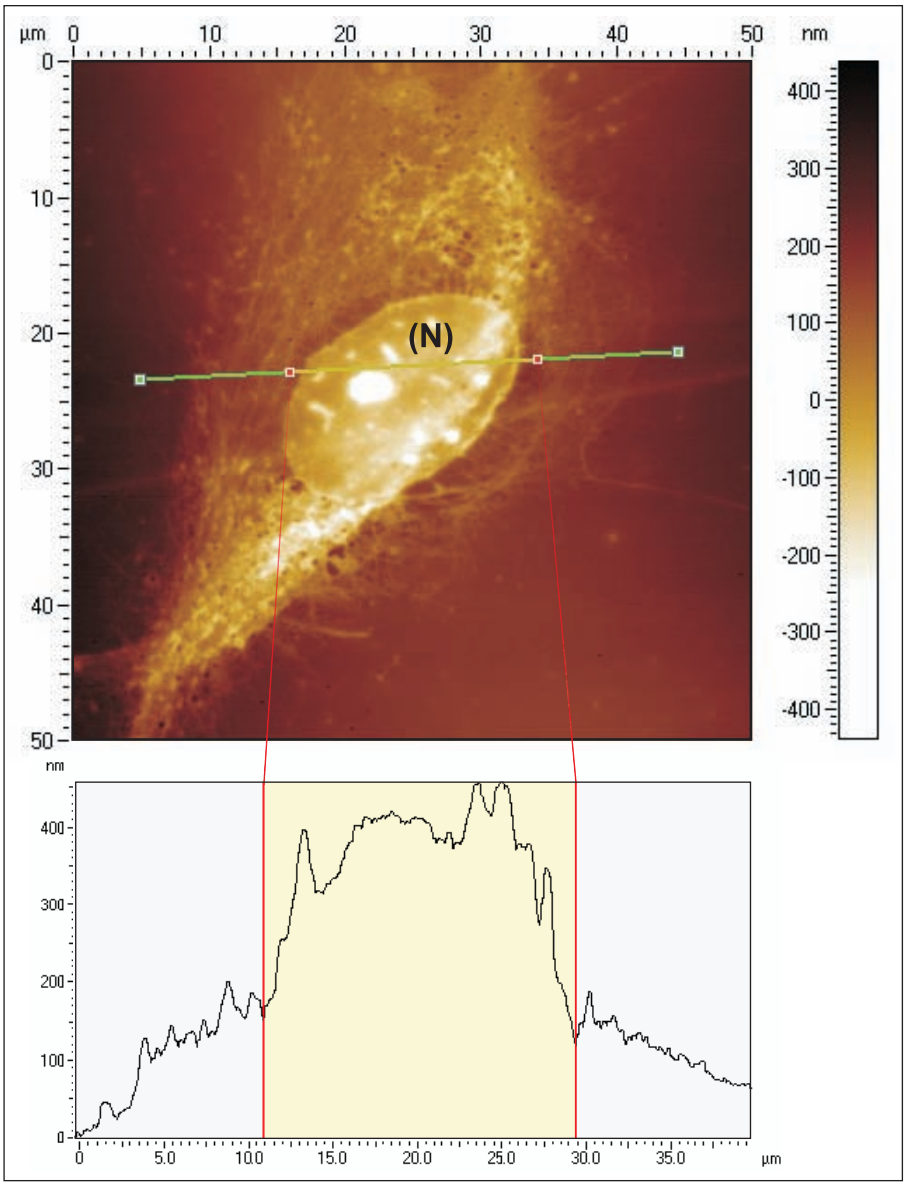

Figure 6.6: A 50 μm AFM scan of a Bioimprint replica showing a malignant endometrial cell with a nucleus (N), seen distinctly protruding from above the surrounding membrane. The scope trace shows the nucleus to be 18 μm wide, extending approximately 300 nm above above the surrounding cell body.

One disadvantage of the AFM when applied to investigate endometrial carcinomas is its limited scan size. Many established 'micro-mutations' are based on characteristics describing overall cell population growth and organisation (Fig. 6.1). Whereas the AFM is only really effective for studying single-cells due to its restricted lateral boundaries (eg. 110 μm^2 - DI 3100 AFM). This drawback is potentially avoided when applied as a complementary technique to conventional optical imaging, and as alternative to methodologies requiring chemical processing. Additionally, using Bioimprint cells, which potentially host diseases, can be replicated and transported without contamination concerns, reducing the necessity for complicated and lengthy documental approval and facilitating out-of-house analysis. Further gain is realised in the ability to keep an indirect specimen record without the need for storage or confinement equipment.

With respect to replica moulding, impressions represent severely 'time-averaged' pictures of cellular condition due to the considerable time for PDMS to cure at incubation temperatures. Over this period artifacts are inevitably introduced by cellular response to the polymer and curing conditions, which are particularly evident by the impact at nuclear locations and likely explain exaggerated pores sizes. An increase in the pore numbers in comparison to replicas of pituitary cells could be a result of the hypoxic affect of the polymer. Equally as likely, are pores being openings on the membrane representing permeation artifacts. Unfortunately, conclusive models describing cell permeability effects using the AFM are limited, and without either seeing their formation or verifying their functionality one can only speculate on their origin.

By fabricating cell topology in a non-degrading polymer a permanent record is created while avoiding many of the inherent difficulties associated with cellular imaging using the AFM. Being able to view and potentially characterise cell variations at micro and nanoscales presents a remarked improvement over conventional optics. In addition to the higher resolution of the AFM a significant advantage over radiation scattered imaging devices is the production of imagery in 3D. When integrated with a more suitable replication technique (eg. UV-Bioimprint - Chapter 5), a system

utilising the sensitivity of the AFM to image cell topography contained in a more suitable medium will provide an ideal method to study fusion pores. With visual verification ultimately being the mainstay for cancer diagnosis cellular analysis using the AFM enables characterisation of morphological abnormalities at the nanoscale. However, without controls it is difficult to deduce if the various shapes and forms are potential markers specific to malignancies, or whether they are artifacts induced by the replication process.

Chapter 7

Biochip

To advance the integration of automated laboratory systems for single-cell identification and analysis it is useful to position cells into organised arrangements. Using an electrokinetic phenomena known as dielectrophoresis (DEP), non-uniform AC electric fields generated by interdigitated microelectrode arrays provide an ideal method for manipulating and controlling particles [111]. An electrode array chip known as the *'Biochip'* has been developed to trap single-cells within cavities for high resolution analysis. In one method cells are captured on the Biochip using positive and negative DEP forces by placing cavities at maxima and minima areas of electric field intensity, respectively.

The motivation for development of the Biochip is to substitute the requirement of prolonging culture times in order to reduce cell heights. Instead by efficiently placing cells within cavities their heights are lowered to within a set-scan level enabling faster time-to-analysis.

7.1 Background

Electrokinetic interaction of AC fields with cells presents an electrically controllable method of trapping living cells based on their unique dielectric properties. Cellular dielectric properties act as an invisible fingerprint, whereby composition and

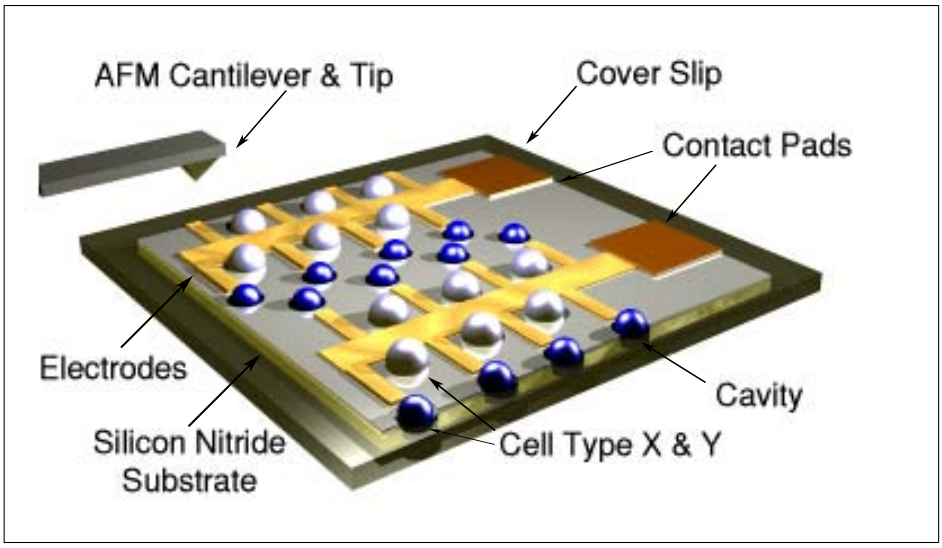

Figure 7.1: Illustration of the Biochip concept: Cells are trapped within cavities by a series of interdigitated electrodes where they are then scanned using the AFM.

structure rich data, which is the cell itself, are the fundamental drivers for DEP. Utilising the cell's unique response to the electric field gradients an induced DEP force directs the particle to high and low field gradients generated by the irregular electrode structures.

The main components and concept of the Biochip system are illustrated in Fig. 7.1 - an array of micro-cavities are aligned between a series of interdigitated electrodes. Cavities etched within the surface of the Biochip at regions of intense and weak fields act as incubators, trapping cells at known positions on the substrate's surface. Each cavity has a unique locator enabling single-cell handling, addressing and identification throughout experimentation.

Submersion and immobilisation of cells within cavities allows 'upper-body' AFM analysis of the cellular structure. The cell protrudes enough of its surface to enable imaging of the exposed cellular body (above the cavity) without breaching its Z-limitation. A 3D AFM image of this concept is illustrated in Fig. 7.2, whereby a series of 10 μm latex beads are trapped within cavities alongside a planar interdigitated electrode by positive DEP. Separately, using the 'pointed' microelectrode configuration on the Biochip, Fig. 7.3 shows a single bead trapped within a cav-

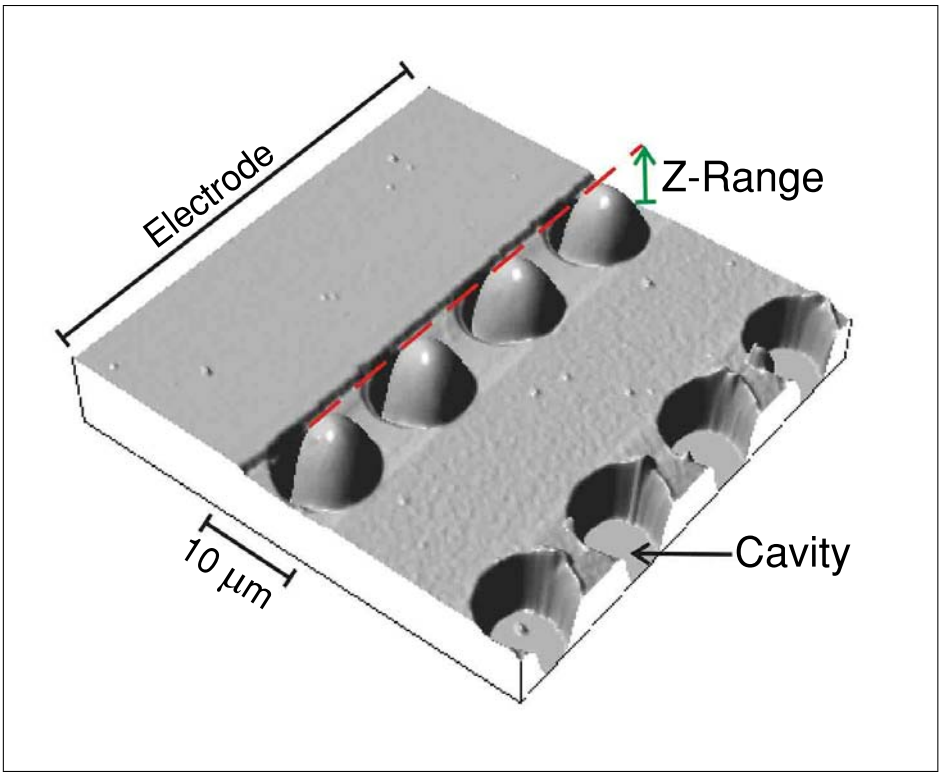

Figure 7.2: AFM micrograph showing a series of 10 μm polystyrene microspheres trapped in cavities alongside a planar electrode system on the Biochip. The image illustrates how by submersing particles within the substrate one can work within the Z-range of the AFM.

ity by positive DEP. An AFM's Z-range as discussed in Chapter 2 is defined as the scannable height range (at its set-point) imposed by the piezoelectric tube. Without placement of microspheres within cavities, height in the positive 'Z' direction from the substrate would significantly exceed its range (6 μm - DI 3100 AFM), resulting in a 'tip retraction' and image loss thereafter. Cavities also serve the purpose of anchoring cells in position and preventing the probe from dragging the object during scanning.

In this chapter an integrative approach for capturing, trapping and precisely positioning cells at known locations using the Biochip is developed and tested. Fabrication of the platform is presented along with a demonstration of the platforms suitability for AFM analysis using Bioimprint.

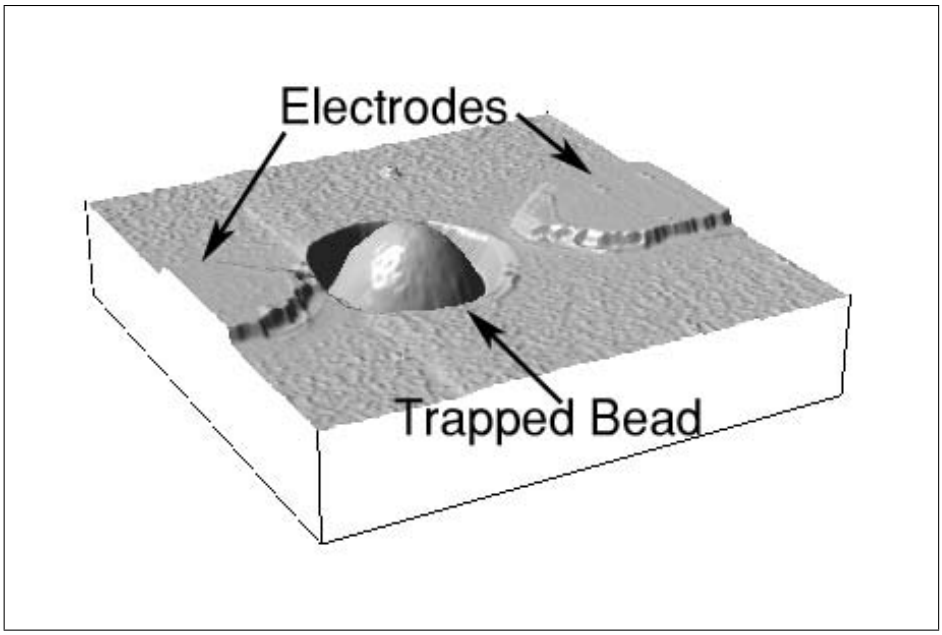

Figure 7.3: 3D AFM image (air-tapping mode) of a bead on the Biochip trapped within a cavity using positive DEP by the interdigitated pointed electrodes.

7.1.1 Dielectrophoresis

AC electrokinetics provides a frequency controllable method for positioning and manipulating cells. A cell present in a uniform electric field will experience no net force as a result of the cancelation of Coulomb charges. If however, the field is non-uniform and varying in magnitude across the cellular space, non-equilibrium Coulomb charges will create a net DEP force [112]. The interaction of dipole moments induced in the cell with the gradients of electric fields results in movement of the cell toward or away from regions of intense electric field gradients by forces known as positive and negative DEP, respectively. The magnitude of these forces is given by the time-averaged DEP equation [113]:

$$F_{DEP} = 2\pi r^3 \varepsilon_m \varepsilon_0 Re[U(\omega)] \nabla |E_{rms}|^2 \tag{7.1}$$

where r, ω, ε_0, ε_m and E_{rms} represent the particle radius, radian field frequency, vacuum permittivity, dielectric constant of the cells suspending medium, and the rms value of the external field strength, respectively. The Clausius-Mossotti (CM) factor,

denoted by U(ω), defines the effective polarisability of the particle and describes its frequency response. For each cell dielectric properties will be unique and create a frequency dependent DEP force governed by the CM factor, which in the case of an uniform spherical particle is given by:

$$U(\omega) = \frac{\epsilon_p^* - \epsilon_m^*}{\epsilon_p^* + 2\epsilon_m^*} \tag{7.2}$$

with ϵ_m^* and ϵ_p^* representing the frequency dependent permittivities of the medium and particle, respectively. The complex permittivity of the particle suspension medium is $\epsilon^* = \epsilon$-j(σ/ω) with ϵ and σ being the respective permittivities and conductivities and ω the angular frequency. From the frequency dependent response of the CM factor it is apparent that DEP manipulation is best suited to being controlled by AC fields. As predicted by the polarity of $Re[U(\omega)]$, cells may experience either positive (F_{DEP}), or negative (-F_{DEP}) DEP by attracting, or repelling from regions of higher or lower electric field gradients, respectively. If $Re[U(\omega)]$ is < 0 then the cells are repelled from the electrodes using negative DEP, on the other hand, if $Re[U(\omega)]$ is > 0 then the cells will be attracted to the electrode edges by positive DEP. That is, among other factors when a cell is more conductive than its suspending medium positive DEP occurs, otherwise, if the medium is more conductive negative DEP occurs.

7.1.2 Single-Shell Model

In addition to the fundamental DEP equation introduced by Pohl (eq. 7.1), Irimajiri [114] has adapted the complex permittivity to include the interfacial dielectric behaviour for a particle with an infinite number of shells. This allows the inclusion of a more complex and accurate structural model of DEP response, when considering each layer as an individual homogenous particle in a medium representing each neighbouring interface, be it another shell, or the suspension. Figure 7.4 illustrates the homogenous compartmental parameters for a single-shell particle - this simplified model describes the permittivity and conductivity of a core surrounded by

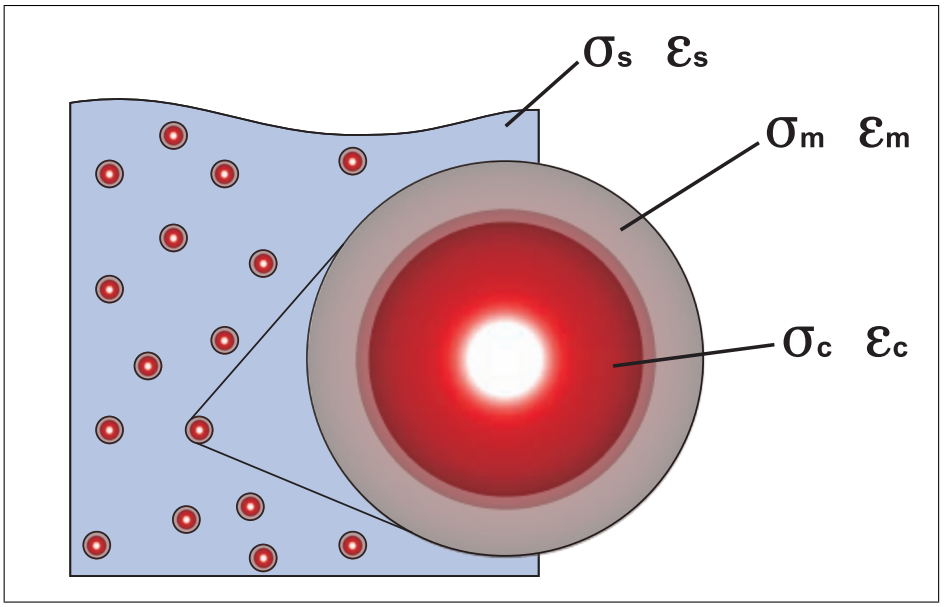

Figure 7.4: Single-shell particle describing the permittivity and conductivity of the cytoplasmic core, surrounded by a membrane shell in a medium suspension denoted by subscripts 'c', 's' and 'm', respectively.

a shell representing the membrane as homogenous dielectrics in the cellular body. However, in reality cellular compartments are highly diverse and consist of an infinite number of structured molecules. From eq. 7.2 each layer has its own complex permittivity with the dispersion at each interfacial layer combining to a yield a total dielectric response given by:

$$\varepsilon^*_{\text{tot}} = \varepsilon^*_2 \frac{\left(\frac{r_2}{r_1}\right)^3 + 2\frac{\varepsilon^*_c - \varepsilon^*_m}{\varepsilon^*_c + 2\varepsilon^*_m}}{\left(\frac{r_2}{r_1}\right)^3 - \frac{\varepsilon^*_c - \varepsilon^*_m}{\varepsilon^*_c + 2\varepsilon^*_m}} \tag{7.3}$$

where the subscripts 'c' and 'm' denote the cytoplasm-core and membrane layers, respectively, and r_1 and r_2 are the widths of each interfacial layer. The frequency dependent DEP forces exerted on a single-shelled spherical particle can be predicted by modeling the real part of the CM factor given in eq. 7.2.

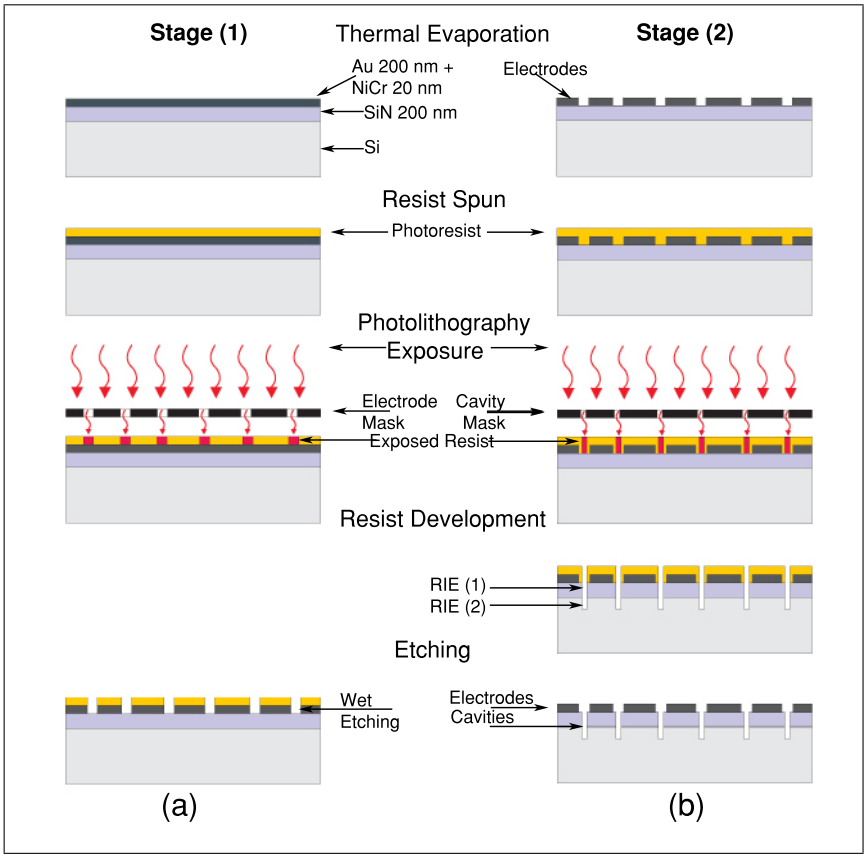

Figure 7.5: Pattern transfer scheme for the two-stage Biochip fabrication processes: (a) Formation of the electrode microsystems by metallic thermal evaporation, photolithography and wet etching processes. (b) Followed by alignment of cavities with respect to electrodes using photolithography and reactive-ion-etching techniques.

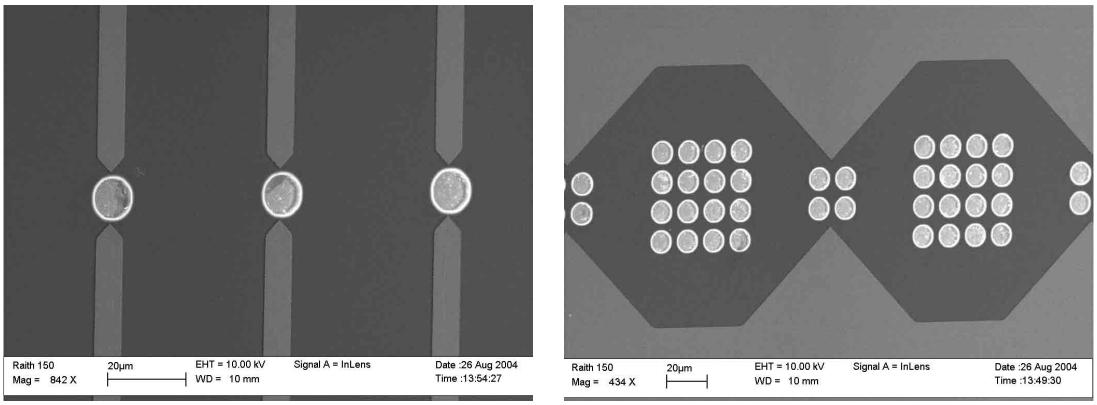

(a) Pointed Electrodes (b) Triangular Electrodes

Figure 7.6: Scanning electron micrographs of two of the Biochip configurations showing a series of 10 μm cavities fabricated between set of (a) pointed interdigitated microelectrodes designed solely for positive DEP. (b) Cavities aligned between a triangular electrode are designed to capture and separate two different cell types by positive and negative DEP collectively.

7.2 Inter-Cavity Electrode Design

Two separate Biochip designs alternating the position and configuration of the cavities with respect to the electrodes were investigated. The electrodes and cavities of each scheme was fabricated using a two-stage process with photolithography, wet/dry etching and metallic deposition techniques. The first stage of creating the electrodes shown in Fig. 7.5 (a) was common for both configurations. Firstly, a thin 20 nm adhesive film of nickel-chrome along with a 150 nm layer of gold were thermally evaporated onto a 10 cm wafer, insulated with either a 2 μm thick silicon-nitride layer, or comprised entirely of quartz (Silicon Quest Int'l). The electrodes are formed after gold and then nickel-chrome wet-etching through a photolithography fabricated 1.5 μm positive resist mask - AZ1518 (Clariant Corp., NJ, USA), which was developed for 15 s in AZ300MIF (Clariant Corp., NJ, USA) and UV exposed for 12 secs using the mask aligner.

For the Biochip configuration that investigated cavities positioned between the interdigitated electrodes the second stage of fabrication was continued according to Fig. 7.5(b) - a mask defining an array of 10 μm single-cell cavities were precisely aligned between the electrodes using the mask aligner operated in vacuum contact

Table 7.1: Process parameters for the fabrication of cavities by reactive ion etching of silicon-nitride and silicon.

Etch Material	Etch Rate (nm/m)	Gases	Flow Rate (sccm)	RF Power (W)	Temp (K)	Process Pressure (mTorr)
SiN	45	CHF_3/Ar	30/25	200	253	15
Si	500	SF_6/O_2	90/8	150	173	70

mode. Cavity positions between the electrode were based on the recorded responses of Polybead® polystyrene 10 μm microspheres - Polysciences Inc. (PA, USA) and Sphero^{TM} carboxyl ferro-magnetic 8.0-8.9 μm particles - Spherotech Inc. (IL, USA) under negative and positive DEP conditions. The cavity sizes were selected based on the approximate mean-average diameter of pituitary cells after dispersion.

After exposure and development the photoresist is hard-baked (185 °C, 1 hr) and cavities 2-3.7 μm deep are etched through the silicon nitride layer and into the silicon substrate by two RIE runs with the etch parameters from Table 7.2 using an Oxford Instrument's Plasmalab 80 Plus etcher. An initial low pressure etch removed the insulating silicon-nitride layer creating an anisotropic etch mask for final etch into the silicon substrate. These parameters were crucial for ensuring a low surface roughness to create a smooth environment for cell adhesion. The depth of the cavity has been optimised to immobilise the cell as well as expose enough of the cell body for AFM imaging without breaching the Z-limit of the AFM.

Finally, the wafer was diced into 20 × 20 mm individual Biochips with a wafer dicing saw (Tempress Model 602, CA, USA) using diamond dicing blades S2530-for silicon, and Z3030-for quartz (Dynatex International, CA, USA). Each Biochip contains 5 integrative microelectrode systems designed to be simultaneously tested. Two different electrode systems are shown in Fig. 7.6 - (a) the pointed/'finger' electrodes are designed to attract cells that respond to positive DEP using cavities located between the electrode tips. Whereas, the electrodes in Fig. 7.6 (b) combines traps located at both positive and negative DEP regions to separate cells that respond to either the intense or weak field regions.

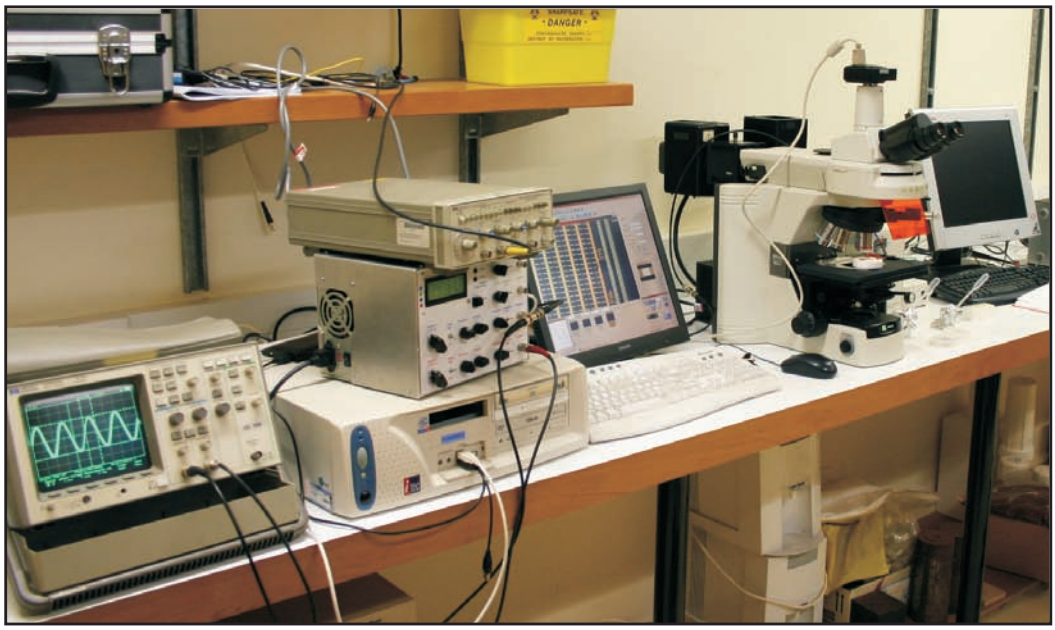

Figure 7.7: DEP experimental setup - the function generator and oscilloscope are connected to a holder containing the Biochip and observed under a microscope equipped with a digital camera imaging system.

7.2.1 Cell Trapping

Using various electrode geometries to periodically create fields of high and low intensity, cells were respectively positioned by positive and negative DEP, via frequency control or changing medium properties, namely conductivity. To position cells within cavities by positive DEP, pituitary cells were washed and resuspended (1500 rpm, 5 min) in a solution comprised of Tris (0.18 mM) Glycine (47 mM) and Dextrose (5 mg/ml) (Tris-Gly-Dex) [115] in de-ionised water (DIW) with an estimated conductivity of $\sim$ 1.7 mS/m. The medium constituents ensures short-term viability of cells but its low ionic content and lack of nutrients is not well suited for prolonged culture. The dielectric properties of the aqueous medium are dominated largely by ionic conductivity and dipoles. A low conductive medium was selected due to the inability of ionic charges to move freely through the liquid, generating a more polarisable cellular body and thus increasing the net DEP force while avoiding electrolysis. Otherwise, the Tris-Gly-Dex was supplemented with DMEM (dispersion medium) solution until negative DEP dominated.

One method of applying the signal to the electrodes used a holder designed to horizontally steady the Biochip during trapping. After 70-100 μl of the cell suspension was pipetted onto the Biochip power was applied to the electrodes for periods up to 1 hr. A limited volume of cell suspension is placed on top of the Biochip while pin-connect needles deliver the desired signal to the contact pads. At higher voltages Ohmic heating can cause hydrodynamic effects that result in formation of an inhomogeneous liquid medium, allowing the creation of space charges in the bulk that interact with the externally generated electric field. The effect of this interaction is fluid motion in and around the cavity structures and levitation of cells above the substrate [116].

Another concern was the medium loss due to thermal evaporation and the fluctuating ionic content, which led to the development of another method for capturing cells referred to as the 'dipstick' technique. In this method the entire Biochip was submersed within the suspension until cells became trapped, the platform was then removed and placed in a solution comprised of incubation media.

Voltage operating conditions required for DEP can be generated by existing electrical and electronic equipment and are low enough to be interfaced directly to the electrodes without compromising structural integrity. As shown in Fig. 7.7 experiments using the Biochip holder were carried out in a room temperature of 21 °C with cell trapping observed using an Olympus BX-60 or Nikon microscope equipped with a digital camera. Power to the microelectrodes in both configurations was delivered by a sinusoidal AC wave between 1 kHz and 13 MHz with a voltage range of 1-25 $V_{\text{p-p}}$, using a function generator - HP3312A, Hewlett Packard (CA, USA). Signals applied to the Biochip were continually monitored with an oscilloscope - HP4523, Hewlett Packard (CA, USA). In the case of the dip-stick method, the generator leads were connected to the contact pads using a set of miniature aluminium clips. Alternatively, the Biochip holder used a set of pointed needle-contacts to apply power to the electrodes, which were connected to the generator using a set of crocodile clips.

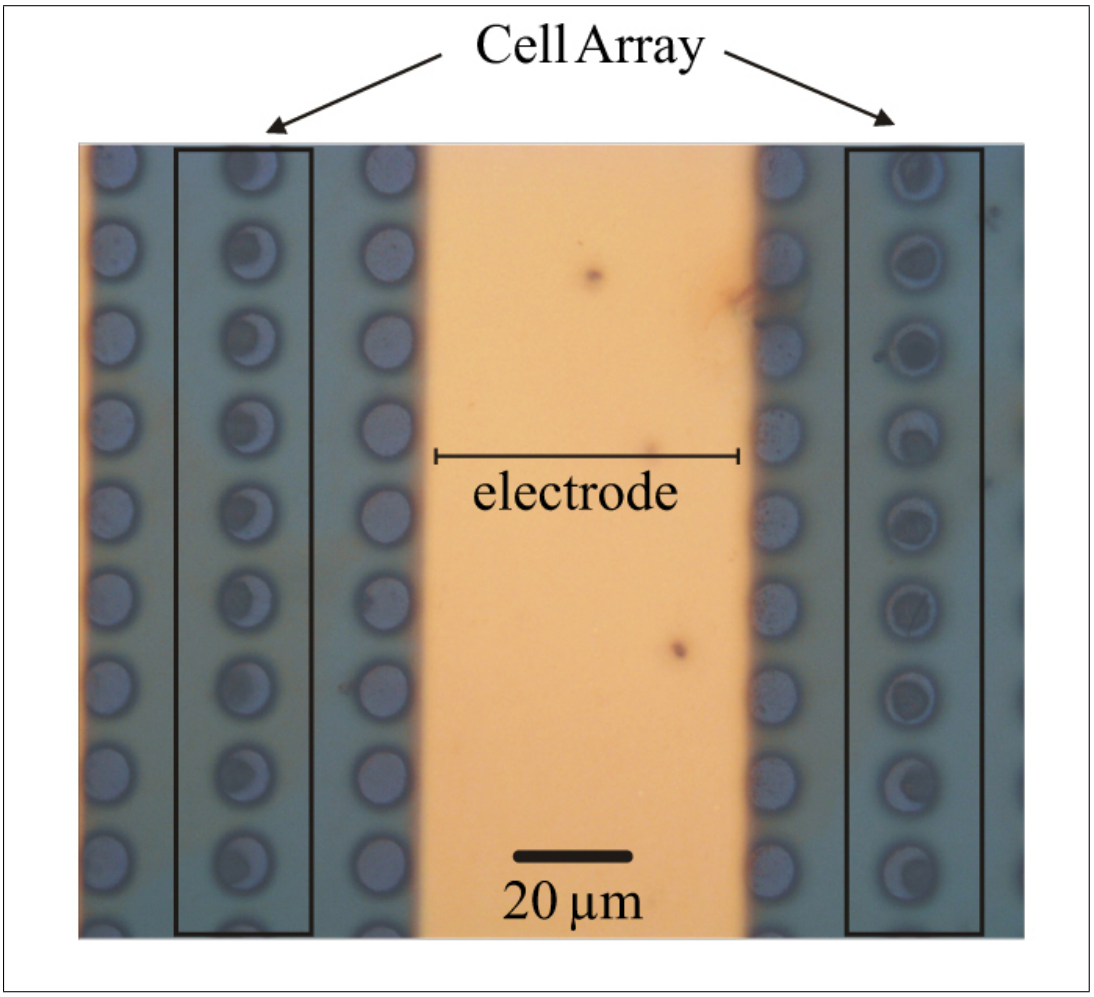

Figure 7.8: Photograph of a large array of pituitary cells captured within 10 μm cavities by a planar interdigitated microsystem using negative dielectrophoresis. The suspending medium was Tris-Gly-Dex supplemented with DMEM using an AC applied voltage at 13.5 $V_{p\text{-}p}$ at a frequency of 1.2 MHz.

7.3 Results

Stable trapping of anterior pituitary cells by negative DEP in Tris-Gly-Dex solution supplemented with dispersion medium is illustrated in Fig. 7.8 - an organised array of cells are directed to the weak field regions occupied by cavities using a parallel series of electrodes. A sinusoidal 1.2 MHz waveform at 13.5 $V_{\text{p-p}}$ amplitude was applied for over an hour, which considerably diminished cell viabilities but resulted in good cell organisation - in this instance each cell is seen occupying its own cavity, but in reality cells often landed outside of cavities because of the difficulty in predicting DEP response over the complete electrode area.

One method to attract cells into cavities by positive DEP is to decrease the conductivity of the suspension. Figure 7.9 illustrates trapping of pituitary cells by positive DEP using the pointed interdigitated microelectrodes. Cells were suspended in a complete solution of Tris-Gly-Dex and the voltage set-point was reduced to 8 $V_{\text{p-p}}$ to ensure minimal cell damage from the intense electric field gradients. Typically, cells became steady within the hydrophillic exposed silicon cavities between a period of 30-60 min, whereby DEP was then discontinued.

Even though cells are depicted as being relatively evenly distributed within cavities across the electrode face (Figs. 7.9, 7.8) it was difficult to consistently achieve such a high degree of cell-cavity efficiency. Inevitably cells were positioned by electrodes independent of cavities and they frequently landed at non-specific areas. Especially with negative DEP, upon removal of the signal cells trapped outside of cavities readily dissipated to take random positions on the Biochip, seemingly from the weak holding forces and low viabilities. Additionally, with positive DEP when compared to homogenous microspheres, which settled within cavities directly adjacent to electrodes (Fig. 7.2), the complex compartmental properties of pituitary cells often resulted in cells taking equilibrium positions slightly offset on the electrode rather than completely within cavities (most noticeably at higher voltages). Due to DEP localisation lower voltages only worsened the situation - weaker forces decreased the effectiveness of the system and made it difficult to influence cells, especially those

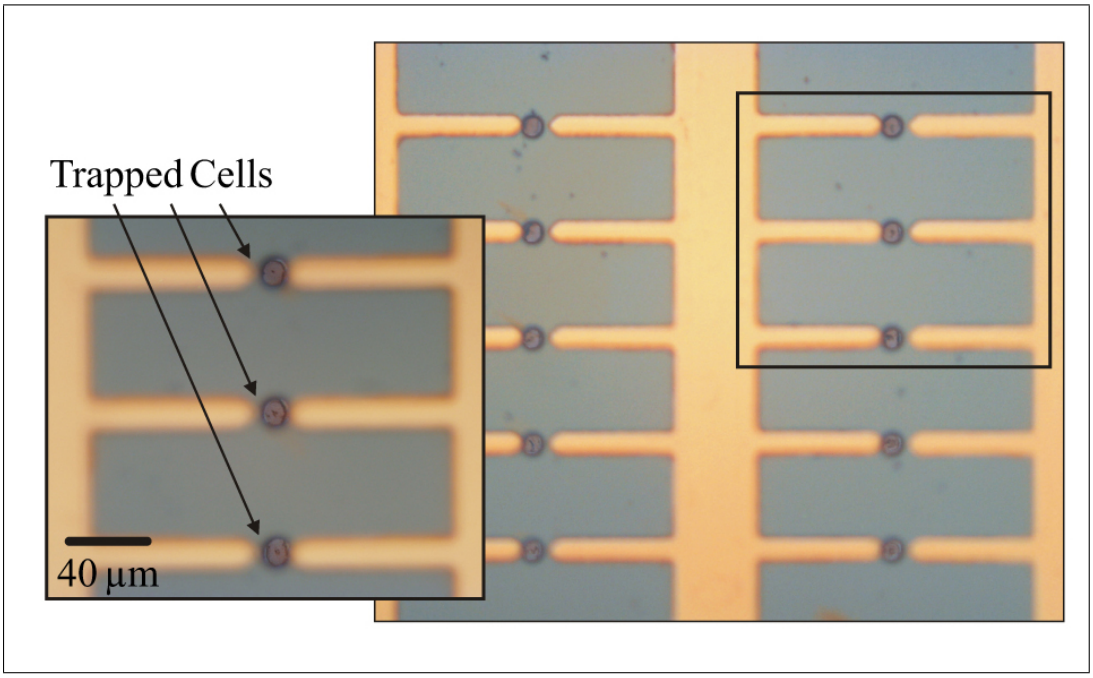

Figure 7.9: Photograph showing pituitary cells captured within 10 μm cavities by a pointed interdigitated microsystem using positive dielectrophoresis. The suspending medium was Tris-Gly-Dex of conductivity 1.7 mS/m, with an AC voltage of 8 $V_{p\text{-}p}$ at a frequency of 930 kHz. A magnified region of the array clearly shows the cells trapped within the cavities.

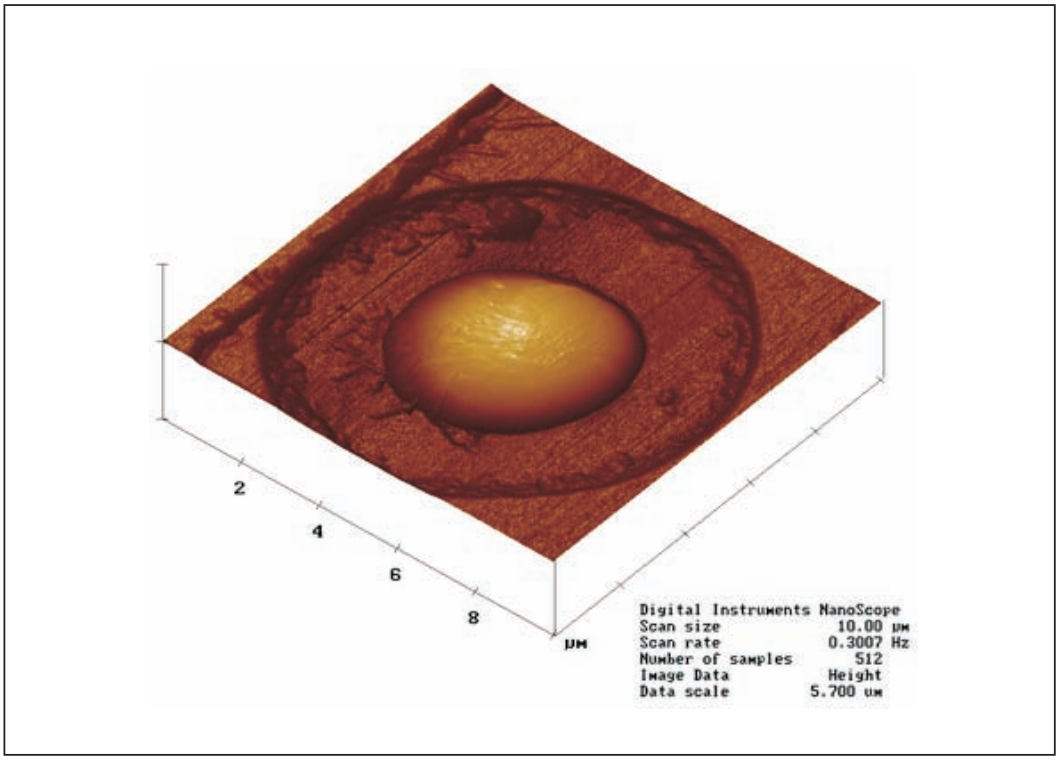

Figure 7.10: 3D AFM of an anterior pituitary cell within a shallow cavity on the Biochip after positive DEP.

landing at decayed DEP positions (ie. outside of field range). In general if cells were not sufficiently contained within cavities prior to signal removal, external forces (eg. hydrodynamics) resulted in their rearrangement within hours of trapping. Though some cells still remained within cavities after trapping as shown in the 3D AFM image - Fig. 7.10 taken in air-tapping mode after using positive DEP to trap cells within cavities with the planar electrode microsystem. Nevertheless, almost all cells deviated from their initial trapping positions after removal of the DEP signal and fluid aspiration, which was also in part caused by the shallow cavities trailed in this case. Finally, the non-physiological environment meant that cell viabilities diminished rapidly and the DEP trapping conditions were not suitable for living cell studies on osmotically sensitive pituitary cells.

In the following investigation a new method was developed to overcome many of these issues, which is integrated with Bioimprint to illustrate the advantage of using

a system designed to replicate cancer cells trapped by positive DEP.

7.3.1 Cavity-on Electrode Design

From the deficiencies of the first Biochip configuration an improved method was developed for positioning cells within cavities by changing the orientation of the existing electrode-cavity mask design. By exposing selective sites in the form of cavities designed to incubate single-cells, this time above the interdigitated electrode plane, high intensity DEP spots in the shape of the cell are formed as individual cavities. Regions around the cavities on the electrode are suppressed by the insulating polymer mask, providing isolated locations for more effective cell trapping by positive DEP. This design is unsuited for negative DEP due to the absence of cavities positioned at definitive minima field areas. Cavities were fabricated by spinning a 1.7 μm layer of photoresist (AZ1518) at 3000 rpm for 40 secs and an isotropic profile created after a 32/65 secs exposure and development process, respectively. A thicker resist ensured the unexposed regions of the electrode were insulated and only the cavities were dominant in DEP regulation. Finally, the 10 cm wafer was hard-baked at 185 °C for 2 hrs before dicing.

Another advantage of the Biochip is its scalability - different cell types are easily accommodated by modification of the cavity features. If the deviation from the original mask dimensions is not too excessive, adjustment of the fabrication parameters, namely exposure and development times, can be used to suit the cell size. Owing to the small amount of tissue available in the anterior pituitary and the resources required for its extraction and dispersion, a large proportion of experiments utilised cancer cells due to their prolific growth in culture, abundance and accessibility. Endometrial cancer cells range from $\sim$ 10-25 μm in diameter post enzymic digestion, and are easily accommodated by over exposure and development of the original cavity mask designed for pituitary cells (10 μm).

Figure 7.11 illustrates the method for positioning cells on the Biochip using cavities fabricated above the electrodes. Trapping of cells within cavities is performed by

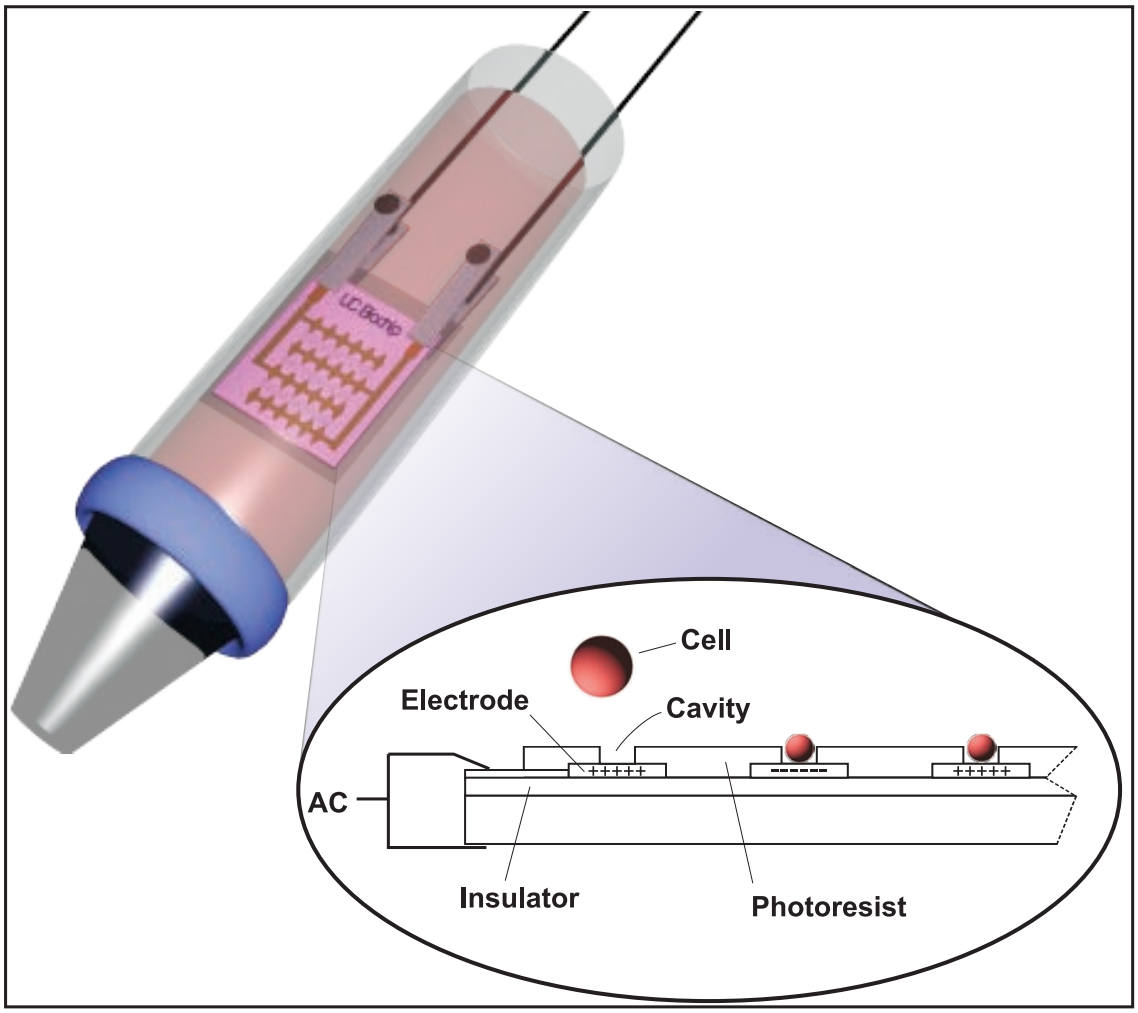

Figure 7.11: A schematic illustration of DEP experimentation using the 'dip-stick' trapping technique - the Biochip is submersed into a sugar-based suspension containing cancer cells and an AC waveform applied to create DEP forces, which captures cells within cavities formed above the electrodes.

vertically angling the Biochip in a suspension of cancer cells suspended in 8.5/0.3 % - sucrose/dextrose sugar solution (estimated conductivity 10 mS/m) [117] contained in a 10 ml plastic tube. The purpose of tilting the device vertically is to minimise the gravitational influence on cell positioning. The tube or container holding the Biochip and cell suspension was submersed in a water bath regulated to 37 °C. The AC signal was delivered by aluminium microclips connected to a set of contact pads on the Biochip using a sinusoidal waveform at a voltage and frequency range of 3-7 V_{p-p} and 500-700 kHz, respectively. Cancer cells were lifted from plates by enzymic (0.1 % trypsin) digestion and kept in incubated in α-MEM supplemented with 10 % FBS until required for experimentation. Each experiment lasted between 5-10 mins, where fresh incubated cancer cells were centrifuged and resuspended in sugar solution. Afterwards each Biochip was washed (α-MEM) and incubated in culture dishes containing α-MEM and 10 % FBS.

7.3.2 Biochip & Cancer Cells

Figure 7.12 illustrates reflected light microscopy images of cancer cells trapped within a number of cavities above the pointed microelectrode design, with each location identifiable by a series of alpha-numeric markers. (a) Two images are combined to highlighted the proportion of cavities occupied by cells (emphasised using asterisks '$*$') - an arrow points to a rogue cell trapped at a position of positive DEP alongside the underlying electrode, illustrating the inability of the photoresist to completely insulate the electrodes. (b) At higher magnification the cells are well incubated within the cavities but at relatively low cell-to-cavity capture efficiencies - only approximately 1:3 cavities were occupied by cells. Low efficiencies were likely due to; cells detaching during the numerous medium exchanges and washes or after DEP, cells dying after passage (enzymic removal from culture dishes) or during DEP, low cell suspension concentrations, large cell sizes/small cavity sizes, or the toxicity of the photoresist during culture.

Using another electrode design, Fig. 7.13 illustrates optical images of endometrial

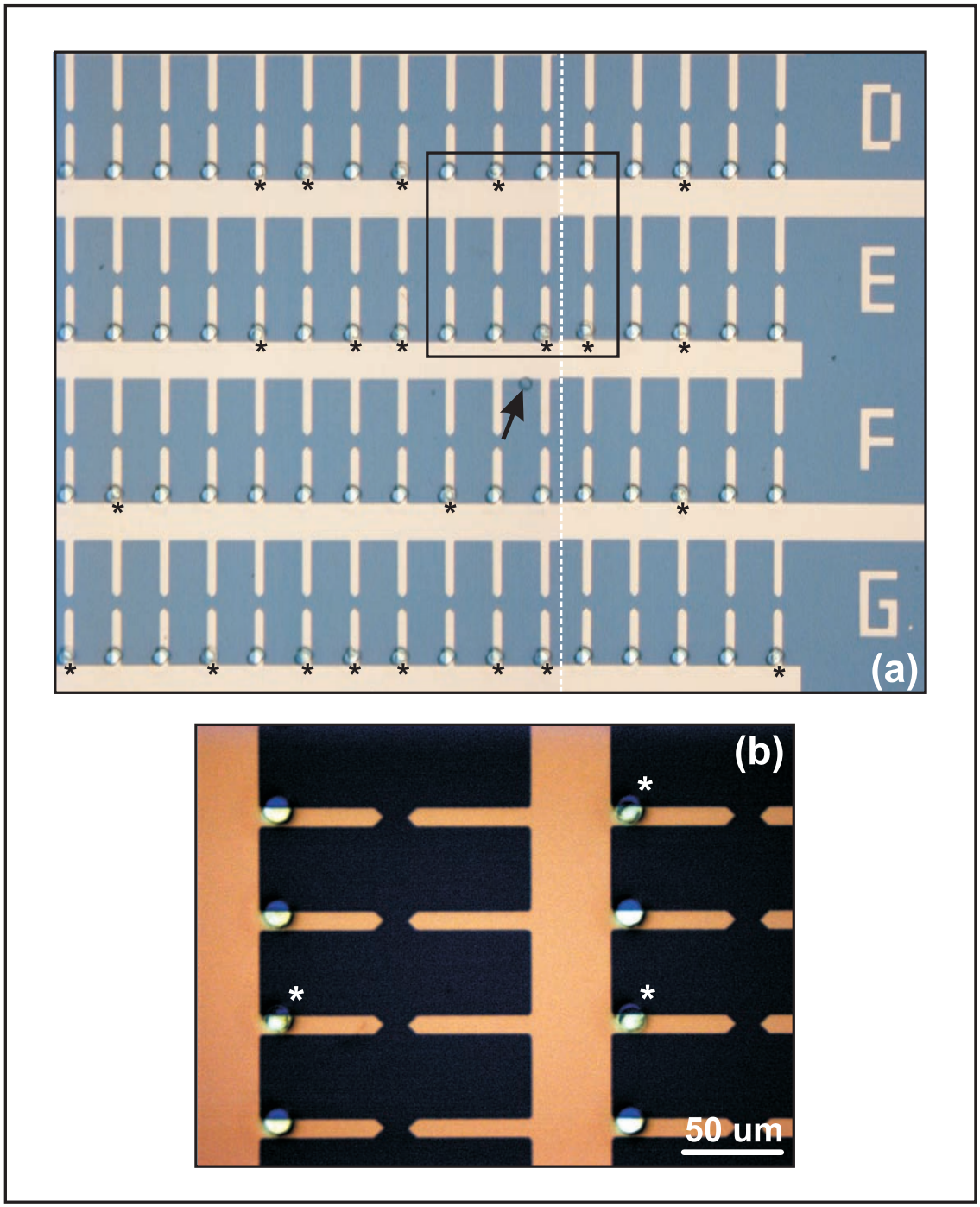

Figure 7.12: Reflected light microscopy images of a series of unstained cancer cells trapped by positive DEP (650 kHz, 10 mins) within cavities fabricated above the pointed microelectrodes after culturing on the Biochip for 1 day. (a) Cells positioned within cavities are denoted by '$*$' whereas the others remained vacant - a rogue cell influenced by the underlying electrodes is highlighted with an arrow. (b) A magnified image depicts 3 cells within cavities amongst 5 which remain unoccupied.

cancer cells trapped within cavities exposed above a planar electrode on the Biochip. For better contrast cells (now dead) in the main image were stained with trypan blue in PBS for 30 mins after initial staining (for 5 mins) confirmed cell viabilities of $\sim$ 90 % by their ability to exclude the dye. DEP was applied for 10 mins between $\sim$ 3-6 V at 500-800 kHz after which cells were cultured for 1 day in α-MEM supplemented with 10 % FBS to promote attachment and adherence to within cavities for subsequent replication. The large variation in cell sizes meant even after over exposure and development of cavities many of the cells were too large, but for some the fit was perfect (see insert Fig. 7.13 - unstained). Cancer cells adhered well to the underlying gold electrodes and the isotropic profile of the cavities provided good support, allowing culture medium for incubation to be exchanged from the sugar solution immediately after DEP experimentation. This system demonstrated that living cancer cells can be cultured on the Biochip after DEP trapping.

For future investigations using longer culture times or wanting to apply solvents to cells on the Biochip for dehydration and drying, cavities will need to be fabricated in more biocompatible and solvent-resistive materials, one of which is available as a negative resists - for example, SU-8 MicroChem (MA, USA). One method to accommodate this type of material is to transpose the original mask designed for positive photoresists using a lift-off technique. Resist was spun (3000 rpm, 1 min) on a 12.5 cm chrome-coated quartz mask plate and soft-baked at 100 °C degrees for 1 min. The positive cavity pattern was exposed in hard-contact mode for 3 mins in UV light (1 mW/cm^2) and developed for 1 min. The mask was then placed directly above the source and 40 nm of gold was evaporated. After lift-off in acetone and a brief ultrasonification the chrome was wet-etched away to create the negative cavity mask shown in Fig. 7.14. Unfortunately, due to time constraints new materials were unable to be tested using this mask pattern.

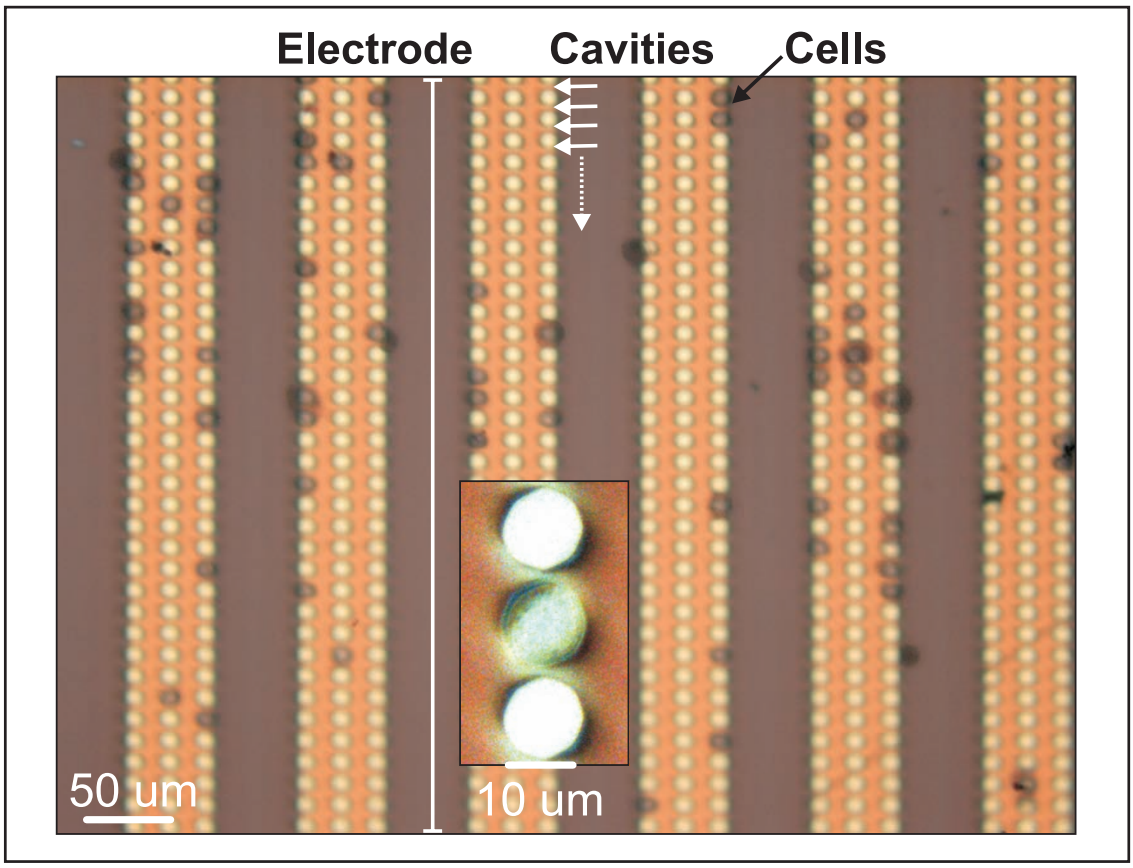

Figure 7.13: Optical image showing trypan blue stained cancer cells trapped in cavities above a planar microelectrode system cultured for 1 day on the Biochip after capture at 600 kHz for 10 mins (insert cell unstained).

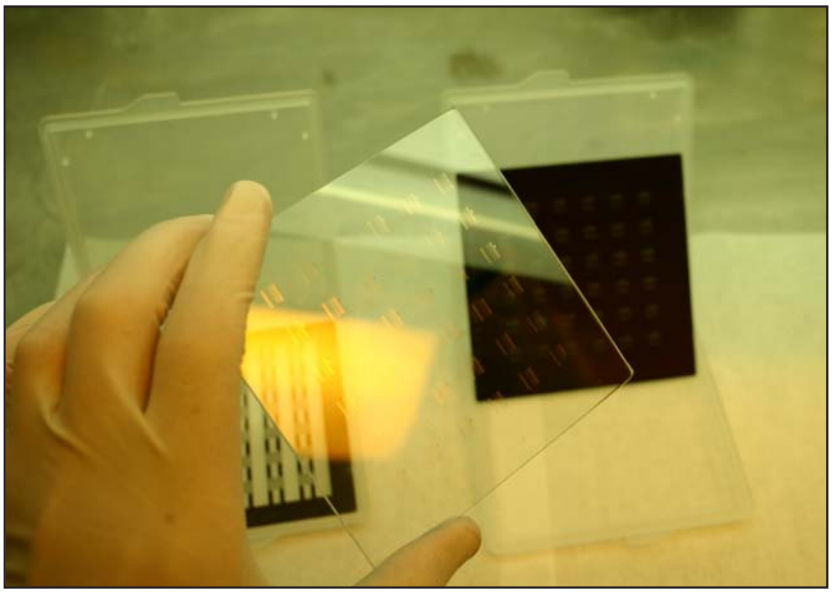

Figure 7.14: Negative cavity mask intended for patterning cavities using negative resists created by a lift-off technique from the old mask plate (right-foreground).

7.3.3 Bioimprint and the Biochip

For high resolution microscopy it is useful to appoint cells to locations, which are easily addressed and observed in electron-vacuum or scanning probe conditions. A key aspect of this research focuses on techniques to enable effective analysis of cells by AFMy. The integration of the Biochip with the Bioimprint replication scheme facilitates integration of the AFM by positioning cells into organised and addressable arrangements.

Using Bioimprint AFM images of cell replicas trapped by positive DEP on the Biochip are fabricated in a PDMS elastomer using the replica moulding technique described in Chapter 5. To create molecular imprints of cells DEP forces need to overcome external influences to remain steady upon removal of the fluidic-suspension bulk. After blotting and evaporation of the PBS washing solution from the Biochip, DEP forces are overcome by a combination of forces acting to disperse cells from their trapping positions, namely the fluidic surface tension, loss of the fluidic interface, DEP force variation and turbulent fluid motion. These effects combined to cause cells to dissipate resulting in a random dispersion of cells.

Generally, without cavities the DEP forces required to steady cells in their incipient trapping positions during their removal from suspension required large driving voltages in excess of 15 V_{p-p}, and for positive DEP extremely low conductive solutions. Even still, forces were often too weak and cells regularly dispersed. As electrolysis and electrochemical reactions are prominent with more conductive suspensions required for negative DEP, which in turn require the frequency to be raised simultaneously, greater voltages are implemented without affecting electrode integrity when using positive DEP. Furthermore, the magnitude of CM factor from Eq. 7.2 predicts theoretical boundaries of 1.0 and 0.5 for positive and negative DEP, respectively, increasing the potential for higher forces holding cells under positive DEP conditions.

The main challenge of using DEP as a positioning tool is the accuracy of particle placement. In a duopolar system 2D cell movement and control by DEP is imprecise as cells are positioned at locations confined to a plane alongside, or grouped within a region between the interdigitated electrodes by positive or negative DEP forces, respectively. To determine an optimal configuration for replication of cells positive DEP was investigated using yeast, blood and human endometrial cancer cells.

Figure 7.15 shows a collation of adjoining AFM images created by PDMS replication of yeast cells, which were trapped alongside a triangular electrode by positive DEP after removal of the DIW solution. While this practically illustrates the integration of Bioimprint and Biochip methodologies these conditions are undesirable for studies on living systems because of the high voltages, unphysiological suspension medium, replication conditions and non-cavity capture. Furthermore, in this configuration positioning and movement are only achieved along a planar axis defined by the shape of the microelectrodes. Even though AFM imaging is effective in this arrangement, single-cell studies are difficult due to their randomness along the electrode edge.

As well as providing identification cavities also steadied cells during processing without needing high voltages or low conductive solutions, which in the absence of cavities were mandatory for maintaining cell positions upon fluid exchange or removal.

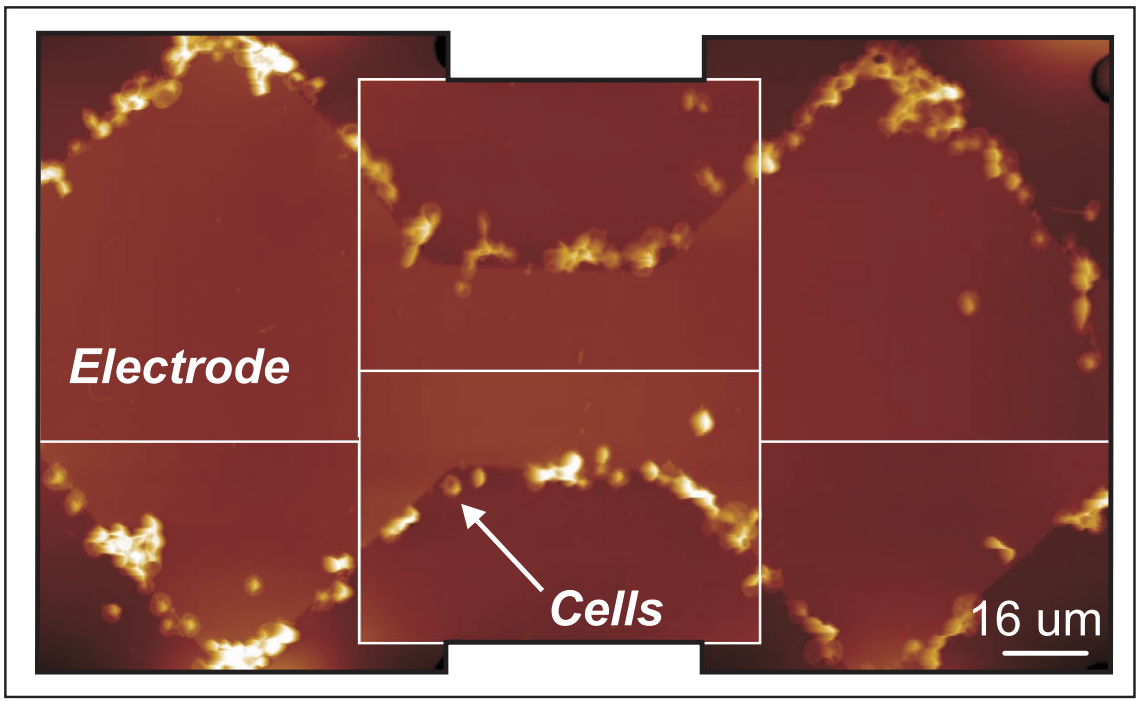

Figure 7.15: Collation of adjoining AFM images depicting Bioimprints of yeast cells aggregated alongside a triangular interdigitated microelectrode by positive DEP on the Biochip.

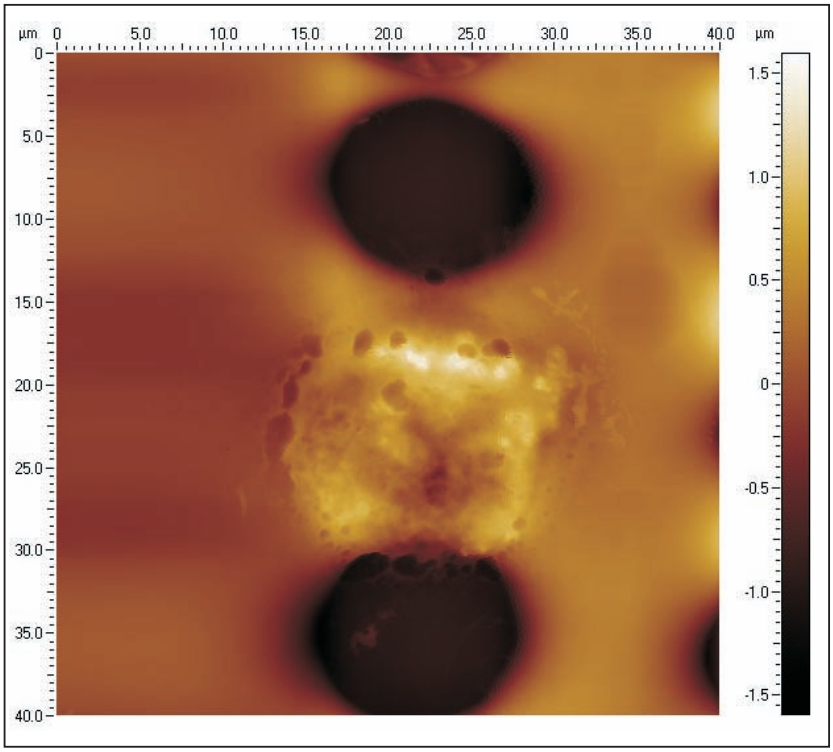

Figure 7.16: AFM image of a Bioimprint depicting an endometrial cancer cell trapped within a cavity by positive DEP between two remaining vacant above a planar interdigitated electrode.

Figure 7.16 depicts an AFM image of an endometrial cancer cell replica fabricated in PDMS and trapped within a cavity positioned between two remaining vacant. Due to the delicacy of applying the polymer over a surface containing cells loosely attached, after trapping Biochips were incubated for 1 day to promote cell attachment and to avoid complete incorporation of the cell into the polymer during replication. In this instance the poor cell-to-cavity captures rates were attributed to weak DEP trapping fields (caused by close inter-cavity proximities) and the excessive number of cavities.

7.4 Discussion

There are numerous applications for lab-on-a-chip devices designed to position cells at definitive locations. Single-cells can be identified, addressed, imaged more effi-

ciently, integrated with existing automated analytical devices or applied as a micro-positioning platform. While other electrode systems with quadrupolar designs show promise in the accurate positioning of single cells by DEP [118] these often require more complex designs and electronics. An advantage of the current system is in its simplicity, adaptability and scalability - the Biochip is easily modified to different sized cells by adjusting the diameter of the overlying cavities. Novelty of the Biochip is in being able to rapidly trap single cells at definitive positions for analysis by a broad range of microscopy tools.

DEP created from a series of interdigitated electrodes often resulted in cell aggregates forming at areas of high or low electric fields without precise control over single-cell position or location. By doubling cavities as electrodes, cells can be directed and isolated at dynamic DEP regions rather than inducing DEP independent of cavity location. Utilising the positive DEP forces generated from cavities we have demonstrated that individual cells can be captured, replicated and imaged using the AFM.

Traditionally, negative DEP has been regarded as the preferred manipulative technique for living systems due to positive DEP creating intense field gradients known to induce harmful forces on the cell membrane. However, at low enough voltages positive DEP can be applied to successfully trap living cancer cells using a sugar solution, which can be aspirated and exchanged for another solution without completely disrupting cells positioned by positive DEP. A crucial factor in the effectiveness of attaching living cells within cavities was in the use of samples immediately after ($<$ 30-60 mins) being lifted by enzyme digestion from culture plates, regardless of whether they had been kept at physiological conditions up until experimentation. It was suspected that after enzyme digestion of plated cells from culture, if not presented with a suitable binding substrate over time the suspended cell's readiness to bind onto new surfaces rapidly decreased. It was crucial that cells attached within cavities swiftly as long-term suspension in the sugar solution was detrimental for cell viability.

Usefulness of DEP in weak voltages is often limited due to the exponential decay of electric potential away from the electrode edges. Near-ranging DEP effects influence cells only when in proximity to the cavities and forces at lower voltages were often too weak to trap cells effectively. Hence, it was difficult to produce scalable cell arrays in these conditions, which resulted in low cell-to-cavity capture ratios. On the other hand the likelihood of cell aggregates collecting in any given cavity was also low because of the preference of cells to locate within unoccupied cavities. At higher voltages one would expect to achieve more scalable cell arrays but at a cost of achieving single cell-to-cavity exclusivity and maintaining cell viability.

Analysis of cancer cells was considerably more difficult in comparison to imaging non-malignant cell types. Rapid proliferation and growth *in vitro* caused substantial cell movement and activity. Given that the Z-height limitation of the AFM (DI 3100) is $\sim 6\ \mu m$ it was often difficult to image whole cancer cells without breaching this boundary, or otherwise, needing to manually step the piezo-tube during scanning. Conventional methodology traditionally succeeded in overcoming this limitation by extending culturing times up to several days in an effort to decrease cell heights. Or otherwise, as in Chapter 6, avoiding this problem all together by imaging single cells and avoiding dividing cells with large heights. An advantage of scanning cells within cavities is they facilitate AFMy by decreasing their Z-range to within the AFM's limit without needing to prolong culture times, or avoid certain cells completely. Furthermore, the reduction in culture times should significantly decrease the amount of medium and reagents required, as well as the overall wait-time for cell imaging.

In this investigation a PDMS elastomer was used to demonstrate the ability to replicate cells trapped using DEP. At the current conditions heat-curing is known to cause cell dehydration as reported in earlier studies on cancer (Chapter 6) and pituitary (Chapter 5) cells. Nevertheless, cavities on the Biochip were seen to insulate cells and promote hydration during fluid clearing from the surface, allowing the top of the cell to be imaged while preventing excessive exposure. The UV-Bioimprint process, which makes use of photo-initiated elastomers was not applied here largely due to the difficulty of using the mask aligner to apply polymer onto

small Biochip (20 × 20 mm) samples, which could of easily damaged this expensive piece of equipment (eg. polymer spilling and clogging outlets and seals).

While curing times are slow when implemented using the replica moulding technique, future investigations will incorporate a UV-Bioimprint methodology with the Biochip to enable imaging of organised cell replicas at near-native states. Even though photo-initiated polymers cure in UV within minutes, on average AFM scanning of a living cell takes equally as long, depending on scan rate, size and resolution (lines per frame). Subsequently, imagery taken from cells in these methods are equally progressive representations of cellular state.

Chapter 8

Summary Remarks

The AFM has great promise as a high resolution analytical tool but *in situ* cell imaging remains notoriously difficult. The very nature of scanning a sharp probe in proximity to, or in contact with a soft cellular membrane, while achievable requires stringency and precision that is not routine nor easily automated for large-scale cellular analysis. For each cell, scanning requires manual adjustment of several parameters based on a balance of forces determined by a countless number of variables. Besides being one of the most sophisticated and robust instruments for surface characterisation the AFM remains fundamentally limited when imaging dynamic events due to its weak time resolution. The problem begins with the serial operation of the AFM, and sequences picturing discrete events more than likely depict parts of a dynamic process. Although the AFM is often promoted as being capable of imaging living cells in real-time, its sequential scanning nature and temporal resolution is unable to contend with the millisecond pace of cellular mechanisms in most cells. Difficulty in operating the AFM in fluid prevented exocytosis from being captured, or for that matter, any images that confidently depicted active fusion pores whatsoever. Given the rapid function of exocytosis in pituitary cells, efforts were subsequently directed toward exploring established and alternative techniques in an attempt to visualise fusion pores in ambient conditions.

Variation in exocytotic or endocytotic features observed in chemically fixed cells

indicates the diverse functionality and complex nature of cells in the anterior pituitary. Throughout this work cells seemingly displayed both total and transient mechanisms of fusion pore function, possibly because of their differential modes of action (ie. exo-/endocytosis), transitional stage (eg. hemifusion, full fusion, 'stalking') or influence from artifacts (eg. permeation). Chemical fixation, dehydration and drying are frequently used in biology to preserve cells and tissues but little is known about the distortions these chemicals create on the plasma membrane at the nanoscale.

In this research fusion pores were characterised according to those appearing consistently in fixed cells. Even though pores referred to as craters and channels displayed similarities to other models described in literature (eg. pits and depressions, hemichannels), further work is required to establish a definitive link. Another scenario proposed in this work is that some images were related by a procession of stages culminating in transient and/or total exocytosis. Alternatively, it is equally likely that various pore structures are part of separate entities and are regulated by different mechanisms. However, for each hypothesis without directly visualising events it is difficult to reliably conclude the exact sequence or nature of the fusion pores presented in this research. The co-existence of differential fusion mechanisms is another theory potentially explaining the different types of pores observed but one which is considerably more speculative and is yet to be confirmed for cells in the anterior pituitary.

Inconsistencies amongst fusion pores imaged in chemically fixed and replicated cells hindered investigation of theories speculating on the diversity of exocytotic function in pituitary cells, due to the increased possibility of some of the observed characteristics of pores being artifacts. While differences in membrane topography are explained by several scenarios resulting from deficiencies with either Bioimprint or fixation methodology, images of cells from each method also shared similarities. Cells were comparable to each other with respect to their shapes, profiles and appearance of unique features, such as extrusions, molecules and even artifacts (when Bioimprint and fixation were combined). Despite their variations fusion pores also displayed

similar features including, spherical dimensions, aggregation and localisation to sites on the membrane around the nuclei or on the cell periphery. Fusion pores described generically as 'major openings' were observed in replicas and chemically fixed cells alike, providing crucial evidence to support their association to physiology. The stability and size of major pore openings indicates they are likely linked to events following full fusion or undergoing endocytosis. Absence of other pores from replicas compared to those observed in chemically fixed cells is potentially explained by a limitless number of factors such as permeation artifacts, distortions, polymer encapsulation (ie. complete submersion) or deficiencies (eg. reaction to the polymer, UV light) relating to Bioimprint. Considering that imagery showing pores described as 'craters' were seen to have definite stages is indicative of their unique transitional nature and provides further evidence in support of their dynamic functionality.

Culturing had a large influence on the presence and structure of fusion pores. AFM images of cells taken several days after dispersion resulted in cells flattening, and in comparison to those cultured for shorter times displayed considerable variation in fusion pore numbers and appearance. Culturing seemingly forced the membrane and the intra-cellular granules in close proximity and dramatically increased the visibility of fusion pores on the membrane. On the other hand AFM images of cells taken relatively early in culture displayed bland topographies with a sparse number of fusion pores frequently observed as major pore openings. It remains uncertain whether pores seen predominantly in longer cultures are an abnormal response caused by *in vitro* conditioning or mechanisms relating to *in vivo* physiology.

One aspect of this research focused on determining whether cells displayed different numbers of fusion pores in the presence and absence of stimulation. It is well known that a peak level of LH is detectable in a population of anterior pituitary cells when subjected to GnRH stimuli, but there is little data on how this translates down to the single-cell level. One mechanism for this peak could be from an increase in the number of gonadotrophs responding to stimuli rather than all cells displaying a sudden burst of fusion pores. On one occasion fusion pore numbers in chemically fixed cells subjected to GnRH decreased, albeit possibly in a disproportionate num-

ber compared to estimated gonadotroph cell numbers. In contrast, some stimulated replicas displayed a greater number of pores than those seen at control conditions. Overall establishing a stimuli response from fusion pores was inconclusive but in itself could signify that numbers remain relatively constant during stimulation. Difficulty was in part due to the static nature of all imagery but also because of the inherent challenges in identifying and quantifying fusion pores in chemically fixed gonadotrophs. Determining the topographic response of a cell to a stimulus by examining an overall population using the AFM was largely ineffective. Even with the aid of immunohistochemistry, the dynamics of fusion pores were difficult to characterise. One obvious explanation for the absence of cells displaying heightened states of fusion after application of stimuli is that both fixation and Bioimprint were too slow to decisively capture exocytotic events. Another possibility is that during stimulation the frequency of fusion changes but the number of fusion pores in a cell at any given moment remains constant. Studies were also unable to provide conclusive evidence on the fate of pores after fusion - that is, whether they dilated with the membrane, remained, or were retrieved back into the cell by compensatory endocytosis.

Bioimprint produced images with an excellent likeness to their physical counterparts while being free of many artifacts observed in chemically fixed cells. The overriding advantage of Bioimprint was its ability to examine samples without the addition of cell modifying agents. Replicas were a lot easier to image than actual cells and at the surface displayed profiles appearing in good condition with consistent fusion pore sizes. After cleaning, replicas were removed from any loosely attached material, which often plagued imagery taken from fixed cells and often resulted in scan line effects. Bioimprint produced high quality images of pituitary cells and exceptionally clean results with elastomers proving to be an ideal medium for AFMy. However, issues relating to cell dehydration frequently inhibited Bioimprint from creating consistent replicas and often impressions were captured showing dehydrated cells or otherwise lacked sufficient resolution - problems directly related to the degree of fluid remaining before polymer application. Nevertheless, indirect analysis of cells

by replication is useful for the exploration of cellular ultrastructure in circumstances requiring an alternative methodology for ambient-air visualisation.

The Biochip provided a simple means of organising a randomised suspension of cells. By rapidly trapping single-cells within cavities cells can easily be addressed using the AFM and can even be replicated after a brief culturing period. With aid of cavities to support cells it is possible to exchange and transfer solutions immediately after DEP, which is vital for maintaining a healthy cell population. Creating localised positive DEP forces by exposing cavities on the electrode while insulating surrounding areas provides a more effective means of capturing cells than methods attempting to predict cellular response and cavity position based on electrode geometry. However, given the large variation in cell sizes, inevitably there remained a certain proportion of cells that were too large for cavities. Initially, cavities were designed to provide a means of reducing cell heights to enable the AFM to operate within its Z-limit. However, given the dull and uninteresting imagery observed from cancer cells early on in culture more features and information are extracted from cells grown *in vitro* after several days. Thus the purpose of needing cavities to submerse cells in order to reduce cell heights was unnecessary due to their progressive flattening during culture.

8.1 Recommendations for Future Work

Numerous difficulties prevented Bioimprint from producing consistent and reliable results. In the future an optimum Bioimprint methodology will be one that is fast enough to capture an exocytotic response while minimising the possibility of any adverse cellular distortion. More specifically, one area requiring development is the use of new materials for the fabrication of living cell replicas. While the use of photo-initiators is a step forward from thermal-active elastomers in achieving a single-shot cell impression, attempts should also focus on materials that are not only rapid in curing but non-toxic, at least in the short-term. Development of new polymers may include the use of materials designed to perform multi-functional

tasks (eg. replication and detection). One category of materials briefly trialed and should be further investigated is organic polymers such as hydrogels or collagen, which can be modified to have physiological liquid-solidification phase temperatures or even photo-activated. Another area of development for Bioimprint is to improve methodologies, such as investigating polymer application techniques including using an immersion-imprint method. Exchange and application of polymers with existing water-based mediums is also critical for achieving quality replication. Performing replication *in situ* would reduce problems relating to medium aspiration and eliminate cell exposure during polymer exchange. A high purity of polymer at the cell surface is also critical for achieving good membrane resolution transfer, which could be enhanced through techniques such as centrifugal exchange - whereby existing suspension medium is centrifuged at ultra-low cycles from the surface using a spinner, in direct exchange for the replicating polymer, which is spun on during down-cycle rotation. UV radiation is known to have damaging effects on living systems and the potential for visible light photoinitiators should also be evaluated. With further advancements in Bioimprint it is envisioned that replication techniques will become a more viable option to study cellular ultrastructure at the molecular level.

This work presents several key advances towards understanding fusion pore topology but there still remains significant work to decisively validate a link to exocytosis. Ultimately, studies will need to be rigourously integrated with immunohistochemical techniques. One promising approach is the use of fluorescence through active systems such as using quantum dots to identify hormone specific sites and structures for AFM targeting. Developments may include applying a solution of functional quantum dot bioconjugates targeted to different hormones to identify several sites simultaneously. This would be useful for determining if exocytosis in anterior pituitary cells is regulated by different fusion pores morphologies, as was suspected during this project. Furthermore, as all analysis in this research was performed using static imagery complementary techniques aimed at revealing the dynamic behaviour of fusion pores should also be sought.

Ultimately, future efforts should focus on creating a system fully integrating the

Biochip with the AFM. To achieve this several areas require development before it can become practical to image cells within cavities. One enhancement is to achieve greater cell-to-cavity capture efficiencies through approaches investigating the physical and chemical texturing of cavities or optimisation of the current mask designs. Another recommendation for future work is to explore suitable growth mediums effective for both DEP trapping and cell culturing, eliminating the need to exchange mediums immediately after DEP experimentation. Future investigations should also make use of biocompatible polymers to use as negative resist templates for culturing cells on the Biochip.

Chapter 9

Conclusions

It has been shown that anterior pituitary cells have diverse and complex fusion pore topologies. At least four distinct types or stages of fusion pores were imaged using the AFM with many displaying characteristics and forms unique to those previously reported in literature.

This research provides a comprehensive analysis of fusion pores that will assist researchers in future investigations on the anterior pituitary as well as on exocytosis and endocytosis in general.

Artifacts are introduced as result of chemical fixatives. A Bioimprint technique for permanently creating replica cell impressions has been developed to facilitate cellular analysis by AFMy while in ambient conditions.

Replicas demonstrate excellent fidelity to images of cells taken directly and were absent of fixation artifacts visible as mounds on the membrane, which were seen frequently at locations above the nucleus.

Accurate transfer of cellular structure was achieved down to the molecular level illustrating that elastomers can be used to accurately mould hydrated cells.

The ability to image fusion pores indicates that replication is a useful technique for the study of biological cells at the nanoscale.

The Biochip provides a simplistic means of precisely positioning single-cells within

micro-cavities using either positive or negative DEP. By rapidly creating cellular arrays using single cavity traps, cells can be individually identified and continually monitored from an entire population.

Cavities provided support for cells during medium exchange allowing living cells to be cultured immediately after DEP without needing excessive forces to hold cells in position.

Using Bioimprint to replicate cells on the Biochip combines methodologies designed to enable the effective analysis of cells at the nanoscale.

Appendix A

Appendix

A.1 Dispersion & Stimulation of Anterior Pituitary Cells

The following chapter details the reagents and protocols used for the preparation, dispersion and stimulation of anterior pituitary cells [38].

A.1.1 Reagents

Dispersion Medium

500 ml DMEM including GlutaMaxI, high glucose and 110 mg/L sodium pyruvate with pyridoxine-HCl [Gibco cat. no. 10569-010].

1. 1.80 g HEPES [Sigma cat. no. H-0763]
2. 1.5 g BSA [Gibco cat. no. 30063-572]
3. 4.0 ml Penicillin/Streptomycin [Gibco cat no 15140-148]

Mix everything well then adjust the pH to between 7.2-7.4. Filter the medium into a sterile bottle with a Steritop Millipore filter (Millipore cat. no. SCGPT05RE) in

a laminar hood and store at 4 °C. This medium is fine for a few months but requires the addition of L-glutamine at $\sim$ 2 monthly intervals.

Medium 199 (with Earles salt):

Powdered Medium 199 (M199) with Earle's salts and L-glutamine but without sodium bicarbonate [Gibco cat. no. 400-1100EB].

1. 950 ml DIW
2. 2.20 g $NaHCO_3$
3. 5.95 g HEPES [Sigma cat. no. H-0763]
4. 1.0 g BSA [Gibco cat. no. 30063-572]
5. 10 ml Penicillin/Streptomycin [Gibco cat. no. 15140-148]

To make 1 L mix everything well then adjust the pH to 7.2-7.4. Filter the medium into a sterile bottle using a Steritop Millipore filter (Millipore cat. no. SCGPT05RE) and store at 4 °C.

Trypan Blue:

To make a 0.4 %(w/v) solution, 40 mg Trypan Blue (C.I. 23850; Direct blue 14) [Sigma T-6146] was mixed with 10.0 ml PBS (physiological) and stored at room temperature.

To use, mix thoroughly with the same quantity of cell suspension and allow the cell suspension-trypan mixture to stand for at least 5 mins (but no more than 15 mins). If the cells are exposed to Trypan Blue for extended period of times, viable cells as well as non-viable cells, may begin to stain.

Pepsol:

The following were mixed and refrigerated;

0.1 ml Pepsol, 0.1 M HCl, 99.9 ml DIW, 0.1 g BSA [Gibco cat. no. 30063-572].

PBS (physiological) (10x):

Mix:

- 80.0 g NaCl
- 2.0 g KCl
- 14.4 g Na_2HPO_4
- 2.4 g KH_2PO_4
- 1 L DIW

This recipe makes 1 L at 10 × concentration. Mix all above using a magnetic stirrer if necessary and autoclave at 15 lb for 20 mins in order to store as a concentrate. Dilute 10 fold for usage, adjust pH to 7.40 and store at 4 °C.

A.1.1.1 Enzyme Preparation

Trypsin

To make a concentrated solution of 50 mg/ml mix 100 mg trypsin (Sigma cat. no. T-8253) with 2 ml of PBS (physiological) then aliquot 30 μl or slightly more into tubes.

Trypsin Inhibitor

Mix 300 mg trypsin inhibitor (Sigma cat. no. T-9003) in 6 ml of PBS (physiological) to make a 50 mg/ml concentrated solution, 100 μl of which is then aliquotted into tubes.

DNase

Mix 150 mg DNase (Sigma cat. no. DN-25) in 3 ml of PBS (physiological), then aliquot at 40 μl or slightly more into tubes - the concentration is 50 mg/ml.

If sterility is of concern filter the mixtures through a Millipore filter in a sterile hood first before aliquotting into tubes. Keep frozen in a -20 °C freezer until required.

A.1.2 Procedure

Adult female Sprague-Dawley or Wistar rats were anaesthetised with halothane until they were non-responsive, after which they were decapitated using a mechanical

driven guillotine. The posterior pituitary and the fine membrane covering the pituitary were discarded and the anterior gland transferred to warm dispersion medium in a sterile tube.

A.1.3 Cell Dispersion

Before pituitary extraction the solutions for digestion, inhibition and trituration were prepared according to the recipes given by[1]:

Digestion solution (Solution A)

- 1 ml dispersion medium
- 30 μl trypsin (50 mg/ml)
- 10 μl DNase (50 mg/ml)

Quick Trypsin Inhibitor (TI) solution (Solution B)

- 1 ml dispersion medium
- 50 μl trypsin inhibitor (50 mg/ml)
- 20 μl DNase (50 mg/ml)

Trituration solution (Solution C)

- 5 ml dispersion medium
- 50 μl trypsin inhibitor (50 mg/ml)
- 20 μl DNase (50 mg/ml)

Immediately after extraction of the anterior pituitary gland approximately 1 ml of warm dispersion medium was placed onto a sterilised glass Petri-dish lid (6 cm diameter) and cut up with a sterile surgical blade until fine. All tissue was collected in a sterile 5 ml Khan tube and centrifuged at 1500 rpm for 5 mins. The supernatant was aspirated and discarded and cells were resuspended in the digestion solution

[1]Volumes are designed for 1 pituitary, if several are prepared simultaneously multiply accordingly.

(Solution A). Cells were mixed well by shaking manually in a water-bath at 37 °C for 11 mins. At the end of the digestion period the enzyme was halted by the addition of Solution B and after a few minutes centrifuged again at 1500 rpm for 5 mins with the supernatant aspirated and discarded.

Cells were resuspended in approximately 2 ml of Solution C and gently triturated to separate cells from connective tissues approximately 20 times with an 18 gauge needle and 1 ml syringe. After allowing the bulk of the tissue to settle for 2 mins the supernatant containing cells was collected and the process repeated until the rest of the trituration solution was used. All the supernatant was filtered through a cell strainer (70 μm mesh) and centrifuged at 1500 rpm for 5 mins and resuspended in 2 ml of incubation medium per pituitary. The solution was triturated again lightly to make a stock cell solution.

For culturing the cell solution was resuspended in M199 supplemented with 10 % FBS (Gibco cat. no. 10091-148) and depending on the application cell were either plated on Petri-dishes, substrates (in Petri-dishes) or well-plates in a 37 °C incubator with 5 % CO_2.

A.1.4 Stimulation of Pituitary Cells

GnRH was prepared by dissolving 5 mg GnRH (Sigma cat. no. L-7134) in 2.0 ml DIW and adding 3.0 ml pepsol. 100 μl of the solution was mixed with 900 μl pepsol to make GnRH at 10^{-5} concentration. The solution was frozen and diluted in M199 depending on the desired concentrated.

A.2 Tissue Preparation and Dispersion of Endometrial Cancer Cells

The following details the reagents and protocols used for the preparation and dispersion of endometrial cancer cells [39].

Minimum essential medium alpha medium (α-MEM)

- 1 packet α-MEM powder (Gibco cat. no. 11900-024 with glutamine)
- 2.2 g $NaHCO_3$
- 10 ml Penicillin streptomycin
- 1 g BSA

α-MEM powder was added to 950 ml DIW water and $NaHCO_3$ (both stirred after each addition), and the pH adjusted to 7.4 $\pm$ 0.2-0.3 before sterilising by membrane filtration.

Collagenase dissolving buffer:

To make 500 ml the following reagents were mixed;

4.0 g NaCl, 0.2 g KCl, 0.19 g Na_2HPO_4, 0.03 g KH_2PO_4, 0.05 g $MgSO_4.7H_2O$, 0.05 g $MgCl_2.6H_2O$, 495 ml DIW. Followed by the addition of; 0.5 g Glucose, 0.175 g $NaHCO_3$, 0.092 g $CaCl_2.2H_2O$, 5.0 ml penicillin streptomycin. After mixing the buffer pH was adjusted to physiology, sterilised and kept at 4 °C.

Collagenase solution:

50 mg collagenase Type 1A (Sigma, cat. no. C-2674) and 50 ml collagenase dissolving buffer were mixed, well dissolved and sterilised, making a brownish coloured concentrate (1 mg/ml).

A.2.1 Tissue Dispersion

To disperse cells from endometrial carcinomas:

1. Tissue was finely diced into small pieces using a scalpel blade and placed in 1 mg/ml collagenase for 30-45 mins depending on tissue quantity and type.
2. Cells were centrifuged and resuspended in culture medium (no FBS) twice and triturated each time.
3. Dispersion was checked and if not evenly distributed the digestion process was repeated for a period of time determined by the degree of clumping.

A.2.2 Cell Passage/Splitting

To split/passage cells *in vitro* (the following volumes are for flasks):

1. Medium was removed.
2. Cells were washed with 10 ml sterile, physiological PBS and incubated for 3-5 mins.
3. Supernatant was discarded and 2 ml trypsin added until cells lifted (approximately 6-12 mins depending on confluence).
4. 10 ml of α-MEM medium containing 10 % FBS was added to stop digestion.
5. Cells were gently triturated until dispersed and plated in 3-5 flasks depending on confluence.

References

[1] Schneider SW, Sritharan KC, Geibel JP, Oberleithner H, and Jena BP. Surface dynamics in living acinar cells imaged by atomic force microscopy: Identification of plasma membrane structures involved in exocytosis. *PNAS USA*, 94(1):316–321, 1997.

[2] Gundelfinger ED, Kessels MM, and Qualmann B. Temporal and spatial coordination of exocytosis and endocytosis. *Nature Rev. Mol. Cell Biol.*, 4(2):127–139, 2003.

[3] Nanavati C, Markin VS, Oberhauser AF, and Fernandez JM. The exocytotic fusion pore modeled as a lipidic pore. *Biophys. J.*, 63(4):1118–1132, 1992.

[4] Jahn R, Lang T, and Südhof TC. Membrane fusion. *Cell*, 112:519–533, 2003.

[5] Lang J. Molecular mechanisms and regulation of insulin exocytosis as a paradigm of endocrine secretion. *Eur. J. Biochem.*, 259(1):3–17, 1999.

[6] Burgoyne RD and Morgan A. Secretory Granule Exocytosis. *Physiol. Rev.*, 83(2):581–632, 2003.

[7] Söllner TH. Intracellular and viral membrane fusion: a uniting mechanism. *Curr. Opin. Cell. Biol.*, 16:429–435, 2004.

[8] Lee J-S, Mayes MS, Stromer MH, Scanes CG, Jeftinija S, and Anderson LL. Number of Secretory Vesicles in Growth Hormone Cells of the Pituitary Remains Unchanged After Secretion. *Exp. Bio. and Med.*, 229(7):632–639, 2004.

[9] Fesce R, Gonzalez F, Valtorta F, and Meldolesi J. Neurotransmitter release: fusion or kiss-and-run? *Trends Cell. Biol.*, 4:1–4, 1994.

[10] Elhamdani A, Azizi F, and Artalejo CR. Double Patch Clamp Reveals That Transient Fusion (Kiss-and-Run) Is a Major Mechanism of Secretion in Calf Adrenal Chromaffin Cells: High Calcium Shifts the Mechanism from Kiss-and-Run to Complete Fusion. *J. Neurosci.*, 26(11):3030–3036, 2006.

[11] Williams RM and Webb WW. Single granule pH cycling in antigen-induced mast cell secretion. *J. Cell. Sci.*, 113(21):3839–3850, 2000.

[12] Ma L, Bindokas VP, Kuznetsov A, Rhodes C, Hays L, Edwardson JM, Ueda K, Steiner DF, and Philipson LH. Direct imaging shows that insulin granule exocytosis occurs by complete vesicle fusion. *PNAS*, 101(25):9266–9271, 2004.

[13] Harata NC. Kiss-and-run and full-collapse fusion as modes of exo-endocytosis in neurosecretion. *J. Neurochem.*, 97(6):1546–1570, 2006.

[14] Sokac AM and Bement WM. Kiss-and-Coat and Compartment Mixing: Coupling Exocytosis to Signal Generation and Local Actin Assembly. *Mol. Biol. Cell*, 17(4):1495–1502, 2006.

[15] Pickett JA. Compound exocytosis: Mechanisms and functional significance. *Traffic*, 7(2):109–116, 2006.

[16] Jena BH, Cho S-J, Jeremic A, Stromer MH, and Abu-Hamdah R. Structure and composition of the fusion pore. *Biophys. J.*, 84(2):1337–1343, 2003.

[17] Tixier-Vidal A and Farquhar MG. *The anterior pituitary, Structure and funciton of pituitary cells (pg. 84-127).* Academic Press, New York, 1975.

[18] Department of Pathology, Virginia Commonwealth University, Richmond VA. Pituitary gland lecture; anatomy, physiology, regulatory factors and hormones. *http://www.pathology.vcu.edu/education/endocrine/endocrine/pituitary/index.htm*, 2005.

[19] Anderson LL, Jeftinija S, and Scanes CG. Growth hormone secretion: Molecular and cellular mechanissm and *in vivo* approaches (minireview). *Exp. Bio. Med.*, 229:291–302, 2004.

[20] Binnig G, Quate CF, and Gerber Ch. Atomic force microscope. *Phys. Rev. Lett.*, 56:930–933, 1986.

[21] Binnig G, Gerber Ch, Stoll E, Albrecht TR, and Quate CF. Atomic resolution with atomic force microscope. *Europhys. Lett.*, 3:1281, 1987.

[22] Digital Instruments, Santa Barabara CA, USA. Nanoscope®, command reference manual. Version 4.42, 1999.

[23] Dürig U, Gimzewski JK, and Pohl DW. Experimental observation of forces acting during scanning tunneling microscopy. *Phys. Rev. Lett.*, 57:24032406, 1986.

[24] Martin Y, Williams CC, and Wickramasinghe HK. Atomic force microscope-force mapping and profiling on a sub 100-angstrom scale. *J. Appl. Phys.*, 61(10):4723–4729, 1987.

[25] Meyer G and Amer NM. Erratum: Novel optical approach to atomic force microscopy. *Appl. Phys. Lett.*, 53(24):2400–2402, 1988.

[26] Butt HJ. Measuring electrostatic, van der waals, and hydration forces in electrolyte solutions with an atomic force microscope. *Biophys. J.*, 60(6):1438–44, 1991.

[27] You HX and Yu L. Atomic force microscopy imaging of living cells: progress, problems and prospects. *Meth. Cell Sci.*, 21:1–17, 1999.

[28] Le Grimellec C, Lesniewska E, Cachia C, Schreiber JP, de Fornel F, and Goudonnet JP. Imaging of the membrane surface of mdck cells by atomic force microscopy. *Biophys. J.*, 67(1):3641, July 1994.

[29] Persson BNJ. The atomic force microscope: Can it be used to study biological molecules? *Chem. Phys. Lett.*, 141:366368, 1987.

[30] Digital Instruments, Santa Barbara, CA. Scanning probe microscopy training notebook.

[31] Binnig G, Rohrer H, Gerber Ch., and Weibel E. Tunneling through a controllable vacuum gap. *Appl. Phys. Lett.*, 40(2):178–180, 1982.

[32] Binnig G, Rohrer H, Gerber Ch., and Weibel E. Surface studies by scanning tunneling microscopy. *Phys. Rev. Lett.*, 49(1-5):5761, 1982.

[33] Von Ardenne M. The scanning electron microscope: Theoretical fundamentals (in german). *Z. Tech. Phys.*, 109:553–572, 1938.

[34] Russell P, Batchelor D, and Thornton JT. Sem and afm: Complementary techniques for high resolution surface investigations. *Application Note AN46, Veeco Instruments Inc., U.S.A*, 2004.

[35] NT-MDT Company, Moscow, Russia. Application note: Spm techniques. *Common techniques for imaging and measuring surface morphology: What is scanning probe microscopy?*, page 3.

[36] Hell SW. Towards fluorescence nanoscopy. *Nat. Biotech.*, 21:1347–1355, 2003.

[37] Pawley JB. *Handbook of Biological Confocal Microscopy*. Plenum Press, New York, 1995.

[38] Evans JJ and Nagase J. Tissue preparation / in vitro (static incubation) and stimulation of dispersed anterior pituitaries with gonadotrophin-releasing hormone. *M.VITS-2*, pages 1–10, Modified 09/2005.

[39] Nagase J. Dispersion and culture of endometrial tumour tissue in vitro. *M.VITS-3 and -4*, pages 2–3, Modified and Printed 02/2005.

[40] Leong A S-Y, Fixation and Fixatives, http://home.primus.com.au/royellis/fix.htm.

[41] Braet F, De Zanger R, and Wisse E. Drying cells for sem, afm and tem by hexamethyldisilazane: a study on hepatic endothelial cells. *J. Microscopy*, 186(1):84–87, 1997.

[42] Araujo JC, Teran FC, Oliveira RA, Nour EAA, Montenegro MAP, Campos JR, and Vazoller RF. Comparison of hexamethyldisilazane and critical point drying treatments for SEM analysis of anaerobic biofilms and granular sludge. *J. Elec. Microscopy (Tokyo)*, 52(4):429–433, 2003.

[43] Evans JJ and Nagase J. Immunohistochemistry for LH/FSH and pcreb and c/ebpβ of dispersed anterior pituitaries after stimulation with gnrh and oestradiol on chamber slides. *M.IHCC-2 - LCPR Application Note, Christchurch School of Medicine*, Modified 2005.

[44] Häberle W, Hörber JKH, and Binnig G. Force microscopy on living cells. *J. Vac. Sci. Technol. B*, 9(2):1210–1213, 1990.

[45] Henderson E, Haydon PG, and Sakaguchi DS. Actin filaments dynamics in living glial cells imaged by atomic force microscopy. *Science*, 257(1944), 1992.

[46] Haydon PG, Lartius R, Parpura V, and Marchese-Ragona SP. Membrane deformation of living glial cells using atomic force microscopy. *J. Microscopy*, 182(114), 1996.

[47] Putman CA, van der Werlf KO, de Grooth BG, van Hulst NF, and Greve J. Viscoelasticity of living cells allows high resolution imaging by tapping mode atomic force microscopy. *Biophys. J.*, 67(1749), 1994.

[48] Radmacher M, Fritz M, Kacher CM, Cleveland JP, and Hansma PK. Measuring the viscoelastic properties of human platelets with the atomic force microscope. *Biophys. J.*, 70(556), 1996.

[49] Schaus SS and Henderson ER. Cell viability and probe-cell membrane interactions of xr1 glial cells imaged by atomic force microscopy. *Biophys. J.*, 73(1205), 1997.

[50] Le Grimellec C, Lesneiewska E, Giocondi M-C, Finot E, Vié V, and Goudonnet J-P. Imaging of the surface of living cells by low-force contact-mode atomic force microscopy. *Biophys. J.*, 75(695), 1998.

[51] Shao Z, Yang J, and Somlyo AP. Biological atomic force microscopy: from microns to nanometers and beyond. *Annu. Rev. Cell Dev. Biol.*, 11:241–65, 1995.

[52] Fritz M, Radmacher M, and Gaub HE. Granula motion and membrane spreading during activation of human platelets imaged by atomic force microscopy. *Biophys. J.*, 66(1328), 1994.

[53] Radmacher M, Tillmann RW, and Gaub HE. Imaging viscoelasticity by force modulation with the atomic force microscope. *Biophys. J.*, 64(735), 1993.

[54] You HX and Yu L. Atomic force microscopy imaging of living cells: progress, problems and prospects. *Methods Cell Sci.*, 21(1), 1999.

[55] Hoh JH and Schoenenberger C-A. Surface morphology and mechanical properties of mdck monolayers by atomic force microscopy. *J. Cell Sci.*, 107:1105–1114, 1994.

[56] Monck JR and Fernandez JM. The exocytotic fusion pore. *J. Cell Biol.*, 119(6):1395–1404, 1992.

[57] Sabatini DD, Bench K, and Barrnett RJ. Cytochemistry and electron microscopy. the preservation of cellular ultrastructure and enzymatic activity by aldehyde fixation. *J. Cell Biol.*, 17:19–58, 1963.

[58] Hopwood D. *Fixation and Fixatives, In: Bancroft JD & Stevens A, eds. Theory and Practice of Histological Techniques*. Churchill Livingstone, Edinburgh, Scotland, 1977.

[59] Braet F, Seynaeve C, De Zanger R, and Wisse E. Imaging surface and submembranous structures with the atomic force microscope: a study on living cancer cells, fibroblasts and macrophages. *J. Microscopy*, 109(3):328–338, 1998.

[60] Kamal A and Goldstein LSB. Connecting vesicle transport to the cytoskeleton. *Curr. Op. Cell Bio.*, 12(4):503–508, 2000.

[61] Kumar S and Hoh JH. Probing the machinery of intracellular trafficking with the atomic force microscope. *Traffic*, 2:746–756, 2001.

[62] Doussau F and Augustine GJ. The actin cytoskeleton and neurotransmitter release: An overview. *Biochimie*, 82(4):353–363, 2000.

[63] Alberts B, Alexander J, Lewis J, Raff M, Roberts K, and Walter P. *Molecular Biology of the Cell: 4th Edition*. Garland Science, New York, NY, 2002.

[64] Liu F, Arce FT, Ramachandran S, and Lal R. Nanomechanics of hemichannel conformations: Connexin flexibility underlying channel opening and closing. *J. Biol. Chem.*, 281(32):23207–23217, 2006.

[65] Paul Hansma's Website, Dept. of Physics, University of California - Santa Barabara (USA). Applications of afm; biophysics. *http://hansmalab.physics.ucsb.edu/afmapp.html*.

[66] Cho S-J, Cho J, and Jena BP. The number of secretory vesicles remains unchanged following exocytosis. *Cell Bio. Int.*, 26(1):2933, 2002.

[67] Angleson JK, Cochilla AJ, Kilic G, Nussinovitch I, and Betz WJ. Regulation of dense core release from neuroendocrine cells revealed by imaging single exocytic events. *Nature Neurosci.*, 2:440–446, 1999.

[68] Fujita H, Kurihara H, and Miyagawa J. Ultrastructural aspects of the effect of calcium ionophore a23187 on incubated anterior pituitary cells of rats. *Cell and Tissue Res.*, 229(1):129–136, 1983.

[69] Betz WJ Cochilla AJ, Angleson JK. Differential Regulation of Granule-to-Granule and Granule-to-Plasma Membrane Fusion during Secretion from Rat Pituitary Lactotrophs. *J. Cell Biol.*, 150(4):839–848, 2000.

[70] Evans JJ, Pragg FL, and Mason DR. Release of luteinizing hormone from the anterior pituitary gland in vitro can be concurrently regulated by at least three peptides: gonadotrophin-releasing hormone, oxytocin and neuropeptide y. *Neuroendocrin.*, 73:408–416, 2001.

[71] Sørensen JB. Formation, stabilisation and fusion of the readily releasable pool of secretory vesicles. *Pflügers Arch. - Euro. J. Physiol.*, 448(4):347–362, 2004.

[72] Heuser JE, Reese TS, Dennis MJ, Jan Y, Jan L, and Evans L. Synaptic vesicle exocytosis captured by quick freezing and correlated with quantal transmitter release. *J. Cell Biol.*, 81(2):275–300, 1979.

[73] Qdot® antibody conjugation kit user manual (pn 90-0078, rev 8). *Invitrogen, CA, USA*, 17 Jan 2006.

[74] Bullivant S and Ames A 3rd. A simple freeze-fracture replication method for electron microscopy. *J. Cell. Biol.*, 29:435–447, 1966.

[75] Pfefferkorn G and Boyde A. Review of replica techniques for scanning electron microscopy. *Scan. Elec. Micro. (Part I) - Proceedings of the 7th Annual Scanning Electron Microscope Symposium, Chicago, IL*, pages 75–82, 1974.

[76] Hasty DL and Hay ED. Freeze-fracture studies of the developing cell surface. ii. particle-free membrane blisters on glutaraldehyde-fixed corneal fibroblasts are artifacts. *J. Cell Sci.*, 78:756–768, 1978.

[77] Sjöstrand FS and Baker RF. Fixation by freeze-drying for electron microscopy of tissue cells. *J. Ultrastruct. Res.*, 1:239, 1958.

[78] Hall CE. A low temperature replica method for electron microscopy. *J. Appl. Phys.*, 21(61), 1950.

[79] Gersh I. The preparation of frozen-dried tissue for electron microscopy. *J. Biophys. Biochem. Cytol.*, 2(37), 1956.

[80] Sampson J. A method of replicating dry or moist surfaces for examination by light microscopy. *Nature*, 191(4791):932–933, August 1966.

[81] Forslind B. Replication techniques for dry and wet biological surfaces. *Scanning Microscopy*, 13(1):133–139, 1999.

[82] Yan M and Ramström O. *Molecularly imprinted materials; Science and Technology*. Marcel Dekker, New York, NY, 2005.

[83] Mosbach K. Molecular imprinting. *Tren. Biochem. Sci.*, 19(1), 1994.

[84] Mosbach K and Ramström O. The emerging technique of molecular imprinting and its future impact on biotechnology. *Nature Biotech.*, 14(163), 1996.

[85] Ramström O and Ansell RJ. Molecular imprinting technology: Challenges and prospects for the future. *Chirality*, 10(195), 1998.

[86] Mingarro I, Abad C, and Braco L. Interfacial activation-based molecular bioimprinting of lipolytic enzymes. *PNAS USA*, 92:3308–3312, 1995.

[87] Hayden O, Bindeus R, and Dickert FL. Combining atomic force microscope and quartz crystal microbalance studies for cell detection. *Meas. Sci. Technol.*, 14(1876), 2003.

[88] Forslind B. Replication techniques for dry and wet biological surfaces. *Scan. Micro.*, 13(1):133, 1999.

[89] Whitesides GM, Ostuni E, Takayama S, Jiang X, and Ingber DE. Soft lithography in biology and biochemistry. *Ann. Rev. Biomed. Eng.*, 3(1):335–373, 2001.

[90] Weyn B, Kalle W, Kumar-Singh S, Van Marck E, Tanke H, and Jacob W. Atomic force microscopy: influence of air drying and fixation on the morphology and viscoelasticity of cultured cells. *J. Microscopy*, 189(2):172–180, 1998.

[91] Sigma Aldrich Application Note. Applications: Free radical initiators.

[92] Muys JJ, Akaisi MM, Melville DOS, Nagase J, Parguez GM, and Evans JJ. Cellular transfer and afm imaging of cancer cells using bioimprint. *J. Nanobiotech.*, 4(1), 2006.

[93] Muys JJ, Alkaisi MM, and Evans JJ. Bioimprint: Nanoscale analysis by replication of cellular topography using soft lithography. *J. Biomed. Nano.*, 2(1), 2006.

[94] Smith JE and Reese TS. Use of aldehyde fixatives to determine the rate of synaptic transmitter release. *J. Exp. Biol.*, 89(1):19–29, 1980.

[95] Fujisawa S, Kadoma Y, and Masuhara E. Effects of photoinitiators for the visible-light resin system on hemolysis of dog erythrocytes and lipid peroxidation of their components. *J. Dental Res.*, 65(9):1186–1190, September 1986.

[96] Muys JJ, Alkaisi MM, and Evans JJ. Cellular replication and afm imaging using a uv-bioimprint technique. *Nanomed: Nanotech. Bio. Med.*, 2(3):169–176, 2006.

[97] Reith A, Kraemer M, and Vassy J. The influence of mode of fixation, type of fixative and vehicles on the same rat liver: a morphometric/stereologic study by light and electron microscopy. *Scan. Elec. Micro.*, 2(645), 1984.

[98] Chandler DE. Comparison of quick-frozen and chemically fixed sea-urchin eggs: Structural evidence that cortical granule exocytosis is preceded by a local increase in membrane mobility. *J. Cell Sci.*, 72(23-36), 1984.

[99] Morgenstern E. Aldehyde fixation causes membrane vesiculation during platelet exocytosis: a freeze-substitution study. *Scan. Elec. Micro.*, 5:S109–S115, 1991.

[100] Pettitt JM, Humphris DC, Barrett SP, Toh B-H, van Driel IR, and Gleeson PA. Fast freeze-fixation/freeze-substitution reveals the secretory membranes of the gastric parietal cell as a network of helically coiled tubule: A new model for parietal cell transformation. *J. Cell Sci.*, 108:1127–1141, 1995.

[101] McIntyre JA, Gilula NB, and Karnovsky MJ. Cryoprotectant-induced redistribution of intramembranous particles in mouse lymphocytes. *J. Cell Sci.*, 60:192–202, 1974.

[102] Holt SJ and Hicks RM. The fine structure produced in cells by fixatives. *J. R. Microscope Society*, 48:115–131, 1965.

[103] Cope GH and Williams MA. Quantitative studies on the preservation of chlorine and ethanolamine phosphatides during tissue preparation for electron microscopy. i. glutaraldehyde, osmium tetroxide, araldite methods. *J. Microscopy*, 90:31–46, 1969.

[104] Hayat MA. *Principles and techniques of electron microscopy: Biological applications 4th ed.* Cambridge University Press, U.K, 2000.

[105] Chandler DE and Heuser JE. Arrest of membrane fusion events in mast cells by quick freezing. *J. Cell. Biol.*, 86(666), 1980.

[106] Papanicolaou GN and Traut HF. The diagnostic value of vaginal smears in carcinoma of the uterus. *Am J. Obstet. Gynecol.*, 42:193–206, 1941.

[107] Hamby L. Gene expression patterns and breast cancer. *Cancer Genetics News*, 4(1), Spring 2002.

[108] National Cancer Institute (NCI), U.S National Institutes of Health. Understanding cancer. *http://www.cancer.gov*.

[109] Zink D, Fischer AH, and Nickerson JA. Nature reviews. *Nucl. Struct. Canc. Cell*, 4:677–687, 2004.

[110] Ishioka S-i, Sagae S, Ito E, and Kudo R. Ultrastructural study of benign, low-malignant potential (lmp), and malignant ovarian tumors. *Medical Elec. Microscopy*, 37(1):37–44, 2004.

[111] Morgan H, Hughes MP, and Green NG. Separation of submicron bioparticles by dielectrophoresis. *Biophys. J.*, 77:516–525, 1999.

[112] Pohl HA. The motion and precipitation of suspensoids in divergent electric fields. *J. Appl. Phys.*, 22:869–871, 1951.

[113] Jones TB. *Electromechanics of Particles*. Cambridge University Press, New York, NY, 1995.

[114] Irimajiri A, Hanai T, and Inouye VA. Dielectric theory of "multi-stratified shell" model with its application to lymphona cell. *J. Theor. Biol.*, 78(251), 1979.

[115] Gomez R, Ladisch MR, Bhunia AK, and Bashir R. Microfabricated device for impedance-baseddetection of bacterial metabolism. *Mat. Res. Soc. Symp. Proc.*, 729, 2002.

[116] Müller T, Arnold WM, Schnelle T, Hegedorn R, Fuhr G, and Zimmermann U. A traveling-wave micropump for aqueous solutions: comparison of 1 g and microgram results. *Electrophoresis*, (14):764, 1993.

[117] Yang J, Huang Y, Wang X-B, Becker FF, and Gascoyne PRC. Differential Analysis of Human Leukocytes by Dielectrophoretic Field-Flow-Fractionation. *Biophys. J.*, 78(5):2680–2689, 2000.

[118] Voldman J, Toner M, Gray ML, and Schmidt MA. A dielectrophoresis-based array cytometer. *Proc. Transducers '01, 1014 June, 2001, Munich, Germany.*